MARTIN MARIETTA ENERGY SYSTEMS LIBRARIES

3 4456 0384373 1

ornl

ORNL-6767

OAK RIDGE NATIONAL LABORATORY

MARTIN MARIETTA

Use of a Temperature-Initiated Passive Cooling System (TIPACS) for the Modular High-Temperature Gas-Cooled Reactor Cavity Cooling System (RCCS)

C. W. Forsberg
J. Conklin
W. J. Reich

OAK RIDGE NATIONAL LABORATORY
CENTRAL RESEARCH LIBRARY
CIRCULATION SECTION
4500N ROOM 175
LIBRARY LOAN COPY
DO NOT TRANSFER TO ANOTHER PERSON
If you wish someone else to see this report, send in name with report and the library will arrange a loan.
DOE/RB-0170

MANAGED BY
MARTIN MARIETTA ENERGY SYSTEMS, INC.
FOR THE UNITED STATES
DEPARTMENT OF ENERGY

This report has been reproduced directly from the best available copy.

Available to DOE and DOE contractors from the Office of Scientific and Technical Information, P.O. Box 62, Oak Ridge, TN 37831; prices available from (615) 576-8401, FTS 626-8401.

Available to the public from the National Technical Information Service, U.S. Department of Commerce, 5285 Port Royal Rd., Springfield, VA 22161.

This report was prepared as an account of work sponsored by an agency of the United States Government. Neither the United States Government nor any agency thereof, nor any of their employees, makes any warranty, express or implied, or assumes any legal liability or responsibility for the accuracy, completeness, or usefulness of any information, apparatus, product, or process disclosed, or represents that its use would not infringe privately owned rights. Reference herein to any specific commercial product, process, or service by trade name, trademark, manufacturer, or otherwise, does not necessarily constitute or imply its endorsement, recommendation, or favoring by the United States Government or any agency thereof. The views and opinions of authors expressed herein do not necessarily state or reflect those of the United States Government or any agency thereof.

DE F 1332.15
(1-93)
mbines previous
sion of DOE
332.15 and .16.
other editions are
solete.

U. S. DEPARTMENT OF ENERGY
RECOMMENDATIONS FOR THE ANNOUNCEMENT AND DISTRIBUTION OF DEPARTMENT OF ENERGY (DOE) SCIENTIFIC AND TECHNICAL INFORMATION (STI)

(See instructions on reverse side. Use plain bond paper if additional space is needed for explanations.)

OMB Control No. 1910-1400
OMB Burden Disclosure Statement on reverse side

ART I *(DOE, DOE Contractors, Grantees, and Awardees complete)*

A. Product/Report Data

1. (Award) Contract No. DE-AC05-84OR21400

2. Title Use of a Temperature-Initiated Passive Cooling System (TIPACS) for the Modular High-Temperature Gas-Cooled Reactor Cavity Cooling System (RCCS)

3. Product/Report Description

☒ a. Report *(Complete all that apply)*
(1) ☒ Print ☐ Nonprint *(specify)*
(2) ☐ Quarterly ☐ Semiannual ☐ Annual ☐ Final
☒ Topical ☐ Phase I ☐ Phase II
☐ Other *(specify)*

Dates covered _____ thru _____

☐ b. Conference/Meeting/Presentation *(Complete all that apply)*
(1) ☐ Print ☐ Nonprint *(specify)*
☐ Published proceedings
☐ Other *(specify)*

(2) Conference Title *(no abbreviations)*

Location *(city/state/country)*

Date(s) *(m/d/y)* / / thru *(m/d/y)* / /
Sponsor

☐ c. Software—Additional forms are required. Follow instructions on the back of this form.
☐ d. Other *(Provide complete description)*

B. Patent Information

Yes No
☐ ☒ Is any new equipment, process, or material disclosed? If yes, identify page numbers
☐ ☒ Has an invention disclosure been submitted? If yes, identify the disclosure number and to whom it was submitted. Disclosure number
Submitted to
☐ ☒ Are there patent-related objections to the release of this STI product? If so, state the objections.

C. Contact *(Person knowledgeable of content)*

Name
Phone
Position
Organization

ART II *(DOE/DOE Contractors complete/or as instructed by DOE contracting officer)*

A. DOE Identifiers

1. Product/Report Nos. ORNL-6767

2. Funding Office(s) *(NOTE: Essential data)* AF 20 50 10 0

B. Copies for Transmittal to AD-21 (OSTI)

(STI must be of sufficient quality for microfilming/copying.)

☐ 1. One for classified processing
☐ 2. *(number)* for standard classified distribution
☒ 3. Two unclassified for processing
☐ 4. *(number)* for program unclassified distribution
☒ 5. UC/C Category 522
☐ 6. Additional instructions/explanations

(Do not identify Sigma categories for Nuclear Weapons Data reports, and do not provide additional instructions that are inconsistent with C below.)

C. Recommendation *("X" at least one)*

☒ 1. Program/Standard Announcement/Distribution *(Available to U.S. and foreign public)*
☐ 2. Classified *(Standard Announcement only)*
☐ 3. Special Handling *(Legal basis must be noted below.)*
☐ a. Unclassified Controlled Nuclear Information (UCNI)
☐ b. Export Control/ITAR/EAR
☐ c. Temporary hold pending patent review
☐ d. Translations of copyrighted material
☐ e. Small Business Innovation Research (SBIR)
☐ f. Commercializable information
☐ (1) Proprietary
☐ (2) Protected CRADA information
Release date / /
☐ (3) Other *(explain)*
☐ 4. Program Directed Special Handling *(copy attached)*

D. Releasing Official

A. Patent Clearance *("X" one)*
☐ Has been submitted for DOE patent clearance
☒ DOE patent clearance has been granted

B. Released by
(Name) D.R. Hamrin
(Signature) D. R. Hamrin (KB)
(Phone) (615) 574-6752
(Date) June 7, 1994

ORNL-6767

S22
77

Use of a Temperature-Initiated Passive Cooling System (TIPACS) for the Modular High-Temperature Gas-Cooled Reactor Cavity Cooling System (RCCS)

C. W. Forsberg
J. Conklin
W. J. Reich

Date Published: April 1994

prepared by
OAK RIDGE NATIONAL LABORATORY
Oak Ridge, Tennessee 37831-6495
managed by
MARTIN MARIETTA ENERGY SYSTEMS, INC.
for the
U.S. DEPARTMENT OF ENERGY
under contract DE-AC05-84OR21400

MARTIN MARIETTA ENERGY SYSTEMS LIBRARIES

3 4456 0384373 1

CONTENTS

LIST OF FIGURES v

LIST OF TABLES vii

ACRONYMS AND ABBREVIATIONS ix

VARIABLES xi

EXECUTIVE SUMMARY S-1

1. INTRODUCTION 1-1

2. DESCRIPTION OF PROBLEM AND TIPACS REQUIREMENTS 2-1

2.1 CHARACTERISTICS OF MHTGR 2-1
2.2 RCCS: CURRENT DESIGN REQUIREMENTS 2-3
2.3 RCCS: ADDITIONAL DESIRABLE CHARACTERISTICS 2-6

3. DESCRIPTION OF TIPACS 3-1

3.1 SYSTEM DESCRIPTION 3-1
3.2 RCHTS DESIGN 3-3

3.2.1 General Design 3-3
3.2.2 External Heat Exchanger 3-3
3.2.3 Internal Heat Exchanger—Option A 3-3
3.2.4 Alternative Internal Heat Exchanger—Option B 3-5

3.3 TCS 3-9
3.4 TIPACS DESIGN APPLIED TO MHTGR 3-13

4. REACTOR CAVITY HEAT TRANSFER SYSTEM 4-1

4.1 CHOICE OF FLUID 4-1
4.2 HIGH PERFORMANCE FOR NATURAL-CIRCULATION RCHTS 4-1
4.3 STEADY-STATE THERMAL PERFORMANCE CHARACTERISTICS FOR TIPACS WITH INTERNAL HEAT-EXCHANGER DESIGN—OPTION A 4-6

4.3.1 TIPACS Geometry Assumptions for Thermal-Flow Modeling 4-6
4.3.2 Calculated Results and Discussion 4-10

CONTENTS
(continued)

4.4 HIGH TEMPERATURE TRANSIENT OR STEADY-STATE OPERATIONS 4-15

5. TEMPERATURE CONTROL SYSTEM 5-1

5.1 PHYSICS OF THE TCS 5-1
5.2 LIQUID-GAS RESERVOIR 5-4
5.3 HEAT DIODE 5-6

6. OTHER ISSUES 6-1

6.1 ALTERNATIVE DESIGN OPTIONS 6-1
6.2 MONITORING OF PERFORMANCE 6-1
6.3 EQUIPMENT AVAILABILITY 6-2

7. UNCERTAINTIES AND UNKNOWNS 7-1

7.1 MHTGR DESIGN TRADE-OFFS 7-1
7.2 MODEL OF TIPACS UNDER ALL EXPECTED CONDITIONS 7-1
7.3 PROOF-OF-PRINCIPLE EXPERIMENT 7-1
7.4 ENGINEERING SCALE TEST 7-2
7.5 DEVELOPMENT OF ENGINEERING METHODOLOGY 7-2

8. CONCLUSIONS 8-1

9. REFERENCES 9-1

Appendix A: CRITICAL PROPERTIES OF FLUIDS A-1

Appendix B: CO_2 PHYSICAL PROPERTIES BELOW THE CRITICAL POINT B-1

Appendix C: ANALYTICAL MODELS OF TEMPERATURE CONTROL SYSTEM PERFORMANCE C-1

Appendix D: ANALYSIS OF RCHTS D-1

LIST OF FIGURES

Fig. 2.1 Schematic of steam-cycle MHTGR 2-2

Fig. 2.2 MHTGR with conventional RCCS and TIPACS 2-5

Fig. 3.1 TIPACS 3-2

Fig. 3.2 External heat exchanger 3-4

Fig. 3.3 Cross-section view of internal RCHTS heat-exchanger options 3-6

Fig. 3.4 Radiative heat-transfer models of internal heat exchanger 3-8

Fig. 3.5 Relative radiative heat transfer vs hot-wall temperature 3-10

Fig. 4.1 Density of CO_2 vs temperature for different pressures above the critical point 4-3

Fig. 4.2 Thermal expansion coefficient of CO_2 vs temperature for different pressures above the critical point 4-4

Fig. 4.3 Dynamic viscosity of CO_2 temperature for different pressures above the critical point 4-5

Fig. 4.4 Isobaric specific heat of CO_2 vs temperature for different pressures above the critical point 4-7

Fig. 4.5 Thermal conductivity of CO_2 vs temperature for different pressures above the critical point 4-8

Fig. 4.6 Heat transfer per quadrant from reactor vessel at 220° C 4-11

Fig. 4.7 CO_2 mass flow for different ambient air temperatures 4-12

Fig. 4.8 CO_2 inlet and exit temperatures from the internal heat exchanger for different ambient temperatures 4-14

Fig. 4.9 CO_2 temperatures vs reactor vessel temperature for design Option A 4-16

Fig. 4.10 Heat-transfer rates and CO_2 flow rates per TIPACS (one quadrant of reactor vessel) vs reactor vessel temperature for design Option A 4-17

LIST OF FIGURES
(continued)

Fig. 4.11 CO_2 temperatures vs reactor vessel temperatures for design Option B 4-21

Fig. 4.12 Heat-transfer rates and CO_2 flow rates per TIPACS (one quadrant of reactor vessel) vs reactor temperatures for design Option B 4-22

Fig. 5.1 TCS characteristics 5-2

Fig. 5.2 Schematic of TIPACS model parameters 5-5

Fig. B.1 CO_2 phase diagram B-4

Fig. C.1 Schematic of TIPACS model parameters C-4

Fig. C.2 Relative height of RCHTS vs external design temperatures C-6

Fig. C.3 TIPACS with bypass line to minimize TCS height C-8

Fig. C.4 Volume fraction (Y) of external RCHTS vs external design temperature for different internal RCHTS volume fractions C-11

Fig. C.5 Density for CO_2 at various pressures near the critical temperature (304 K) C-14

Fig. C.6 Pressure vs external RCHTS voluem fraction (Y) at various operating temperatures C-15

LIST OF TABLES

Table 2.1 MHTGR design parameters 2-3

Table 2.2 Design requirements for RCCS 2-4

Table 3.1 Physical properties of several fluids near their respective critical points 3-11

Table 3.2 Design parameters for representative TIPACS with internal heat exchanger—Option A 3-14

Table 4.1 Differences between Option A and Option B 4-19

Table A.1 Critical properties A-4

Table B.1 Carbon dioxide liquid and saturation line properties B-5

ACRONYMS AND ABBREVIATIONS

DOE	U.S. Department of Energy
HTGR	high-temperature gas-cooled reactor
MHTGR	modular high-temperature gas-cooled reactor
NTU	number of transfer units
RCCS	reactor cavity cooling system
RCHTS	reactor-cavity heat-transfer system
TCS	temperature-control system
TIPACS	temperature-initiated passive cooling system

VARIABLES

A	=	area (m^2)
C	=	isobaric specific heat (J/kg-K)
D	=	hydraulic diameter (m)
f	=	Moody friction factor
g	=	acceleration of gravity (9.8 m/s^2)
h	=	heat-transfer coefficient (W/m^2K)
h_h	=	height from liquid in expansion reservoir to crossover piping to exterior
h_m	=	minimum height of RCHTS
h_p	=	height of piping above expansion reservoir
h_s	=	static height difference between hot and cold fluid
h_T	=	height of hot-cold transition zone
k	=	thermal conductivity (W/m-K)
L	=	flow length (m)
$\dot{m}$	=	mass flow rate (kg/s)
P	=	pressure (bar)
Q	=	heat load (W)
q	=	heat flux (W/m^2)
R	=	radius (m)
$\Re$	=	ideal gas constant for air (287 J/kg-K)
T	=	temperature (°C)
T_c	=	temperature of critical point of working fluid
T_E	=	temperature of external heat exchangers at lowest design conditions
T_o	=	temperature of initial operation
X	=	fractional height of cold liquid in external zones to total TIPACS height
Y	=	relative volume
Z	=	fractional fluid volume of external heat exchanger

VARIABLES
(continued)

Greek

β	=	isobaric thermal expansion coefficient $-\frac{1}{\rho}\left(\frac{\partial \rho}{\partial T}\right)_p$
ϵ	=	surface emissivity
$\Delta\rho$	=	change in fluid density
ρ	=	density (kg/m^3)
ρ_{L,T_E,P_o}	=	the density of gas at temperature T_E and pressure P_o
ρ_{L,T_o,P_o}	=	the density of liquid at temperature T_o and pressure P_o
ρ_{L,T_E,P_E}	=	the density of liquid at coldest temperature T_E and corresponding pressure for saturated system at P_E
ρ_{G,T_E,P_E}	=	the density of gas at coldest temperature T_E and corresponding pressure for saturated system at P_E
ρ_{L,T_E,P_c}	=	the density of liquid at coldest temperature T_E and pressure of fluid at the critical point P_c
ρ_c	=	the density of fluid at the critical point
ρ_s	=	density of fluid on interior at temperature of initial operation
μ	=	dynamic viscosity (Pa-s)
σ	=	Stefan-Boltzmann constant (5.669×10^{-8} W/m^{2}K^4)

Subscripts

wall	=	wall conditions
b	=	bulk
varp	=	variable properties

VARIABLES
(continued)

Dimensionless groups

Gr	=	Grashof number $[\rho^2\beta(T_w - T_b)D^3/\mu^2]$
Nu	=	Nusselt number (hD/k)
Pr	=	Prandtl number $(\mu C/k)$
Re	=	Reynolds number

$$\bar{C} = \frac{\int_{T_b}^{T_w} C\,dt}{T_w - T_b} \qquad \bar{\rho} = \frac{\int_{T_b}^{T_w} \rho\,dt}{T_w - T_b} \qquad \bar{Gr} = \frac{\rho_b(\rho_b - \bar{\rho})gD^3}{\mu_b^2} \qquad \bar{Pr}_b = \frac{\bar{C}\mu_b}{k_b}$$

EXECUTIVE SUMMARY

Use of a Temperature Initiated Passive Cooling System (TIPACS) for the Modular High-Temperature Gas-Cooled Reactor Cavity Cooling System (RCCS)

C. W. Forsberg, J. Conklin, and W. J. Reich

The Temperature-Initiated Passive Cooling System (TIPACS) is a recently invented passive cooling system. Its use and performance were evaluated for cooling the below-grade reactor cavity of a modular high-temperature gas-cooled reactor (MHTGR). This cavity is one element of the MHTGR's containment/confinement system. The analysis considered reactor cavity cooling for MHTGR reactor vessels with surface temperatures from 220 to 450°C. This corresponds to MHTGR designs with steam and gas turbine power cycles.

TIPACS consists of two subsystems: a reactor-cavity heat-transfer system (RCHTS) and a temperature-control system (TCS). The RCHTS is a single-phase, natural-circulation system that uses carbon dioxide (CO_2) above its vapor-liquid critical point (T >31°C; P >72.85 atm) as the heat-transfer fluid. The vapor-liquid critical point is the state beyond which the difference between the vapor phase and the liquid phase no longer exists and only a supercritical phase remains.

Heat generated by losses from the reactor vessel heats the CO_2 in the reactor-cavity heat exchanger. The warm, lower-density CO_2 flows upward to a natural-circulation, air-cooled external heat exchanger. The CO_2 is cooled as it dumps its heat to the atmosphere; and the cooler, higher-density CO_2 flows downward back to the reactor-cavity heat exchanger. The performance of this natural-circulation heat-transfer system is high compared to other such systems because of the transport and physical properties of CO_2 near the critical point.

The TCS is a passive device that blocks the flow of CO_2 if the interior containment temperature drops below the vapor-liquid critical temperature of CO_2. The control mechanism is driven only by the change of fluid properties near the critical point (i.e., there are no active components). This feature of the TCS avoids overcooling of the reactor cavity under cold-weather conditions.

TIPACS has several potential advantages over existing systems. It is a passive system with no moving parts. The equipment space requirements near the reactor vessel are significantly smaller than those of currently proposed systems. It operates only above a preset temperature, thus avoiding potential overcooling of the reactor cavity during cold-weather reactor shutdown. It provides several advantages in the event of a beyond-design accident. Decay heat from the reactor can be transported to the ground in the case of TIPACS failure. TIPACS, when inoperable, does not create a major thermal barrier between pressure vessel and reactor cavity wall. It consists of robust components arranged in a closed loop; this allows the design of containments with higher resistance to external severe events (assault, etc.) than those of the current reference design. It also allows the option of a sealed containment system. The results of the analysis indicate that the performance of TIPACS exceeds the current concepts for cooling for both normal and accident conditions.

There is one major disadvantage: TIPACS is a new concept that has not been demonstrated. This implies significant uncertainties that can be reduced only by proof-of-principle experiments, detailed models of performance, and economic engineering analysis.

1. INTRODUCTION

A new type of passive cooling system has been invented (Forsberg 1993): the Temperature-Initiated Passive Cooling System (TIPACS). The characteristics of the TIPACS potentially match requirements for an improved reactor-cavity-cooling system (RCCS) for the modular high-temperature gas-cooled reactor (MHTGR). This report is an initial evaluation of the TIPACS for the MHTGR with a Rankine (steam) power conversion cycle. Limited evaluations were made of applying the TIPACS to MHTGRs with reactor pressure vessel temperatures up to 450°C. These temperatures may occur in designs of Brayton cycle (gas turbine) and process heat MHTGRs.

The report is structured as follows. Section 2 describes the containment cooling issues associated with the MHTGR and the requirements for such a cooling system. Section 3 describes TIPACS in nonmathematical terms. Section 4 describes TIPACS's heat-removal capabilities. Section 5 analyzes the operation of the temperature-control mechanism that determines under what conditions the TIPACS rejects heat to the environment. Section 6 addresses other design and operational issues. Section 7 identifies uncertainties, and Section 8 provides conclusions. The appendixes provide the detailed data and models used in the analysis.

2. DESCRIPTION OF PROBLEM AND TIPACS REQUIREMENTS

2.1 CHARACTERISTICS OF MHTGR

The MHTGR is an advanced power reactor (Fig. 2.1; Table 2.1) that has been under development by the U.S. Department of Energy (DOE) and its contractors for several years. The conceptual design of this reactor emphasizes the attainment of safety goals that are more stringent than those currently required by the industry and regulators and requires that these goals be met with passive systems relying solely on the inherent physical characteristics of the system. The vital features of the MHTGR design, with respect to this passive safety goal, are the following:

- Ceramic fuel and core components that are able to withstand very high temperatures with minimal release of fission products. For example, the ceramic fuel itself is able to retain most fission products at 1600°C for hundreds of hours during the most severe accident events.

- A strongly negative core reactivity temperature coefficient under all conditions. This limits maximum power levels to those the reactor core can withstand.

- Slow transient temperature response to abnormal events resulting from low power density and large thermal mass of the core system.

- Provision of a completely passive cooling system to remove that part of the decay heat which eventually reaches the outer surface of the reactor pressure vessel and which then passes by conduction, convection, and radiation into the below-grade concrete structure known as the reactor cavity.

- Provision of a reactor containment/confinement system which further reduces the release of fission products to the atmosphere in the event of leakage of contaminated helium primary coolant. The passively cooled reactor cavity is an important element of that containment approach.

As a result of the combined effects of the previously described features, safety analysis has shown that the maximum temperatures reached during any of the predicted transient events are well within the capabilities of the various materials used. Consequently, fission product releases, even for the most severe events, are low enough such that dose limits at a comparatively close-in site boundary are met.

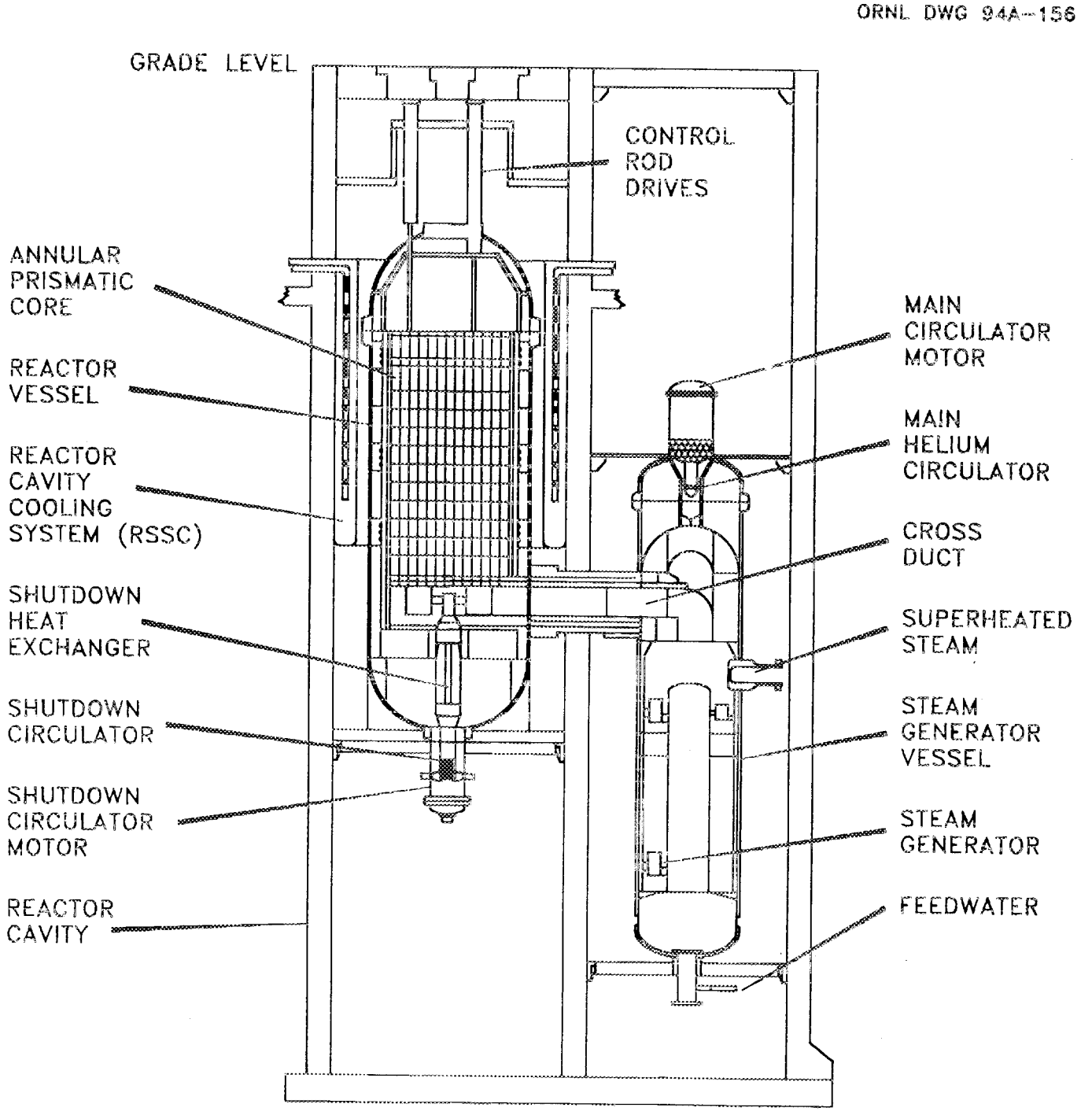

Fig. 2.1. Schematic of steam-cycle MHTGR.

Table 2.1. MHTGR design parameters

Thermal power	450 MW(t)
Electrical power	170 MW(e)
Pressure-vessel height	17.4 m
Pressure-vessel diameter	8.0 m
Reactor-cavity diameter	10.2 m
Calculated design decay-heat removal rate at nominal conditions	3.2 MW(t)

2.2 RCCS: CURRENT DESIGN REQUIREMENTS

In the current reference design, the function of removing heat from the reactor cavity is met by the RCCS. TIPACS is an alternative to the existing RCCS design. The RCCS is required for operations, investment protection, and safety. During normal full-power operation, the return legs of the primary reactor coolant flow path are at a temperature of 288°C; therefore, the reactor and steam generator vessels are also at or near this temperature. Similarly, during the worst cases (i.e., abnormal events in which power to circulate the primary coolant has been lost), the reactor vessel may reach 450°C. The reactor cavity containing the reactor vessel must be continuously cooled.

- Operation requires the cavity to be cooled to limit cavity temperatures below those that would damage other equipment in the reactor cavity and the concrete structure of the reactor cavity. The concrete wall of the reactor cavity has a continuous design temperature limit of 66°C. By placing either the current RCCS or the proposed TIPACS between the reactor vessel and these concrete walls and operating them at sufficiently low temperatures, the concrete may be kept within its acceptable temperature range.

- Safety has similar requirements. If reactor-cavity temperature is limited, the reactor vessel wall temperature is limited (450°C), and the nuclear fuel can not heat up to a temperature where there is significant fuel failure with release of radioactivity from the fuel. This safety feature requires that the pressure vessel not be insulated in order to allow decay heat to move outside via the pressure vessel wall. This also implies a continuous heat loss from the reactor vessel during normal operations.

The required safety system properties of the RCCS include (1) control of reactor-cavity temperature, (2) passive operation—the system should not require any operator action to operate, nor have moving components that could fail, and (3) redundancy—the system should fail progressively so that a partial failure does not result in total loss of cooling capacity. Safety requirements are summarized in Table 2.2.

- Investment protection has similar requirements. Although the reactor system has other multiple heat removal systems (steam generators for power production and an auxiliary shutdown cooling system), a highly reliable RCCS is needed to ensure low economic risk to investors.

Table 2.2. Design requirements for RCCS

Operating condition	Frequency	Expected vessel (or cold-loop helium) temperature[a]	RCCS protecting
Normal: 25–100% power	Continuous	About 220° C	Cavity concrete
Normal: shutdown	Frequent	About 120° C	Cavity concrete
Abnormal: depressurized conduction cooldown	Infrequent design basis event ($10^{-4 \text{ to } -6}$/year)	About 425° C	Vessel, cavity concrete and fuel

[a] For purposes of RCCS thermal analysis, the reactor can be considered as a heated cylindrical vessel. The cold-loop helium temperature controls the reactor vessel interior wall temperature. The external wall temperature will vary depending on how cold is the exvessel environment.

In the current reference design, the function of removing heat from the reactor cavity is provided by a passive system of air ducts (Fig. 2.2). Cooling is provided by this system during all reactor operating states—both normal and abnormal. The system works by natural convectional flow of the air in the ducts by the reactor vessel and has no control system other than the inherent properties of height and temperature differences.

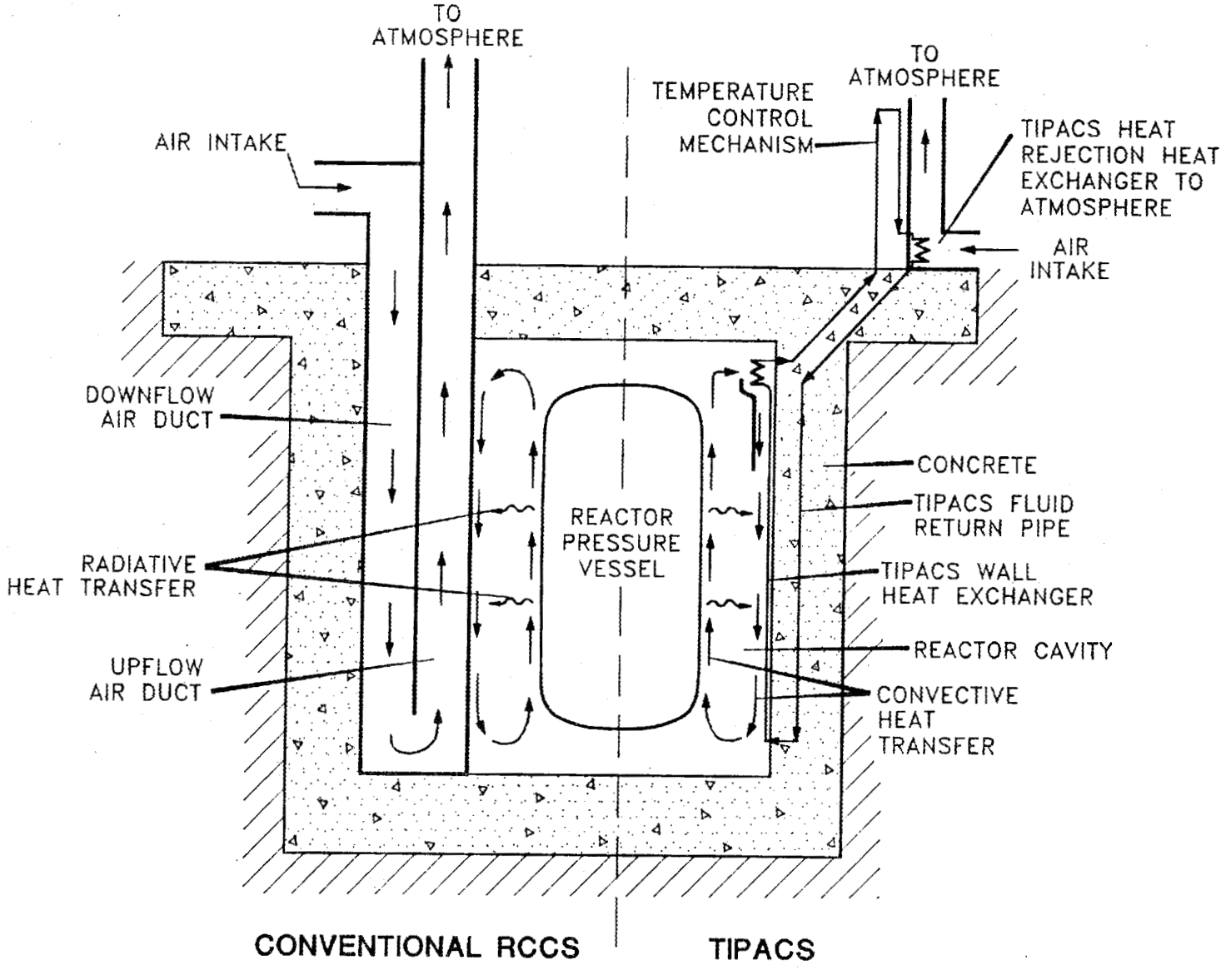

Fig. 2.2. MHTGR with conventional RCCS and TIPACS.

2.3 RCCS: ADDITIONAL DESIRABLE CHARACTERISTICS

In addition to meeting the previously described cooling functions, several added characteristics are desired for an advanced replacement RCCS.

- Fail safe. In the event of a total system failure, it is desirable to have alternative backup inherent safety cooling. With the MHTGR, decay heat can be conducted to the ground in an emergency—provided that the RCCS does not create a significant thermal insulative barrier between the reactor pressure vessel and containment wall. The use of this decay-heat-cooling option should protect the public against major releases of radioactivity, but the resultant higher temperatures may damage the power-producing capability of the reactor. This option is beyond the design basis and is not required of the current system, but it is highly desirable.

- Upgraded containment capability. The cooling system should allow for economic upgrade of reactor silo confinement capabilities, if desired. The National Academy of Sciences (NAS 1992) evaluations of the MHTGR have recommended strengthened containment for unknown or unexpected events. Such studies have recognized the safety features of the MHTGR, but these studies have also supported *strong sealed containment* as a matter of philosophy. The silo containment structure provides intrinsically very high protection of the reactor against external threats and protects the environment against internal accidents. Containment performance is currently limited by auxiliary systems such as the currently proposed RCCS—not the basic silo structure. Large air ducts are difficult to isolate if isolation is desired (isolation systems would destroy current RCCS passive system characteristics) and have limited strength in certain accident scenarios against high-containment building pressures due to the flat surfaces of the RCCSs.

- Improved Economics. The equipment volume for the RCCS system within and next to the reactor cavity should be minimized. By necessity, reactor control, reactor refueling, and primary heat-transfer equipment are near the reactor vessel, thus resulting in confined space. This makes this space very valuable both in terms of capital expense and operating costs if excessively crowded.

- Vented Containment. A pressure-resistant cavity-cooling system would allow the option for filtered and vented containment systems that require a minimum pressure to force gases through filter systems. This is a particularly desirable feature for certain accident sequences in which depressurization of the reactor occurs late in the accident sequence. The size of the filter required to meet this requirement is extremely sensitive to allowable pressure drop. An RCCS that does not limit maximum cavity pressure would greatly simplify design of such filter systems.

- Temperature control. During extended shutdown, avoiding freezing is required if the reactor is located in a cold climate. Any temporary barriers to operation of cooling systems during shutdown should be avoided since they do not result in passive cooling during maintenance or overhaul.

These requirements, system properties, and desired characteristics are the basis for the TIPACS design described herein. This design is a new concept (Forsberg 1993).

3. DESCRIPTION OF TIPACS

3.1 SYSTEM DESCRIPTION

TIPACS, as applied to an MHTGR, is a natural-circulation, single-phase, heat-transfer loop (Figs. 2.2 and 3.1). The proposed heat-transfer fluid is single-phase CO_2 above its critical pressure and temperature (P_c = 72.85 atm; T_c = 31.04°C). The heat exchanger inside the reactor cavity absorbs heat, thus heating the CO_2. The lower-density, hot CO_2 flows upward to an external, natural-circulation, air-cooled heat exchanger. The external heat exchanger cools the CO_2 fluid and dumps the heat into the atmosphere. The cooler, dense CO_2 flows downward to the reactor cavity heat exchanger. Any single MHTGR would have multiple TIPACS units; therefore, no single failure could stop reactor-cavity cooling. The high density of CO_2 (ρ_c = 0.468 g/cm^3), the thermodynamic properties of a fluid near its critical point, and the heat-transfer characteristics result in small equipment sizes compared to the current reference air-cooled RCCS.

TIPACS can be broken into two subsystems: a reactor-cavity heat-transfer system (RCHTS) and a temperature-control system (TCS). The RCHTS has two critical components: (1) the external heat exchangers to dump heat to the atmosphere and (2) the internal heat exchangers to adsorb heat in containment. The RCHTS removes heat from the reactor cavity and rejects it into the atmosphere via natural-circulation air-cooled heat exchangers. When the RCHTS operates, the TCS can be considered to be some unusually shaped piping above the two heat exchangers and connecting the two heat exchangers. The TCS is a control mechanism that allows the RCHTS to operate only above a preset temperature. Below this temperature, the TCS does not allow fluid flow between internal and external heat exchangers. The TCS operation depends upon the geometry of the piping above the heat exchangers and choice of fluid.

The choice of TIPACS heat-transfer fluid is based on multiple considerations. As is described in Sect. 3.3, the operation of the TCS within TIPACS depends upon the changes in fluid properties near the operating fluid critical point. The system begins full operation when a single-phase fluid exists above the fluid's critical temperature (T_c). For

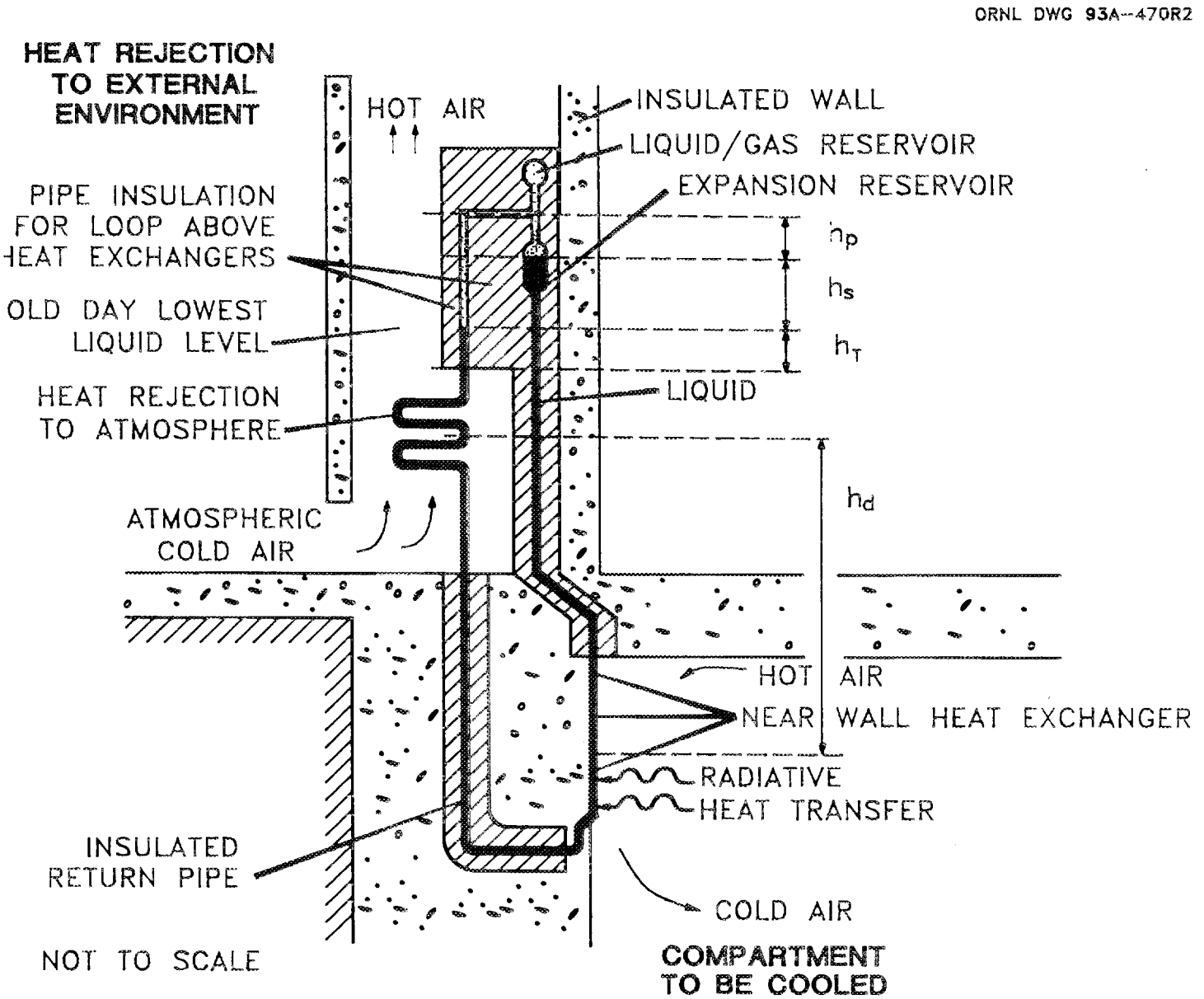

Fig. 3.1. TIPACS

this specific application, it is desired to initiate RCHTS operation between 10 and 40°C. This implies that the fluid must have a critical temperature in this range. Based on engineering considerations (Sect. 4.1), CO_2, with a critical temperature of 31°C, was chosen as the preferred heat-transfer fluid. The following description and figures show a conceptual design for a TIPACS as applied to the 450-MW(th) steam-cycle MHTGR.

3.2 RCHTS DESIGN

3.2.1 General Design

The RCHTS consists of two heat exchangers, the connecting piping, and the CO_2 heat-transfer fluid. The internal heat exchanger absorbs heat in the reactor cavity, while the external heat exchanger dumps the heat into the environment.

3.2.2 External Heat Exchanger

The external heat exchanger is a standard, air-cooled exchanger used for single-phase fluids. It has no unusual characteristics (Fig. 3.2); it consists of tubes with flowing single-phase CO_2 on the inside and natural circulation of air on the outside. The tubes have fins on the outside to improve heat transfer. Air circulation past the external heat exchanger is enhanced by a hot-air stack above the heat exchanger.

3.2.3 Internal Heat Exchanger—Option A

A custom-designed containment heat exchanger with several special design features removes heat from the reactor cavity and transfers it to the single-phase CO_2. There are several requirements for this heat exchanger. During normal operation, the heat exchanger must adsorb heat from the pressure vessel while it keeps concrete containment temperatures below 66°C. Peak internal-pressure vessel temperature during normal operation is ~290°C, with the vessel surface temperature of 220°C. The hot reactor vessel results in a large steady-state radiant heat flux to the concrete wall (~1.5 kW/m^2). To prevent excessive concrete temperatures, the heat exchanger must intercept this radiant heat. If an accident occurs, the radiant heat flux may further increase because

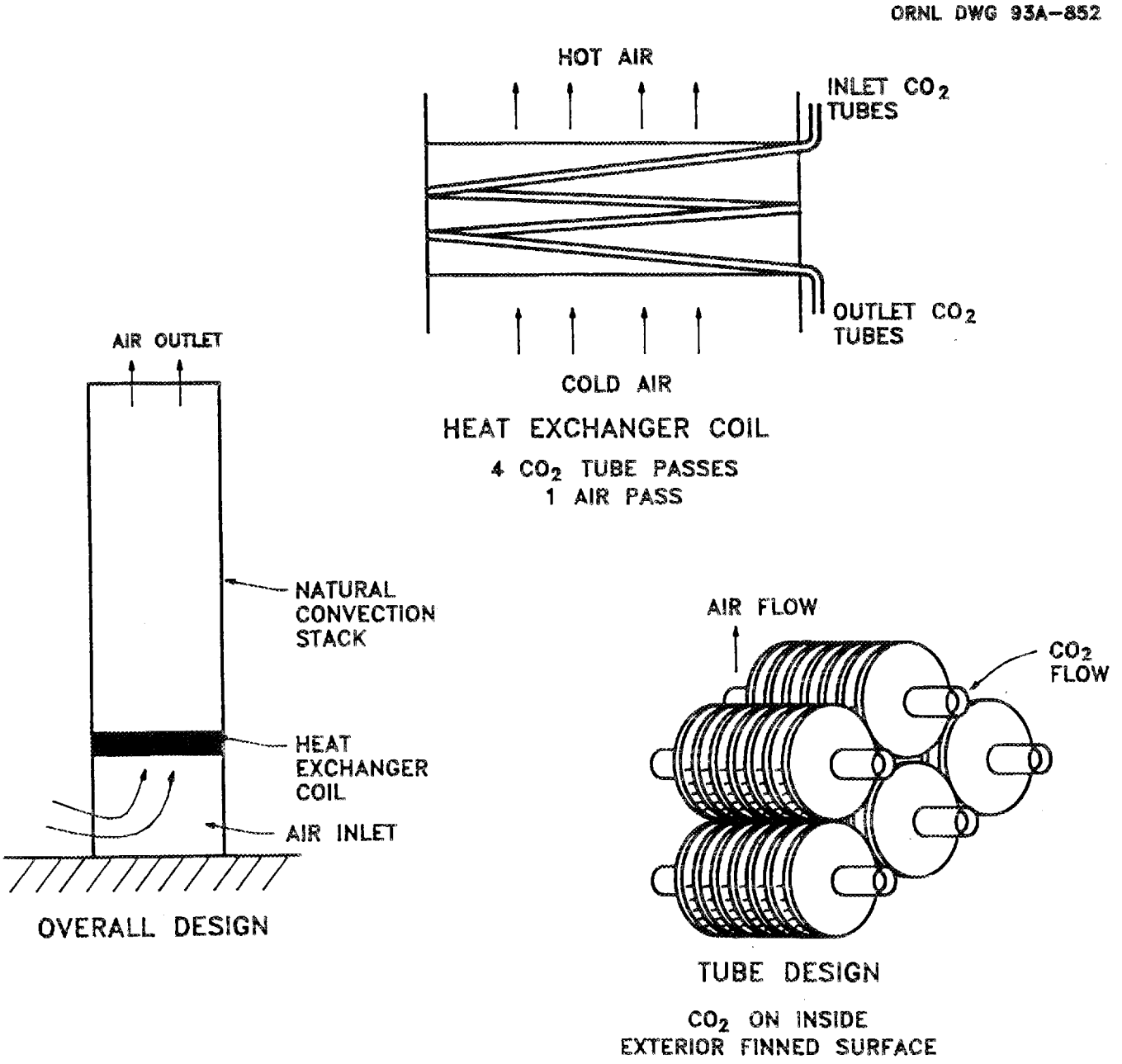

Fig. 3.2. External heat exchanger.

vessel temperatures will increase. Simultaneously, if the TIPACS fails, the radiant heat must transfer directly to concrete with little heat flow resistance from the TIPACS. This allows the heat to be transported to the soil.

There are two internal heat exchanger design options (Fig. 3.3). The choice of options depends upon the expected temperature of the reactor vessel and other design considerations. The proposed heat exchanger—Option A—is a wall of vertical steel pipes with steel plate added between the pipes. It is the mechanically simplest option. The single-phase, high-density CO_2 enters the bottom of the pipes, and single-phase, lower-density CO_2 exits the top. This mechanical design is essentially identical in design to boiler walls in packaged steam generators in the chemical process industry (Ganapathy 1993), and in large utility fossil-fuel plants. In these boilers, the outer boiler wall is both a heat exchanger to convert water to steam and the outer boiler wall. It is called membrane-wall construction. These tube walls have several characteristics:

- The tubes directly absorb radiant heat from the pressure vessel and convective cooling of the air. Most heat transfer (>80%) is by radiant heating during normal and off-normal conditions.

- The steel web between the pipes absorbs radiative and convective heat with the transfer of the heat by conduction through the steel to the nearest tube.

- In the event of TIPACS failure, heat is conducted through the steel tubes and webs and radiates to the concrete liner. Because the thermal conductivity of steel is more than a factor of 10 greater than concrete, the resistance of heat flow by the steel-heat-exchanger structure is very small. Heat conduction is rapid through the tube from the side facing the pressure vessel to the side facing the concrete.

3.2.4 Alternative Internal Heat Exchanger—Option B

For higher temperature operations (gas turbine or process-heat MHTGR) or lower reactor-cavity-wall temperatures, Option B is preferred. Internal heat exchanger—Option B is a double-wall heat exchanger in which there are two steel-tube-membrane walls between the pressure vessel and the reactor cavity (Fig.3.3). Cold CO_2 flows down the tubes next to the reactor cavity wall and then flows up the tubes near the

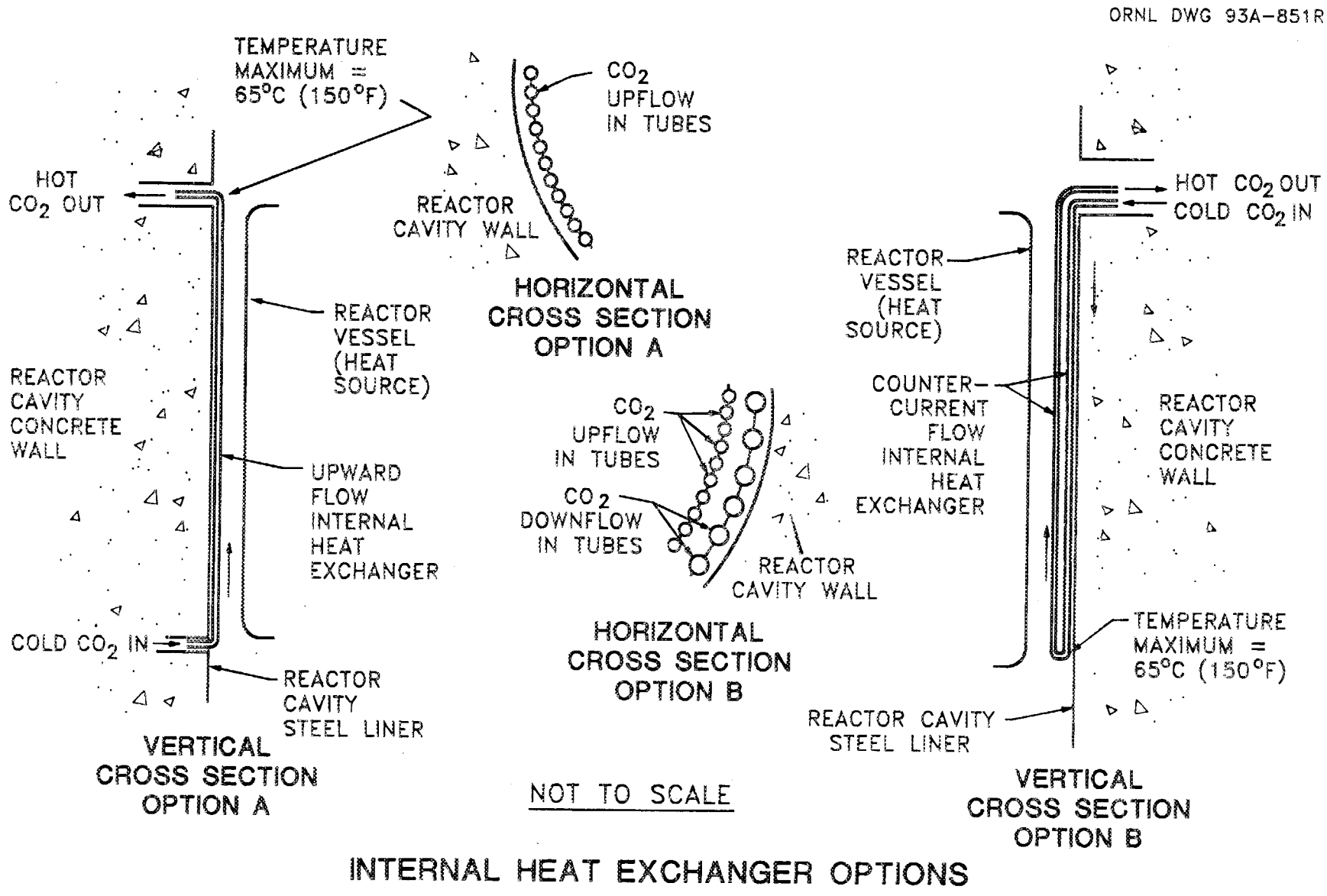

Fig. 3.3. Cross-section view of internal RCHTS heat-exchanger options.

pressure vessel to the external heat exchanger. The tube membrane wall next to the reactor cavity acts as a thermal shield to protect the reactor cavity wall from higher temperatures from the tube membrane wall next to the pressure vessel.

With Option A, the maximum allowable CO_2 temperature is limited by the maximum allowable reactor-cavity-concrete temperature (~66° C). With Option B, the design limit is that the CO_2 temperature at the bottom of the tube membrane wall next to the reactor cavity wall can not exceed 66° C—the maximum allowable reactor-cavity-concrete temperature. Exit temperatures from the tube membrane wall next to the reactor pressure vessel are not limited because the reactor cavity does not see such temperatures.

The two options have very different mechanical designs and very different performance limits, but they have similar thermal and CO_2 flow characteristics. This implies that the results of analysis of one option provide a good estimate of the performance of the other option. The heat-transfer characteristics of Option B result in little heat being adsorbed by the downward flow of CO_2 in the membrane wall while cold reactor cavity wall temperatures are maintained. The downward flowing CO_2 is almost like the downward CO_2 flowing into the insulated pipe as occur in Option A. The reason for this is that reactor-cavity heat transfer between surfaces is controlled by radiation cooling (Fig 3.4). The rate of heat transfer between any two surfaces in the system is proportional to the differences in the temperatures of the two surfaces to the forth power; that is,

$$q = C * [(T2)^4 - (T1)^4] \quad . \qquad \text{Eq. (3.1)}$$

With this type of heat transfer, small increases in the temperature differences between two surfaces imply large increases in the rate of heat transfer.

Option B can be considered as four walls, as shown in Fig. 3.4. Each wall is at a constant temperature. The first wall is the pressure vessel wall, the second wall is the tube membrane wall with upward flowing CO_2, the third wall is the tube membrane wall with downward flowing CO_2, and the forth wall is the reactor-cavity wall. If a design criterion is that the concrete wall cannot exceed 66° C, the tube wall with downward flowing CO_2 cannot exceed 66° C—the same limit as the maximum CO_2 temperature for Option A.

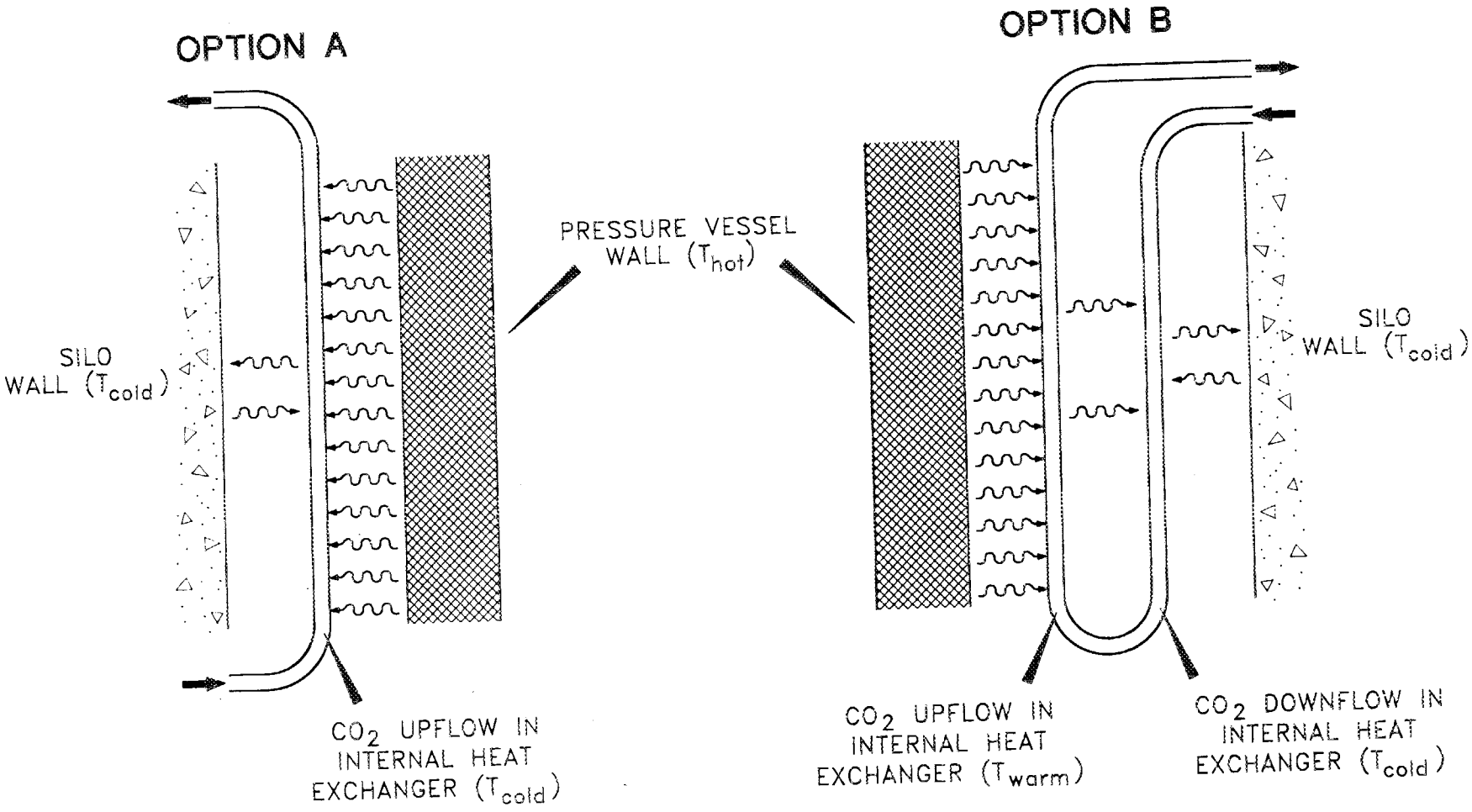

Fig. 3.4. Radiative heat-transfer models of internal heat exchanger.

With this model, the relative heat transfer between various surfaces can be calculated. Figure 3.5 shows the relative heat transfer between two surfaces as a function of the temperature of the hotter surface for two different cold temperature surfaces. Consider a reactor vessel surface temperature of 450° C with an average CO_2 upflow temperature of 100° C that reradiates heat to the wall with downflowing CO_2 at a wall temperature of 50° C. In relative units, the rate of heat transfer between the 450° C wall and the 100° C wall is 2.54 vs 0.08 between the 100° C wall and the 50° C wall. The heat flow to the downward flowing section of the internal heat exchanger is only 3.3% of that to the upflow section. In effect, the downward flow section sees almost no heat flux. This is an intrinsic characteristic of this type of heat-exchanger design.

3.3 TCS

The temperature control capabilities of TIPACS depend upon the two aforementioned heat exchangers and two other passive components. These are shown in Fig. 3.1.

The first component for temperature control is the heat-transfer fluid. It is the special characteristics of the fluid that make the TIPACS feasible. Given that the TIPACS is to operate above a specified temperature, a fluid is chosen whose vapor-liquid critical point matches the temperature above which the TIPACS is to operate. The vapor-liquid critical point is the state beyond which the differences between the vapor phase and the liquid phase no longer exist and only a supercritical fluid phase remains. All liquids, unless they decompose first, have a vapor-liquid critical point. The TIPACS depends on the changes in thermodynamic properties near the critical point. The thermodynamic properties of CO_2 and water are shown in Table 3.1. (Note the rapid changes in physical properties near the critical point.)

Consider now a natural-circulation heat-transfer loop partially filled with a pure compound, such as CO_2, below the critical point, as shown in Fig. 3.1. Carbon dioxide is an example of a fluid that would be used if the enclosure temperature is to remain near room temperature. Liquid CO_2 would fill the bottom of the loop, and gaseous CO_2 would fill the top. The liquid CO_2 in the warm zone would be warmer than the CO_2 outside in

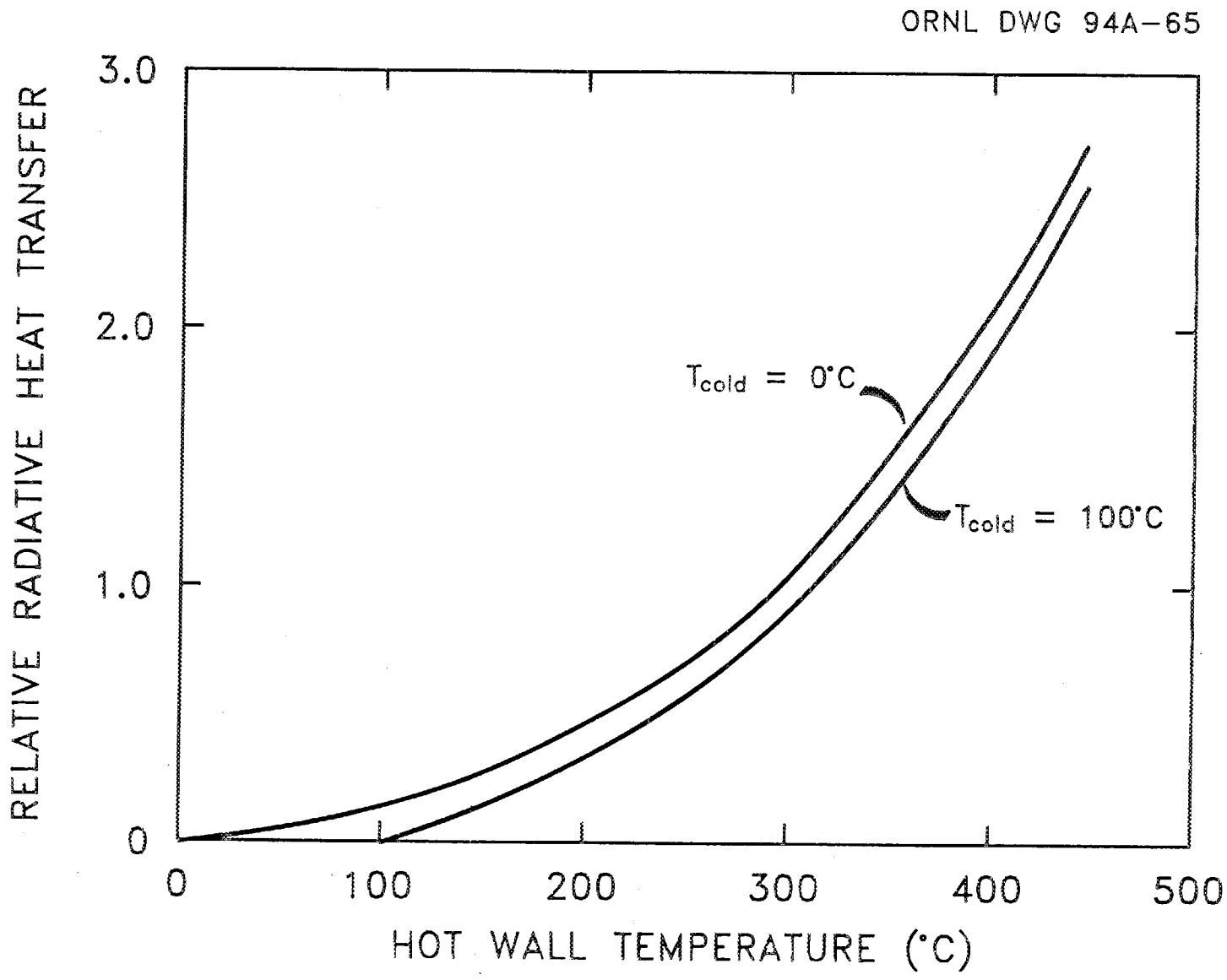

Fig. 3.5. Relative radiative heat transfer vs hot-wall temperature.

Table 3.1. Physical properties of several fluids near their respective critical points (critical point data in bold)

Fluid	Temperature (°C)	Pressure (kPa)	Density (kg/m^3) Liquid	Density (kg/m^3) Gas
Carbon dioxide	0	3,467	929	97
	5	3,939	898	114
	10	4,480	863	134
	15	5,062	823	159
	20	5,702	776	191
	25	6,404	714	238
	30	7,180	601	335
	31.1	**7,384**	**468**	**468**
Water	300	8,600	712	46
	320	11,300	667	65
	340	14,600	611	93
	360	18,700	528	114
	374.14	**22,100**	**317**	**317**

the colder environment and have lower density. The differences in densities would result in differences in elevation—delta height static (h_s) of the fluid in the piping to ensure hydrostatic balance.

The CO_2 critical point (T_c) is 31.04°C (87.8°F). As the reactor cavity temperature rises toward 31.04°C, the specific volume of liquid CO_2 increases rapidly. The expanding volume of liquid CO_2 would quickly raise the level by h_p. Once the liquid CO_2 has reached the level of the piping to the outside exchanger, it would flow to the outside heat exchanger, and the circulation of liquid CO_2 would remove heat from the warm zone to the external environment. When the temperature exceeds 31.04°C—the critical point—the liquid and gaseous forms of CO_2 become a single phase that ensures steady operation of the heat-transfer loop. In practice, these two sequential phenomena occur over such a small temperature range such as to be almost simultaneous events in most real systems—with the observer noting that a two-phase system has become a one-phase system. The very rapid changes in physical properties near the critical point make the device function and activate it over a very small temperature range.

The second key component is the pipe loop extending above both heat exchangers in the natural-circulation heat-transfer loop. This pipe loop (1) is where the liquid-gas interface zones are designed to be at temperatures below the critical point and (2) must be well insulated. This loop is required to prevent heat transfer from the warm inside zone to the colder outside zone when the inside temperature is much below T_c. Consider what would happen if the liquid-gas interface were not in this zone or if the piping were not insulated. In such a case, using the example of CO_2, liquid CO_2 would evaporate (removing heat) in the warm zone; condense in the colder gas-phase zone; and release heat to the cool, outside zone. In effect, a two-phase, natural-circulation heat-transfer loop would begin to operate.

With the pipe loop insulated, hot vapor from the warm zone will heat the vapor space uniformly. Warm liquid CO_2 will condense on internal pipe surfaces above the heat exchanger which is colder and rejects heat to the environment. The liquid temperatures at the gas-liquid interface in the insulated pipe on the outside will match the liquid temperature inside the warm zone. This warm CO_2 with its lower density floats on the

colder liquid CO_2 above the outside heat exchanger. Heat transfer, when TIPACS is not in operation, will be limited to heat loses through the insulation and conduction from warm-to-cold liquid CO_2 in the loop outside over elevation h_T.

TIPACS has the option of including an optional liquid-gas reservoir (Fig. 3.1) at the top of the TCS. This allows liquid expansion to start TIPACS operation before the critical temperature is reached. The performance of this liquid RCHTS is expected to be significantly less than that of the system (see Sect. 5.2) after the critical pressure and temperature have been exceeded.

There are several design considerations in building practical systems.

- The normal liquid-level fluctuations when the TIPACS is not operating must be in the insulated pipe zone at some significant distance (h_i) between the bottom of the insulated zone and the liquid level. (Note that liquid levels will fluctuate depending upon temperatures of the fluid.)

- For practical systems, most of the TIPACS volume should be in the interior warm zone. The fluid is the temperature sensor. Fluid expansion depends upon the amount of warm fluid. Suficient fluid in the warm zone may be easily accomplished by a liquid reservoir above the heat exchanger in the warm zone with fluid temperatures near the temperatures of the warm zone. The precise relative fluid volumes in the cold, hot, and insulated zones are chosen to ensure that gas-liquid interfaces remain in the insulated zones over expected warm- and cold-zone temperature variations below T_c.

3.4 TIPACS DESIGN APPLIED TO MHTGR

Table 3.2 lists the design parameters for a representative TIPACS for the 450-MW(t) steam-cycle MHTGR.

Table 3.2. Design parameters for representative TIPACS with internal heat exchanger—Option A

General design parameters	
Number of TIPACS per reactor	4
Heat duty (nominal - 4 units)	800 kW
Minimum external air temperature	-40°C
Maximum external air temperature	35°C
TIPACS startup temperature	17°C
TIPACS full-operating temperature	31°C
Maximum operating pressure	150 bar
System physical dimensions	
Height	
Internal heat exchanger	17.4 m
Top of internal heat exchanger to ground level	4.5 m
External heat exchanger above ground level	5.0 m
External heat exchanger	1.0 m
Air duct above external heat exchanger	24.0 m
Totals	52.0 m
Reactor cavity diameter	10.2 m
Reactor cavity circumference	32.0 m
Reactor cavity circumference covered by a single TIPACS system	8.0 m
External CO_2 pipe diameter	0.5 m
TCS Dimension Ratios	
Fractional height of RCHTS	0.65
Fractional height of TCS	0.35
Internal volume fraction of internal heat exchanger with piping	0.315
Internal volume fraction of external heat exchanger with piping	0.200
Internal volume fraction of TCS	0.485

Table 3.2. Design parameters for representative TIPACS with internal heat exchanger—Option A (continued)

Internal heat exchanger—Option A	
Type	Vertical pipe
Height	17.4 m
Diameter (nominal)	2 in.
Size	Schedule 80
Number	163
Cavity circumference covered	8.0 m
Nominal radiation heat flux	1.5 kW/m^2
External heat exchanger	
Duty	200 kW
Type	Air-cooled multipass cross counterflow
Design	
Air passes	1
Co_2 passes	4
Dimensions	
Height	1 m
Width	8 m
Length	4 m
Pipe size	2 in.
Pipe thickness	Schedule 80
Pipe length (4 passes)	16 m
Number of parallel pipes	321
Fin pitch	346 m
Fin height	18 mm

Table 3.2. Design parameters for representative TIPACS with internal heat exchanger—Option A (continued)

Operational parameters	
Maximum CO_2 temperature	66° C
Internal pressure-vessel wall temperature	290° C
External pressure-vessel wall temperature	220° C
Temperature (hot day)	
Inlet air temperature	35.0° C
Outlet air temperature	54.6° C
Inlet CO_2 temperature	46.1° C
Outlet CO_2 temperature	55.8° C
Mass flow rate	
Air flow rate	9.27 kg/s
CO_2 flow rate	6.0 kg/s
CO_2 system pressure drop, $\Delta p / p$	0.0091

4. REACTOR CAVITY HEAT TRANSFER SYSTEM

TIPACS has a set of characteristics that define its performance. This results in performance characteristics fundamentally different from those of other systems.

4.1 CHOICE OF FLUID

For this application, CO_2 is the fluid of choice because of several of its characteristics:

- Its critical temperature (T_c) is 31.04°C (87.8°F), which is close to the optimum temperature (above freezing, good working conditions).
- It will not freeze in cold weather [freeze point is -56.6°C (-70°F)].
- It is nontoxic.
- It is inexpensive.
- In its dry state, it is noncorrosive.
- Neutron activation of it is insignificant.
- There is a very large industrial experience-base. It is used to make dry ice and in carbonated beverages. Before the development of chloroflurocarbons, it was widely used as a refrigerant. Its physical heat-transfer and pumping characteristics are well known, and there are multiple suppliers of equipment for handling it. British Magox power reactors use it as a coolant; thus, there is a large experience base in its nuclear applications.

However, there is one disadvantage of CO_2. It has a relatively high critical pressure (~73 bar). Many fluids are available with critical pressures half that of CO_2—but these have other disadvantages, such as flammability.

4.2 HIGH PERFORMANCE FOR NATURAL-CIRCULATION RCHTS

For most fluids in a natural-circulation RCHTS, performance is maximized when (a) the fluid pressure is just above the fluid's critical pressure and (b) the operating temperature-range from hot-to-cold fluid is just above the fluid's critical temperature. This phenomenon is a direct result of the thermodynamic and transport properties of fluids

near their critical points. The TIPACS's TCS requires operating in this region to ensure the initiation of the TIPACS at a preset temperature, but coincidentally because of the very desirable physical properties of fluids, it implies excellent RCHTS performance. In the last several years, because of the very desirable physical properties of fluids near the critical point, there has been increased research (Oka 1993) on the operation of heat-transfer systems in this fluid region.

Four physical properties primarily determine the performance of a natural-circulation heat-transfer system: change in density of the fluid with temperature over its operating ranges, dynamic viscosity, specific heat capacity, and thermal conductivity. These four properties are shown for CO_2 near the critical point. More detailed tables are available in Appendix B.

For a natural-circulation heat-transfer system, large changes in fluid density over the operating range are desired. A high-density fluid should exit via the external heat exchanger, and a low-density fluid should exit via the internal (containment) heat exchanger. The difference in density creates the driving force for fluid transport. As shown in Fig. 4.1, these densities change rapidly near the critical point for CO_2. Figure 4.2 shows the corresponding thermal expansion coefficient.

The second desirable property for a heat-transfer fluid is low fluid viscosity, which will minimize resistance to fluid flow. Many generalized correlations (Green 1984) exist for liquids and gases. The general rule for liquids is that as the temperature goes up, the viscosity goes down. The general rule for gases is that as the temperature goes up, the viscosity goes up. This implies that the viscosity minimum for any fluid is near the critical point. Because generalized correlations are not accurate near the critical point, they can not be used for viscosity predictions, but the minimum measured viscosity is near the critical point. This viscosity effect for CO_2 is shown in Fig. 4.3.

The third desirable property for a natural-circulation RCHTS is high specific-heat capacity. The greater the specific-heat capacity, the more heat that can be removed per unit of fluid mass. For single-phase systems, this property is maximized near the critical

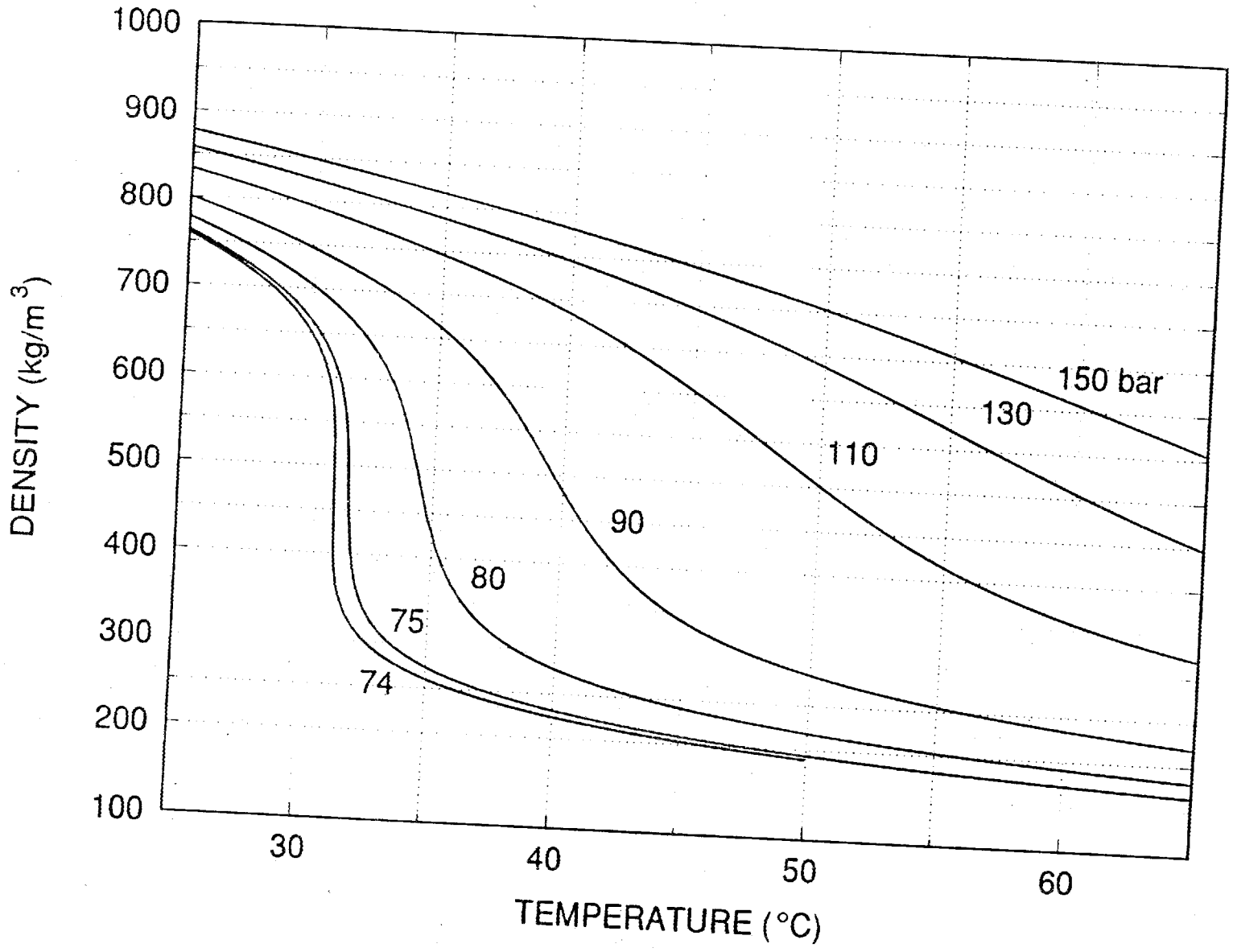

Fig. 4.1. Density of CO_2 vs temperature for different pressures above the critical point.

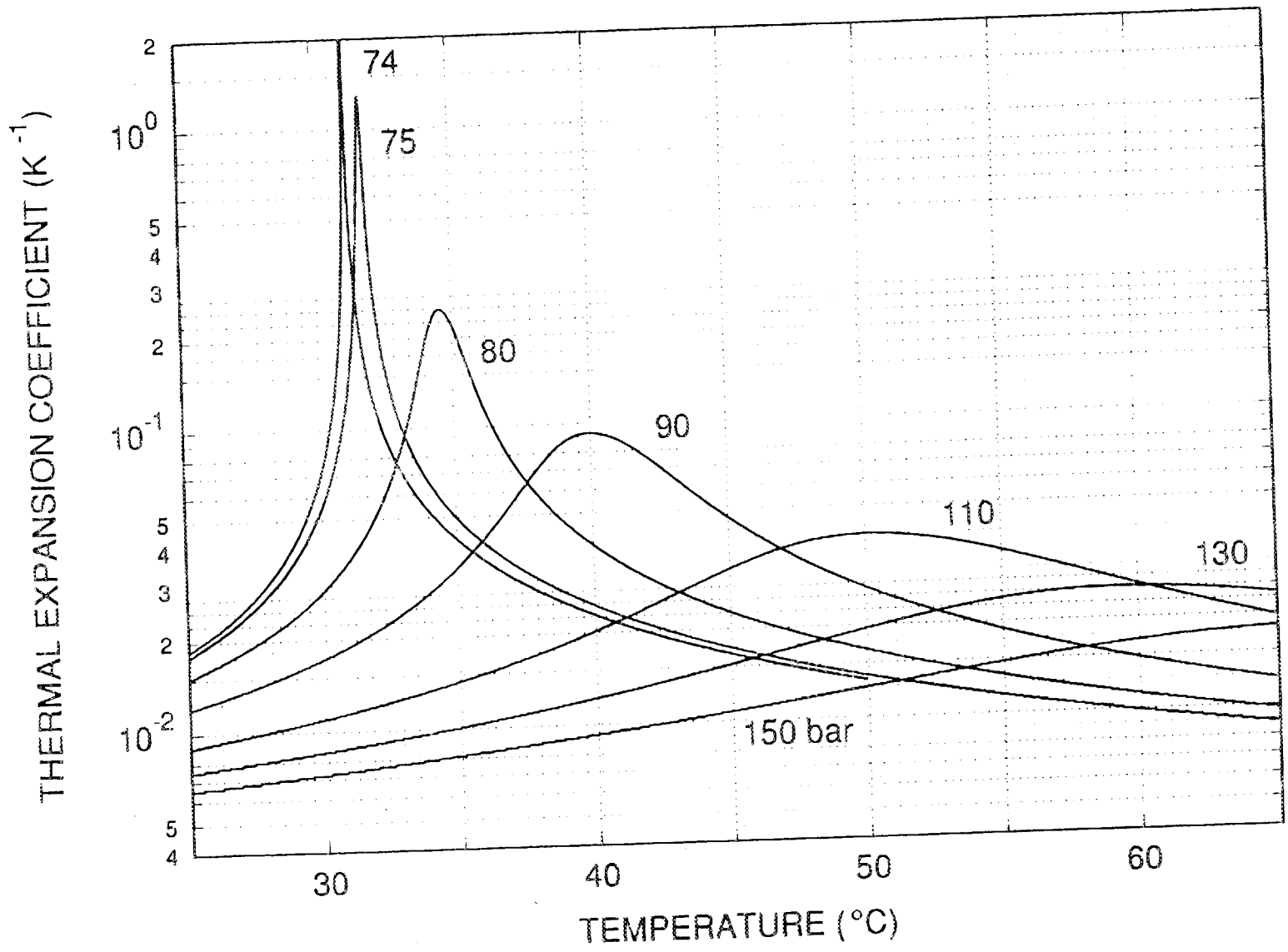

Fig. 4.2. Thermal expansion coefficient of carbon dioxide vs temperature for different pressures above the critical point.

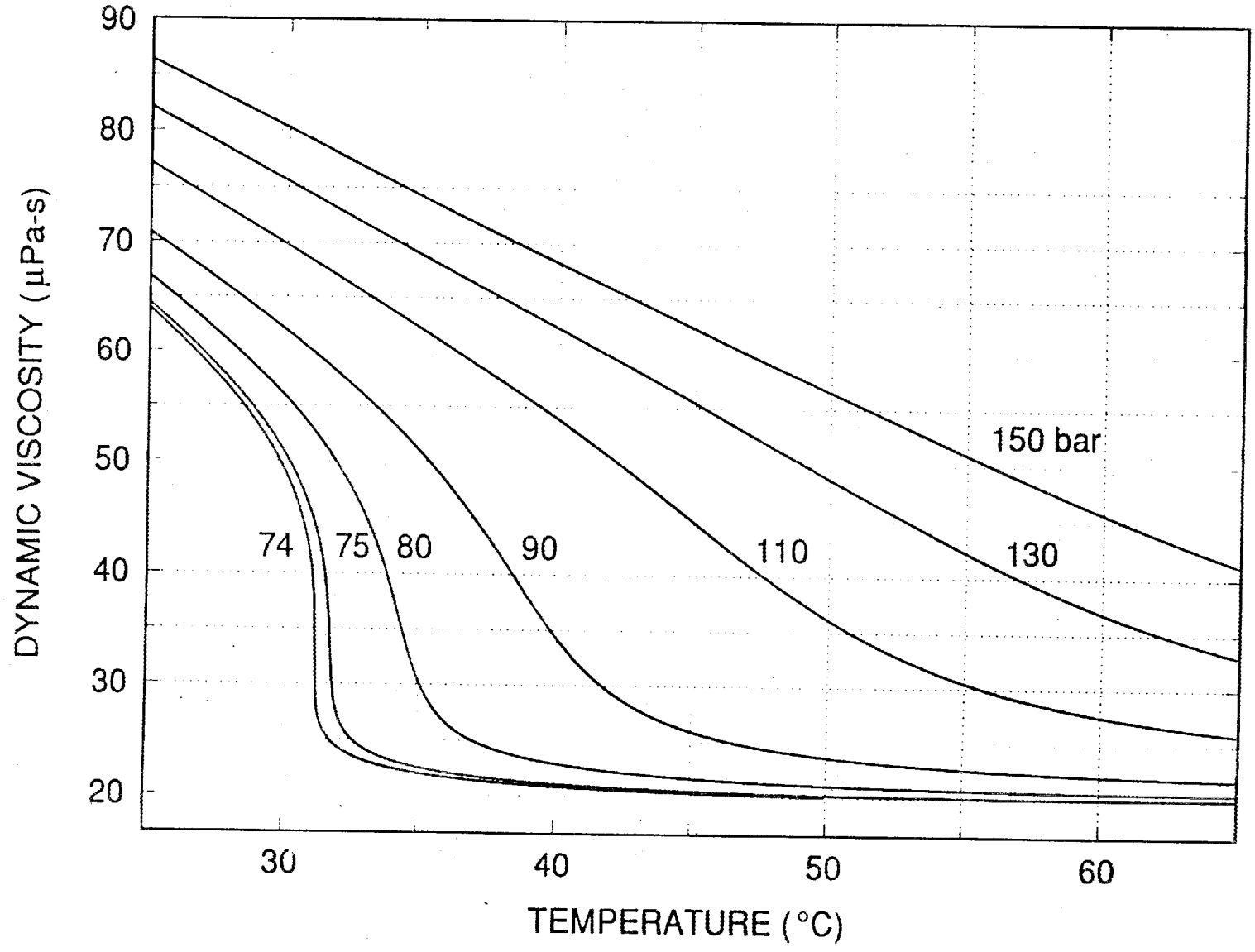

Fig. 4.3. Dynamic viscosity of CO_2 vs temperature for different pressures above the critical point.

point as shown for CO_2 in Fig. 4.4. It is also noted that as pressure increases with increasing temperature in TIPACS, the maximum specific heat increases with temperature. This reaction ensures good performance over an extended range.

The fourth desirable property for a natural-circulation RCHTS fluid is high thermal conductivity. This property is also maximized near the critical point (Fig. 4.5), but it decreases thereafter with temperature. For a TIPACS in a specific application with an MHTGR, this property is not a major concern because heat transfer is primarily controlled by air-side heat transfer in the containment silo and in the exterior heat exchanger.

4.3 STEADY-STATE THERMAL PERFORMANCE CHARACTERISTICS FOR TIPACS WITH INTERNAL HEAT-EXCHANGER DESIGN—OPTION A

A series of design studies were conducted to optimize RCHTS performance for different sets of conditions. The primary design constant was to maintain TIPACS's hottest temperatures below 66°C and, thus, maintain reactor cavity concrete below 66°C. The design methodology is described in Appendix D. The initial design studies evaluated different TIPACSs designs with internal heat exchanger—Option A. This option has a single set of tubes between the reactor vessel and the reactor cavity wall. CO_2 flows in the upward direction.

4.3.1 TIPACS Geometry Assumptions for Thermal-Flow Modeling

To begin analysis, appropriate component sizes and heights for the TIPACS components are assumed. The heights of certain components are fixed, at least by the current design of the MHTGR. These fixed heights are the internal heat exchanger of 17.4 m (matching pressure vessel height) and a concrete thickness above the reactor cavity of 4.5 m. The external heat exchanger was assumed to be 5 m above the ground with a total height of 9.5 m between the top of the internal heat exchanger and the bottom of the external air-cooled heat exchanger. Another fixed height for the thermal-flow performance calculations is the height of the CO_2 piping above the external heat exchanger; the height is determined by the requirements of the TCS to be 15 m (see

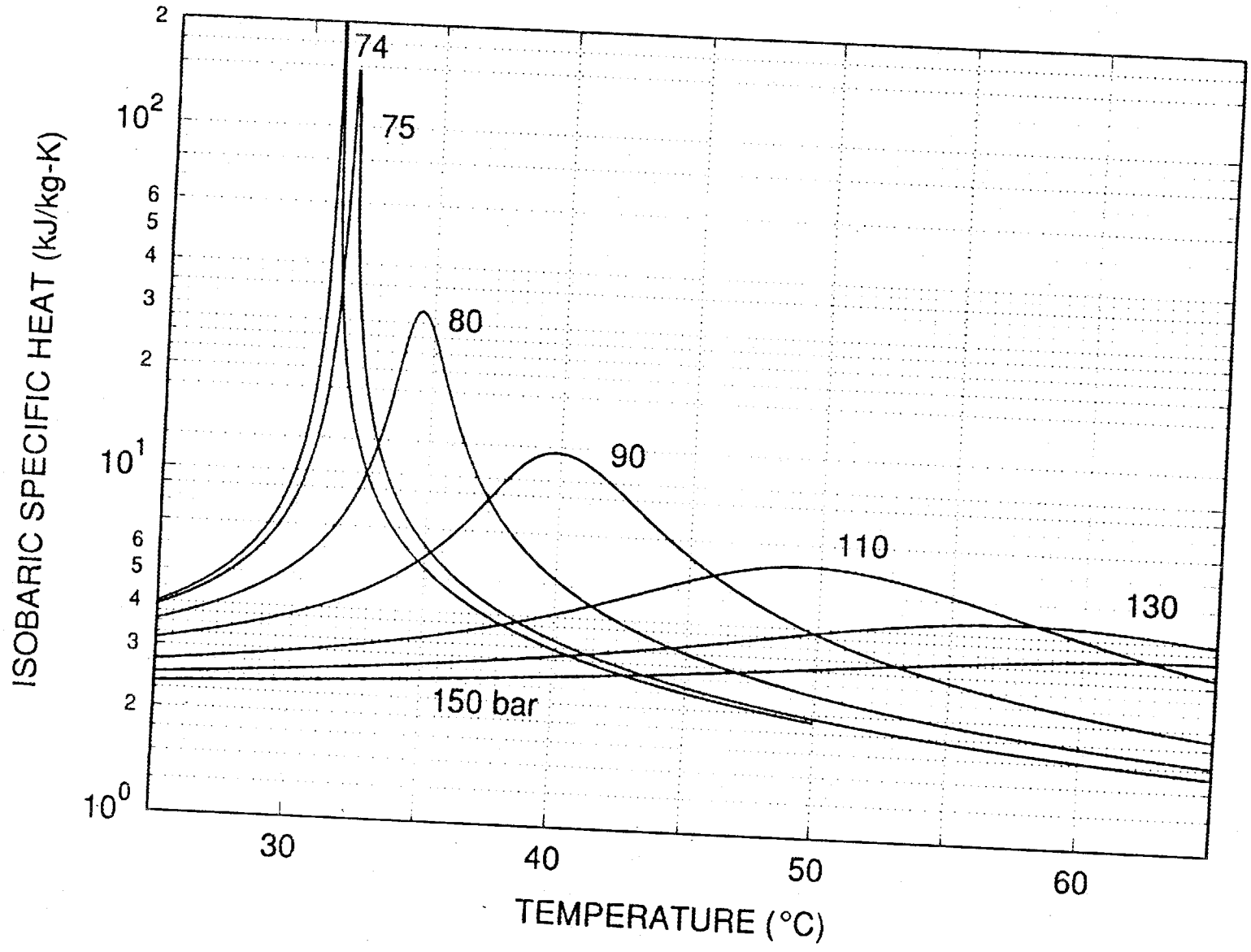

Fig. 4.4. Isobaric specific heat of CO_2 vs temperature for different pressures above the critical point.

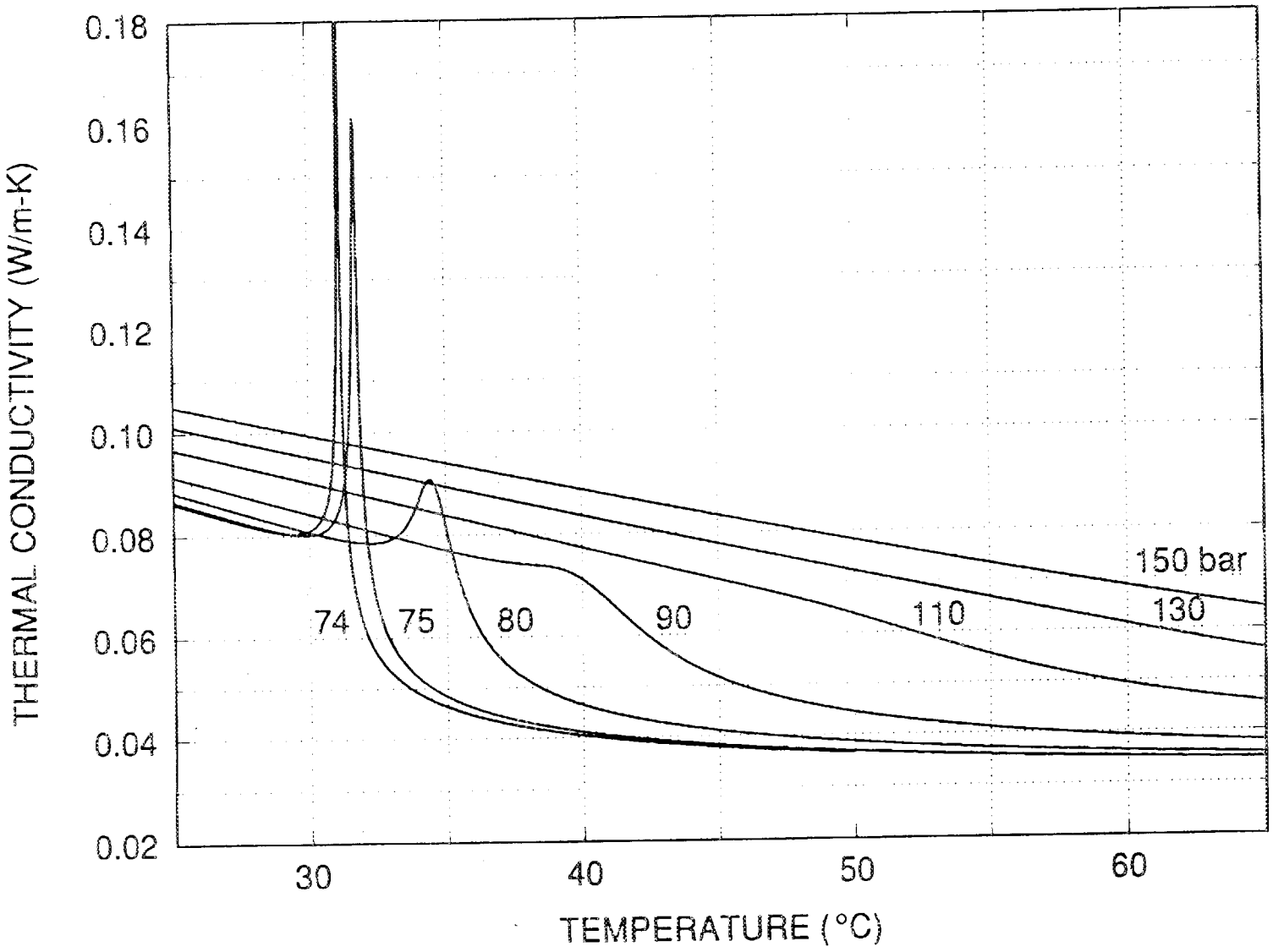

Fig. 4.5. Thermal conductivity of CO_2 vs temperature for different pressures above the critical point.

Sect. 5). The other components are sized appropriately to yield reasonable numbers for loop temperatures at a reasonable height. The mass and energy flows must be balanced.

As a result of initial scoping calculations, reasonable temperatures were calculated for a reactor cavity internal heat exchanger consisting of 2-in. vertical, schedule 80 tubes that touch each other at the outer annulus of the reactor cavity. For this initial model, the external air cooled heat exchanger is a multipass, cross-counterflow arrangement having air-side thermal and flow performance parameters [given in Fig. 10-90 of Kays and London (1984)] with 2-in., schedule 80 tubes for the CO_2 side having circular fins to enhance heat transfer to the air. The dimensions of the modeled external heat exchanger are 8 m wide, 4 m long, and 1 m high. The internal and external heat exchangers were connected by 0.5-m-diam pipes to close the CO_2 loop. The circular reactor cavity is cooled by four TIPACS units; each unit provides cooling for a quadrant of the reactor-cavity silo. The calculations herein are for *one* of these units. For an actual design, however, some interdependence may be necessary.

Calculated CO_2 temperatures are affected by the height of the external heat exchanger and the height of the air stack above the heat exchanger. As expected, the calculated loop temperatures decrease as these two heights are increased. The most significant parameter, however, is the diameter of the pipes in the internal and external heat exchangers because this dimension directly affects the frictional loop pressure drop. The number of parallel tubes in each heat exchanger can be varied to modify the pressure drop up to the maximum that can fit. The height of the external heat exchanger above the concrete ceiling of the reactor cavity (at grade level) is 5 m, and the height of the air stack is 25 m. These heights were based on a combination of practical considerations and results of scoping calculations. The air stack is 30 m above grade and only 5 m above the highest point of the CO_2 loop in the TCS above the external heat exchanger. Hence, the total change in elevation from the bottom of the internal heat exchanger to the top of the air stack is ~52 m. This change in elevation is reasonable for a nuclear reactor plant of this power rating.

4.3.2 Calculated Results and Discussion

For a given design, to calculate system performance, only two parameters need be set—the ambient air temperature and the reactor vessel temperature. For the total simulation of the MHTGR, the reactor vessel temperature is controlled primarily by the internal reactor flow and power conditions and will vary with respect to axial position and time during operation at transient and normal conditions. For these scoping studies, a uniform reactor vessel temperature of 220° C, which approximately corresponds to normal operating temperature, was chosen. This temperature is different for different MHTGR designs and requires resizing the TIPACS components for different MHTGR designs. The air inlet temperature was arbitrarily chosen as ranging from 5 to 35° C, corresponding to cold and hot ambient conditions. The CO_2 pressure in TIPACS was varied from 75 (just slightly above critical) to 150 bar for investigation of TIPACS performance.

The heat transferred from the reactor vessel to a single TIPACS unit (1 of 4) is presented in Fig. 4.6. As expected, the total heat transferred from the reactor increases as the ambient temperature decreases at any given TIPACS system pressure. At a given ambient temperature, however, the heat removed from the reactor varies differently as the pressure is increased. As shown in Fig. 4.6, at an ambient temperature of 5° C, the heat load decreases slightly as the system pressure is increased. At 15° C ambient inlet temperature, the heat load decreases as the pressure is raised from 75 to 80 bar—the heat load increases slightly from 80 to 150 bar. As the ambient temperature is increased to 25 and 35° C, however, the reactor heat load increases as the pressure is increased.

The resultant CO_2 mass flow is shown in Fig. 4.7. At 5° C ambient conditions, the mass flow decreases as the system pressure increases, reaching fairly constant values at a pressure of 90 bar and higher. At an air inlet temperature of 15° C, the mass flow increases with pressure, reaching a fairly constant value for the pressure range from 85 to 100 bar, then showing a slight decrease to a constant value at higher pressure. For 25° C air inlet temperature, the CO_2 mass flow increases with pressure for the range of 75 to 110 bar, at which it levels off to a fairly constant flow. For 35° C air inlet temperature, the CO_2 mass flow increases with system pressure, but it appears also to be reaching a constant value beyond the highest calculated pressure.

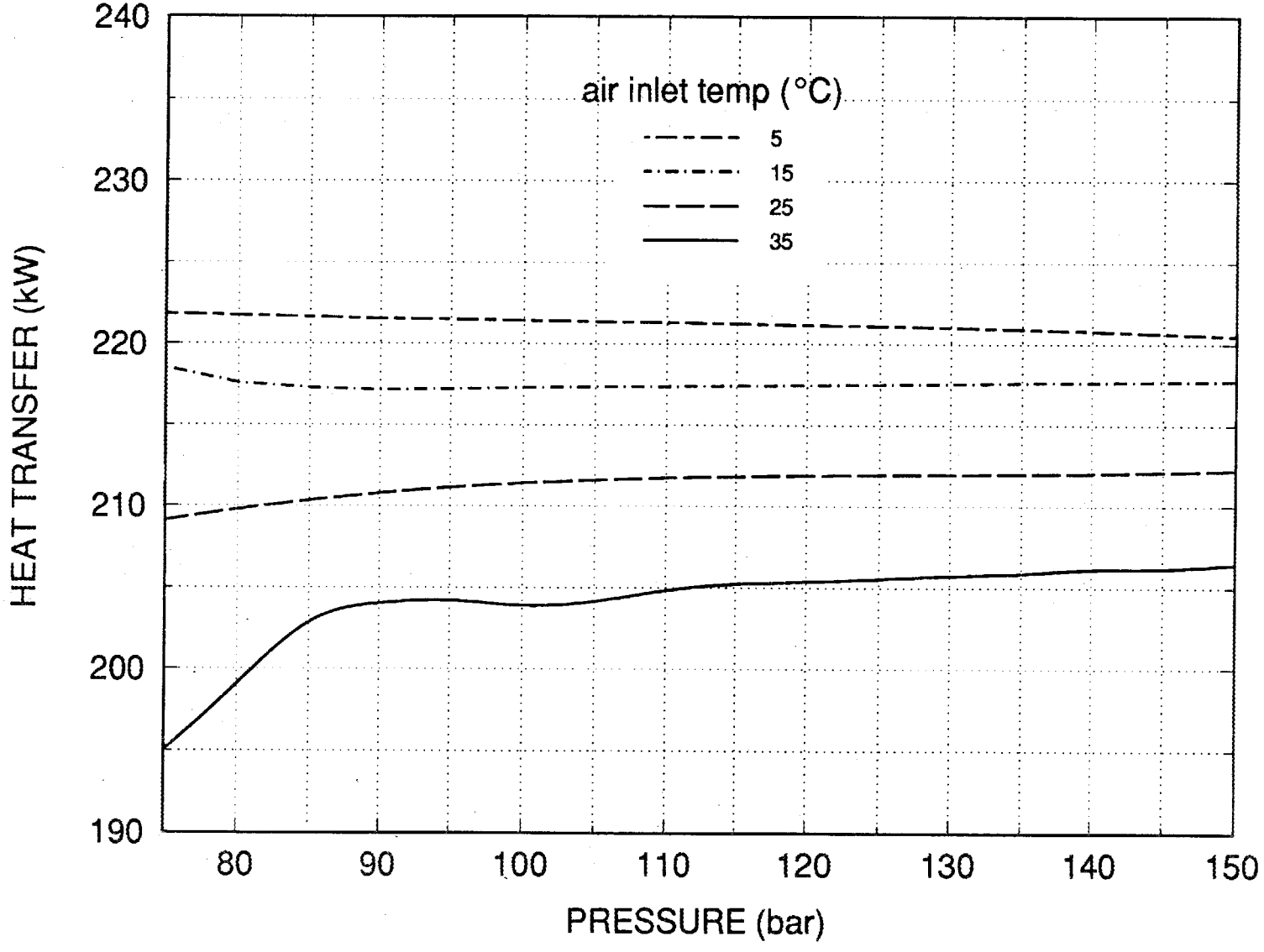

Fig. 4.6. Heat transfer per quadrant from reactor vessel at 220° C.

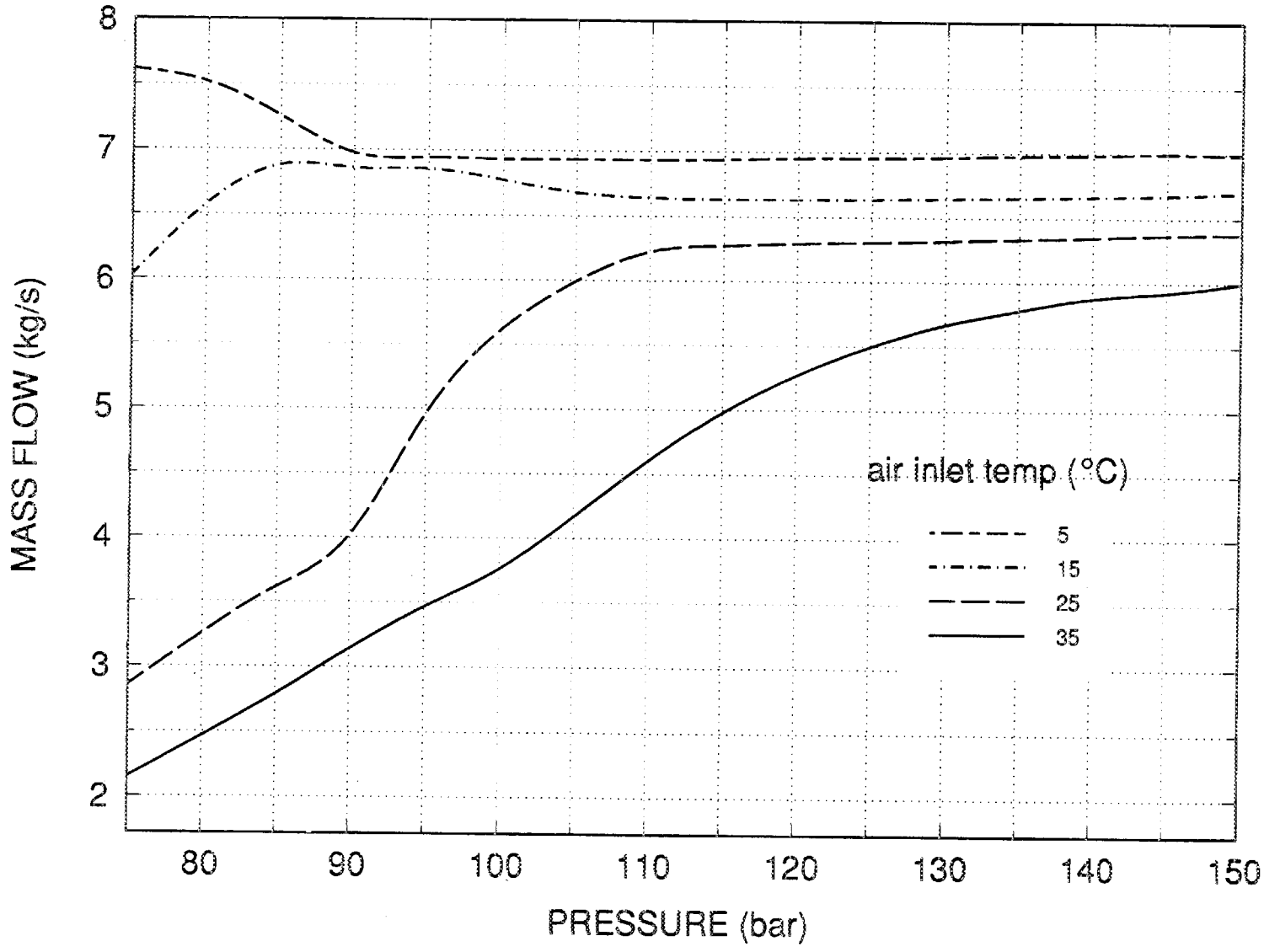

Fig. 4.7. CO_2 mass flow for different ambient air temperatures.

The inlet (bottom) and the outlet (top) temperatures of the internal heat exchanger are shown in Fig. 4.8. Because the outlet temperature is an important parameter (representing a maximum temperature of the reactor-cavity concrete), operating conditions should be chosen so that under normal operation, the maximum temperature of CO_2 should not be >66°C. This temperature is not exceeded for the ambient conditions of 5, 15, and 25°C at any pressure. At an ambient air inlet of 35°C on a hot day, however, the riser outlet temperature of 66°C is exceeded for system pressures <88 bar. Hence, the TIPACS inventory of CO_2 should be sufficient to result in a minimum pressure of 88 bar on a hot day.

Figure 4.8 shows also some interesting effects around the critical point. Note that for an ambient inlet of 5 and 15°C, the difference between the internal heat-exchanger inlet and outlet temperatures increases as the pressure increases. For an ambient air-inlet temperature of 25°C, the difference between the internal heat-exchanger inlet and outlet temperatures decreases as the system pressure increases from 75 to 95 bar, remains constant from 95 to 105 bar, and then increases at higher pressures. Showing a similar trend, the internal heat-exchanger temperature difference for 35°C air inlet temperature decreases as the system pressure increases from 75 to 110 bar, remains constant from 110 to 120 bar, and then increases at higher pressures.

Interestingly, at a 15°C air inlet and a system pressure of 75 bar, the inlet and outlet temperatures straddle the critical temperature by about ±0.5°C. At this point, the mass flow is ~6 kg/s, transferring almost 220 kW of heat per quadrant from the reactor, but only through ~1°C temperature difference, thus reflecting the very *large isobaric specific* heat at or very near the critical point. The external and internal heat-exchanger metal temperatures throughout the entire CO_2 closed loop system are also at or very near the critical temperature. One conclusion that can be drawn here is that if the air-side conditions in the external heat exchanger are such that the critical point of the TIPACS internal loop fluid exists in a large fraction of the external heat exchanger for a particular reactor vessel condition, a significant amount of heat can be removed from the reactor by the TIPACS with a minimal temperature difference around the critical temperature. Further analysis and modeling are necessary to prove this supposition and to develop an

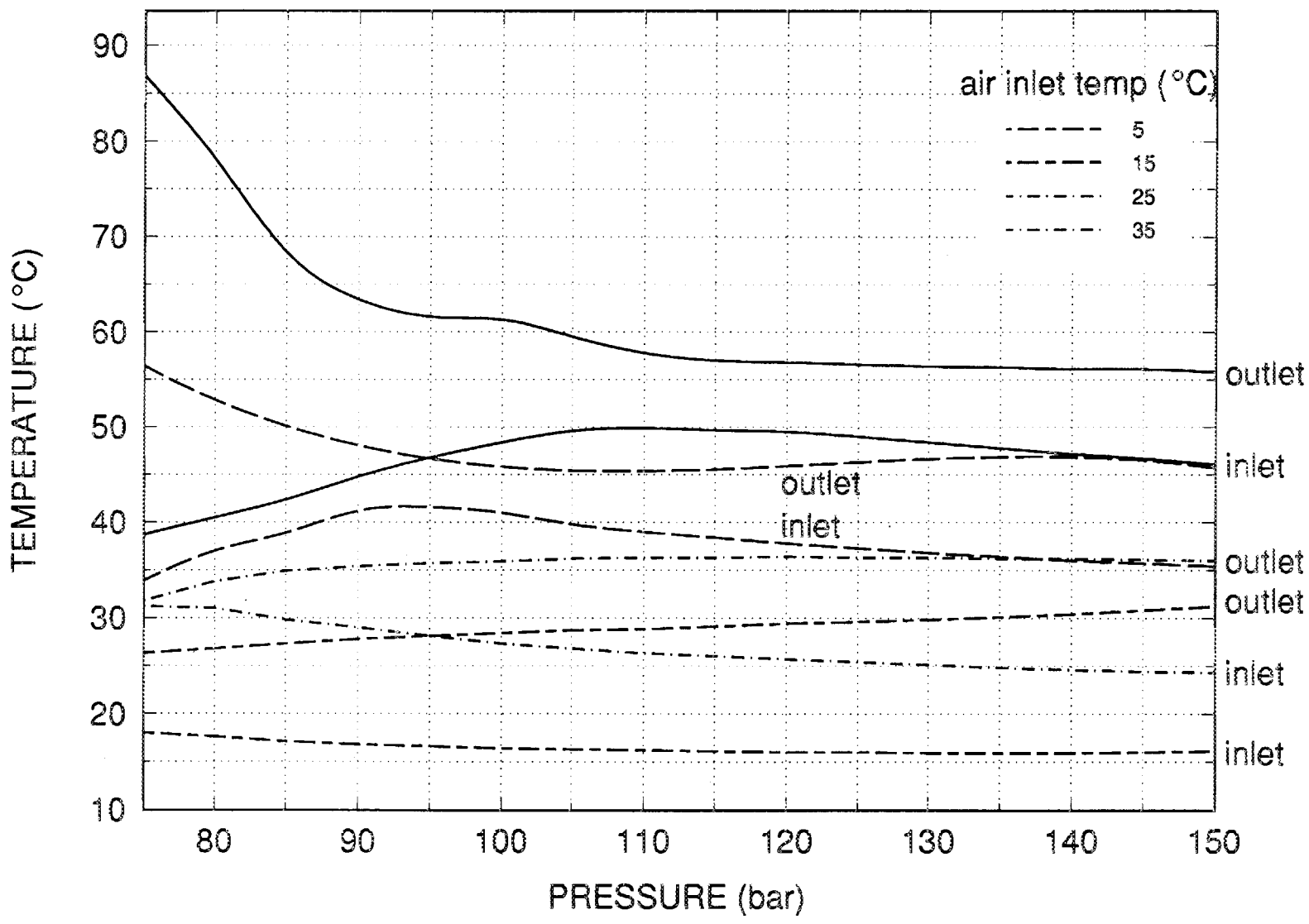

Fig. 4.8. CO_2 inlet and exit temperatures from the internal heat exchanger for different ambient temperatures.

understanding of the necessary design parameters to achieve this desirable condition—perhaps very important under postulated off-normal reactor conditions.

Hence, when the temperature levels and flow conditions are optimum, the TIPACS will remove heat from the reactor very effectively. At other than these favorable conditions, TIPACS will remove a sufficient amount of heat from the reactor vessel and keep the cavity concrete below 66°C, which is a desirable temperature range for steady-state normal operating conditions.

4.4 HIGHER TEMPERATURE TRANSIENT OR STEADY-STATE OPERATIONS

The reactor vessel may occasionally operate at higher temperatures during transients. For different designs, such as the direct-cycle gas-turbine design, the reactor vessel temperature may also be higher. Thus, the computational model was used to compute the steady-state temperatures, flows, and heat transfer of the TIPACS for an ambient air temperature of 35°C and at a CO_2 pressure of 150 bar for higher reactor vessel temperatures. Preliminary designs for the gas-turbine MHTGR indicate possible reactor vessel temperatures as high as 450°C; hence, this initial examination of TIPACS performance at higher temperatures included pressure vessel temperatures up to 450°C.

The temperatures of the CO_2 entering and leaving the internal heat exchanger for the Option A TIPACS design, as described in Sect. 3.2, are shown in Fig. 4.9. At a reactor vessel temperature of ~260°C, the CO_2 temperature at the outlet to the internal heat exchanger rises above 66°C, the nominal design temperature limit for concrete in long-term use. As the reactor vessel temperature increases to 325°C, the CO_2 inlet temperature also rises above 66°C. At a reactor vessel temperature of 450°C, the CO_2 inlet temperature is 81°C, and the outlet temperature is 247°C, which may be an undesirable operating condition of TIPACS design Option A.

The CO_2 mass flow and heat transferred from one quadrant of the reactor vessel to a single TIPACS unit are shown in Fig. 4.10. As expected, the heat transferred from the reactor vessel increases as the reactor vessel temperature increases. Also, the CO_2 mass flow decreases as the vessel temperature increases. This decrease in flow is the result of

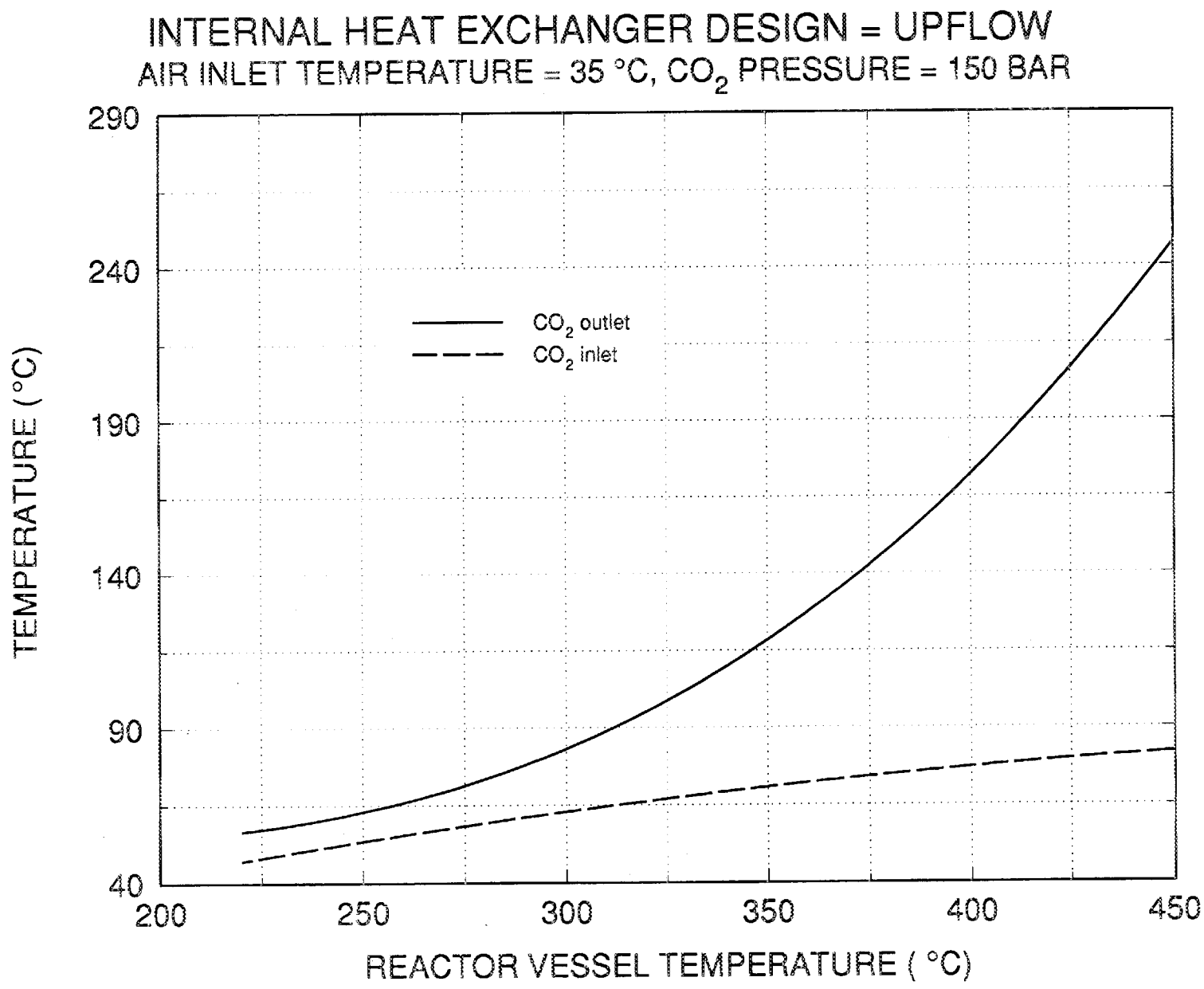

Fig. 4.9. CO_2 temperatures vs reactor vessel temperature for design Option A.

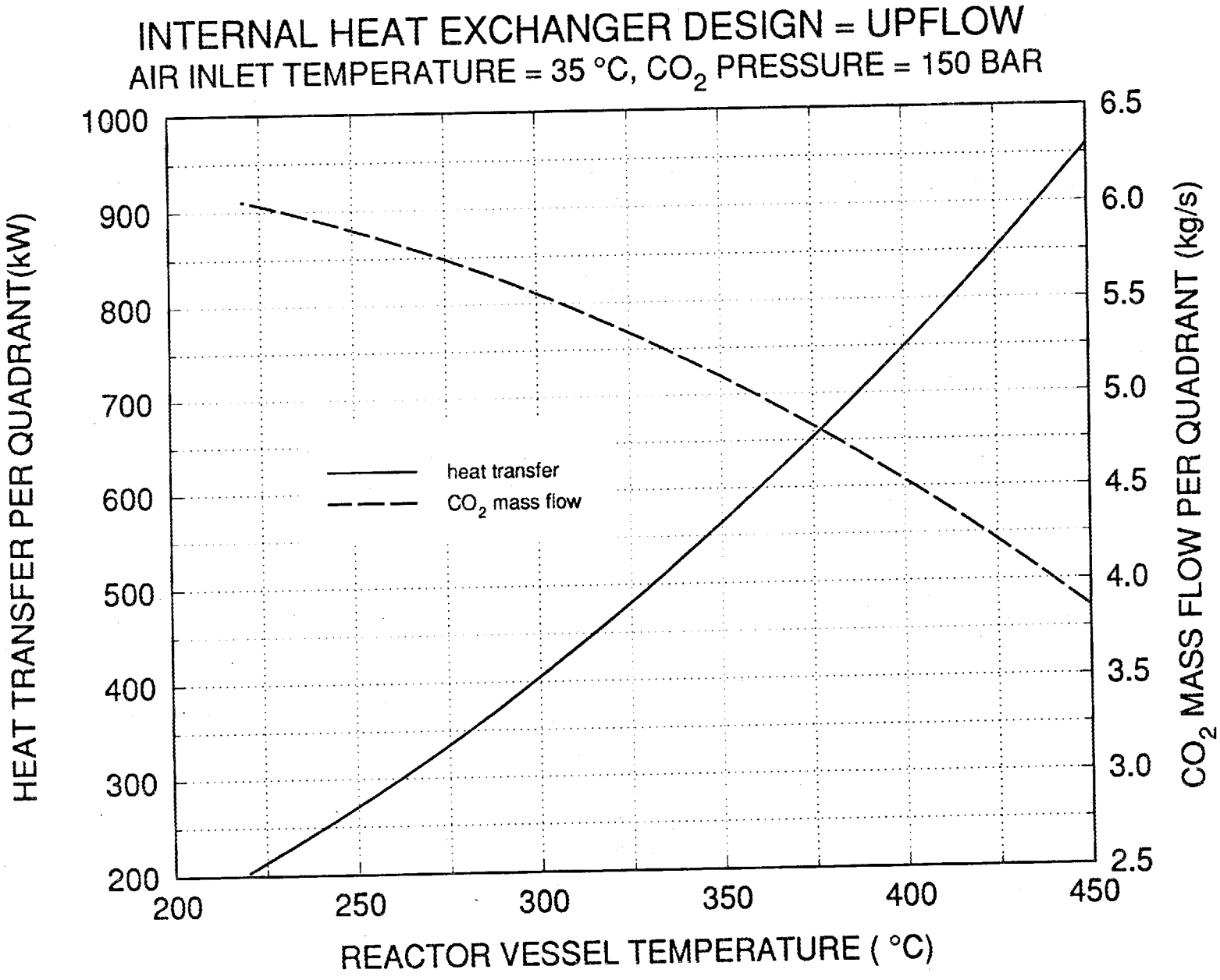

Fig. 4.10. Heat-transfer rates and CO_2 flow rates per TIPACS (one quadrant of reactor vessel) vs reactor vessel temperature for design Option A.

changing physical properties that induce higher frictional pressure losses. The fractional pressure drop increases from 0.0091, at a vessel temperature of 220°C to 0.010, at a vessel temperature of 450°C.

TIPACS design Option B, as described in Sect. 3.2, was also modeled. The external air-cooled heat exchanger and the internal heat exchanger next to the pressure vessel wall is of the same design as Option A, but another row of tubes is used as a "downcomer" to introduce CO_2 to the upflow section of the internal heat exchanger. The differences in the two designs are summarized in Table 4.1. *No regenerative heat exchange between the downcomer and the riser was modeled for this simplified model.* As discussed earlier (Sect. 3.2), radiation transport is limited at low temperatures; hence, only a few percent of the heat is transferred to the downcomer. The temperature of the CO_2 entering the downward flowing section and exiting the upward flowing section of the internal heat exchanger for the Option B design are shown in Fig. 4.11 for an ambient air temperature of 35°C (hot day) and at a CO_2 pressure of 150 bar. The inlet CO_2 temperature is slightly lower, and the outlet temperature is slightly higher as compared to Option A design for a reactor-vessel temperature of 220°C. As the reactor-vessel temperature increases to 450°C, however, the inlet temperature rises to only 68°C, while the outlet temperature rises to 280°C. Because of the design of Option B, the concrete forming the reactor cavity may only slightly exceed, on hot days, the nominal design limit for the concrete (in long-term use) of 66°C. (Note: These scoping studies did not optimize the external air-cooled heat exchanger to limit the temperature seen by the concrete for design Option B.)

The CO_2 mass flow and heat transferred from the reactor vessel for design Option B are shown in Fig. 4.12 for one TIPACS unit that cools one quarter of the reactor cavity. As expected, the heat transferred from the reactor vessel increases and the CO_2 mass flow decreases as the vessel temperature increases. The decreased CO_2 mass flow for Option B is almost half that for Option A due to higher friction losses resulting from the smaller tubes in the downcomer for Option B. The fractional pressure drop increases from 0.0099 at a vessel temperature of 220°C to 0.011 at a vessel temperature of 450°C. The very much increased outlet temperature of 280°C is shown in Fig. 4.11 for design Option B. Figure 4.11 also shows the effect of the buoyancy force and frictional fluid drag forces.

Table 4.1 Differences between Option A and Option B[1]

Property	Option A	Option B
General design parameters	— Identical[2] —	
System physical dimensions	— Identical[2] —	
TCS dimensional ratios	— Identical[2] —	
External heat exchanger	— Identical[2] —	
Internal heat exchanger		
Type	Upflow vertical	Downflow/upflow vertical
Height	17.4 m	17.4 m
Silo circumference covered	8 m	8 m
Surface area facing reactor vessel	139.2 m^2	139.2 m^2
Downflow pipe diameter	0.5 m	2 in.
Downflow pipe size	—	Schedule 80
Downflow pipe number	1	163
Upflow pipe diameter	2 in.	2 in.
Upflow pipe size	Schedule 80	Schedule 80
Upflow pipe number	163	163
Operational parameters		
Exit air temperature (Air in 35°C)		
Vessel at 220°C	54.6°C	58.1°C
Vessel at 450°C	195°C	189.2°C
Mass air flow rate		
Vessel at 220°C	9.27 kg/s	8.9 kg/s
Vessel at 450°C	6.0 kg/s	6.0 kg/s

Table 4.1 Differences between Option A and Option B[1] (continued)

Property	Option A	Option B
Operational parameters (continued)		
Inlet CO_2 temperature		
Vessel at 220°C	46.1°C	45.1°C
Vessel at 450°C	81.3°C	68°C
Exit CO_2 temperature		
Vessel at 220°C	55.8°C	62°C
Vessel at 450°C	247°C	280°C
Mass CO_2 flow rate		
Vessel at 220°C	6.0 kg/s	3.86 kg/s
Vessel at 450°C	3.9 kg/s	2.92 kg/s
Heat transfer		
Vessel at 220°C	207 kw	204 kw
Vessel at 450°C	955 kw	926 kw

[1]All physical differences between options in internal heat exchanger. For Option B, system not reoptimized, only heat exchanger changed.

[2]See Table 3.2.

[3]N/A = not applicable.

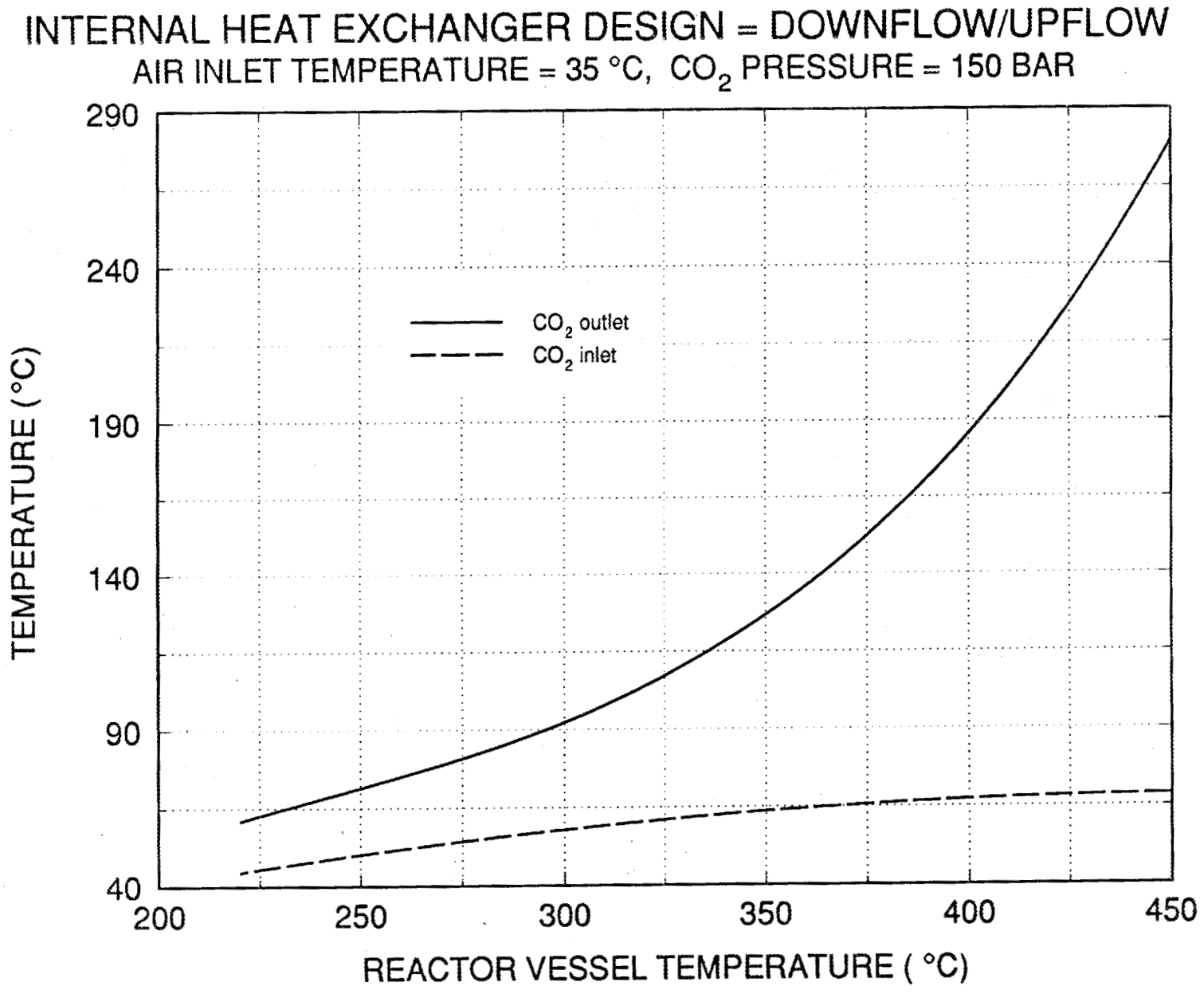

Fig. 4.11. CO_2 temperatures vs reactor vessel temperatures for design Option B.

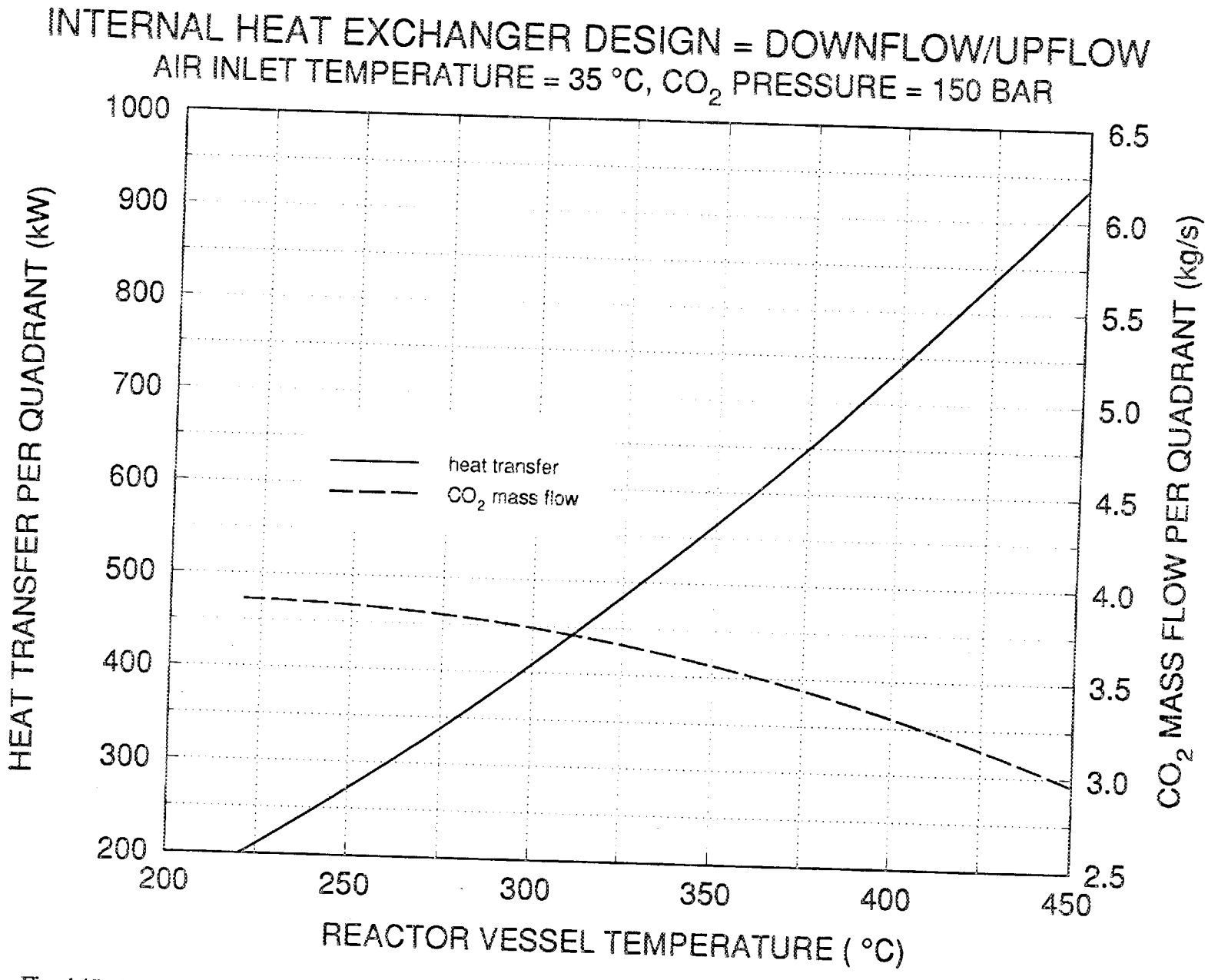

Fig. 4.12. Heat-transfer rates and CO_2 flow rates per TIPACS (one quadrant of reactor vessel) vs reactor temperatures for design Option B.

Thus, Option B may be preferable for the MHTGR, particularly for the direct-cycle gas-turbine variety, if higher reactor vessel temperatures are expected. Further modeling improvements are recommended, particularly to improve the modeling of the external heat exchanger and the possible regenerative heat transfer from the downcomer and riser of Option B.

5. TEMPERATURE CONTROL SYSTEM

The TIPACS is an RCHTS with a thermal switch, the TCS, that turns the system off and on. When the system is off, there is no fluid movement, and the TIPACS is static. When the system is on, there is flowing CO_2. This off-on characteristic allows the initial TIPACS design to be broken into two components—TCS for off-operation and RCHTS for on-operation. The TCS can be considered that part of the TIPACS above the two heat exchangers (Fig. 5.1). The RCHTS is primarily the two heat exchangers.

A series of simplified "models" of the TCS have been constructed to understand TCS behavior, design parameters, and performance limits. Using these models, alternative design options were considered. The actual performance of different TCS designs can be determined with numerical models that can provide more detailed information but do not provide the understanding of the TCS behavior. The details of these models are presented in Appendix C.

5.1 PHYSICS OF THE TCS

The physics of the TCS must be understood in terms of its impact on the design of the TIPACS. Important design parameters are the heights of the TCS and relative volumes of various pipes and tanks. The RCHTS imposes only one significant constraint on the TCS—a minimum pipe diameter for flow of CO_2 fluid from the inside heat exchanger to the outside heat exchanger without excessive pressure drop. TCS operation is dependent upon the expansion of CO_2 until a liquid natural-circulation loop is created or the fluid passes the critical point and becomes a single-phase system. Where the expansion occurs controls TIPACS performance and when TIPACS activates; thus, the relative fluid volumes of various TIPACS components are critical design parameters. For this analysis, the TIPACS can be broken into four sections: the exterior RCHTS zone, the exterior TCS zone, the interior RCHTS zone, and the interior TCS zone. The consequences of locating most of the fluid volume of the TIPACS in each zone can be separately evaluated.

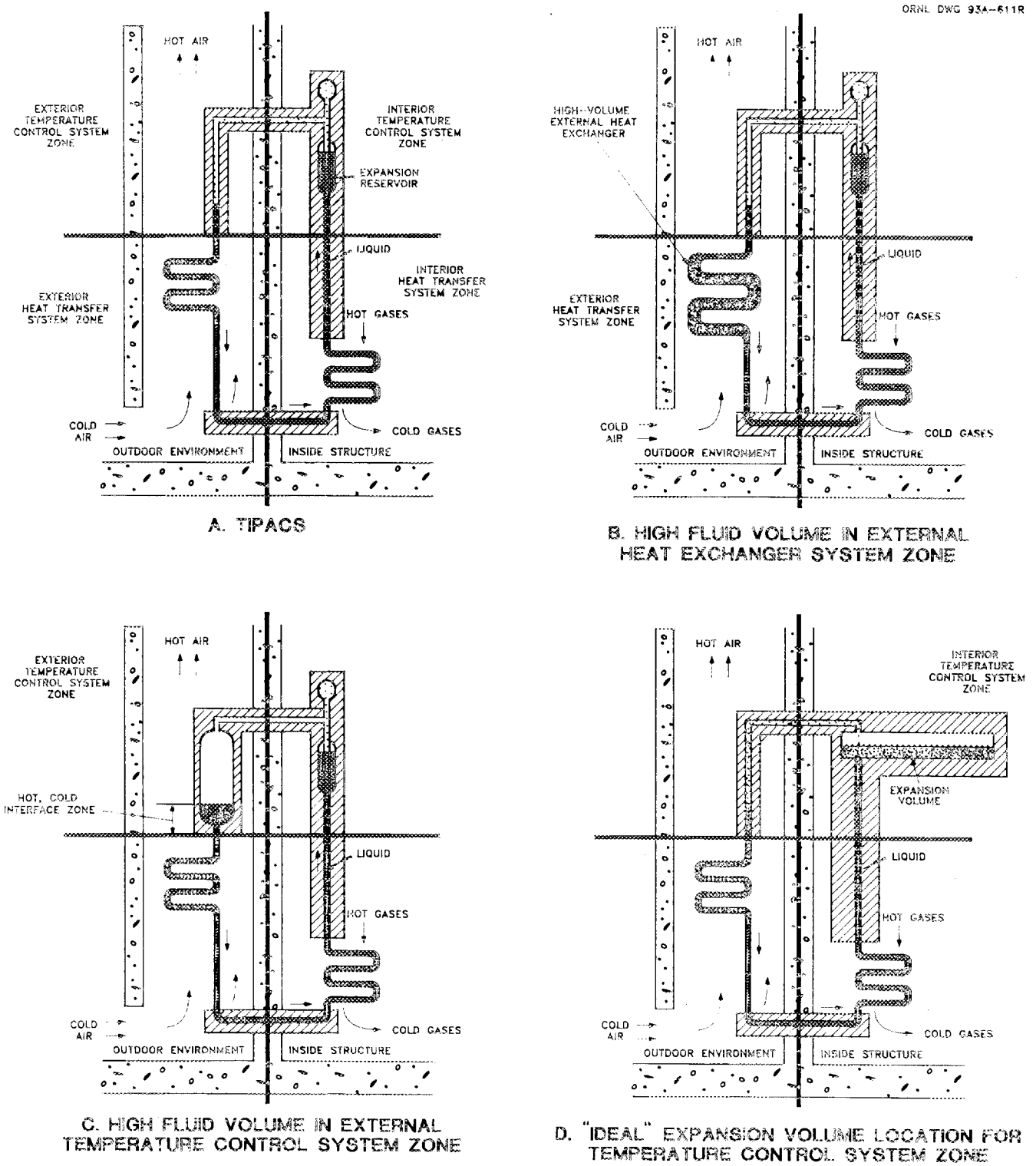

Fig. 5.1. TCS characteristics.

For the first case, let us consider a TIPACS system where most of the volume for fluid is in the exterior heat exchanger [Fig. 5.1(b)]. Fluid temperature determines TIPACS operation. If most of the fluid is in the external heat exchanger, changes in external temperature will control the expansion or contraction of the liquid CO_2 and startup of the heat-transfer loop. The objective, however, is to control operation of the TIPACS by interior temperatures. To meet this design objective of the TIPACS being controlled by interior heat-exchanger temperature, *most of the fluid volume must be in the inside zones of the TIPACS.*

For the second case, let us consider a TIPACS where most of the fluid volume is in the exterior TCS zone [Fig. 5.1(c)]. This zone contains liquid CO_2 that is partly controlled by exterior temperatures. The bottom of the liquid CO_2 in this zone has the same temperature as that of the outside. The top of the liquid zone has the temperature of the interior zone because it is in contact with saturated CO_2 in equilibrium with warm, liquid CO_2 in the interior zone. Just as in the external heat-exchanger zone, there is a strong incentive to minimize the fluid volume of the TIPACS here to ensure that the TIPACS is controlled by interior temperatures. In addition, when the TIPACS is not operating, this zone contains the hot-cold CO_2 transition zone. The smaller the cross-sectional area of this transition zone, the less heat that is conducted from the TIPACS when the TIPACS is not operating.

The previous considerations indicate that for TCS operation, most of the liquid volume when the TIPACS is shut down and cold should be in the internal RCHTS zone. The liquid is the TIPACS's temperature sensor. If the normal design of the RCHTS does not result in most of the liquid in this zone, added storage volume for the liquid must be added to this zone. Because of the natural circulation of the liquid, the temperatures of the interior RCHTS and the interior TCS are expected to be equal.

The optimum volume and geometry of the interior TCS zone are dependent upon three factors. First, as the interior heat exchanger, exterior heat exchanger, and interior TCS zones warm up, the liquid CO_2 density decreases, and the liquid CO_2 volume increases. The expansion volume then fills with liquid CO_2 until the critical point is reached, and the entire TIPACS is filled with a single-fluid expansion. The expansion reservoir volume

must handle the expansion of liquid CO_2 from the coldest design conditions to a few degrees below the critical temperatures without spilling liquid CO_2 into the external loop.

Second, there is a minimum height (h_m) of the interior TCS based on the design of the RCHTS. In a normal standby mode, the liquid on the inside will be hotter than the liquid on the outside and, hence, have a lower fluid density. To maintain a balance between the interior (hot) liquid and exterior (cold) liquid, the liquid heights must vary by height h_s (Fig. 5.2). This implies that the minimum height of the TCS is the sum of the height required for the hot-cold transition zone (h_T) in the outside TCS plus the height h_s.

Third, the height of the TCS is dependent upon the placement and geometry of the expansion volume. The TCS height is minimized if the expansion volume starts directly above the minimum height and is a wide, shallow vessel [Fig. 5.1(d)]. As a wide, shallow vessel, the height of fluid in the inside TCS volume does not change significantly with expansion or contraction of the liquid. In effect, the height of liquid in the inside TCS is fixed, while the height of liquid in the outside TCS varies.

The interior temperature control zone is shown inside the structure to be cooled, but this is not a requirement. Because the TCS is insulated, it may be located inside or outside the structure. There is a requirement that the liquid in the interior heat-exchanger zone freely communicates with the fluid in the interior temperature control zone so that the hottest liquid in a shutdown state can flow by natural convection to the expansion volume.

5.2 LIQUID-GAS RESERVOIR

The TIPACS has the option of including an optional liquid-gas reservoir (Fig. 5.2) at the very top of the TCS. This allows liquid expansion to start operation of the TIPACS before all the gas volume is filled with liquid and the critical temperature is reached. A liquid CO_2 RCHTS is created. The performance of this liquid RCHTS is significantly less than when a single-phase system is created. The liquid is near the boiling point of CO_2; therefore, boiling is likely to occur in the warm zone. This gas-liquid mixture is carried to the exterior TCS zone. Here, the gas-liquid mixture attempts to descend to the exterior

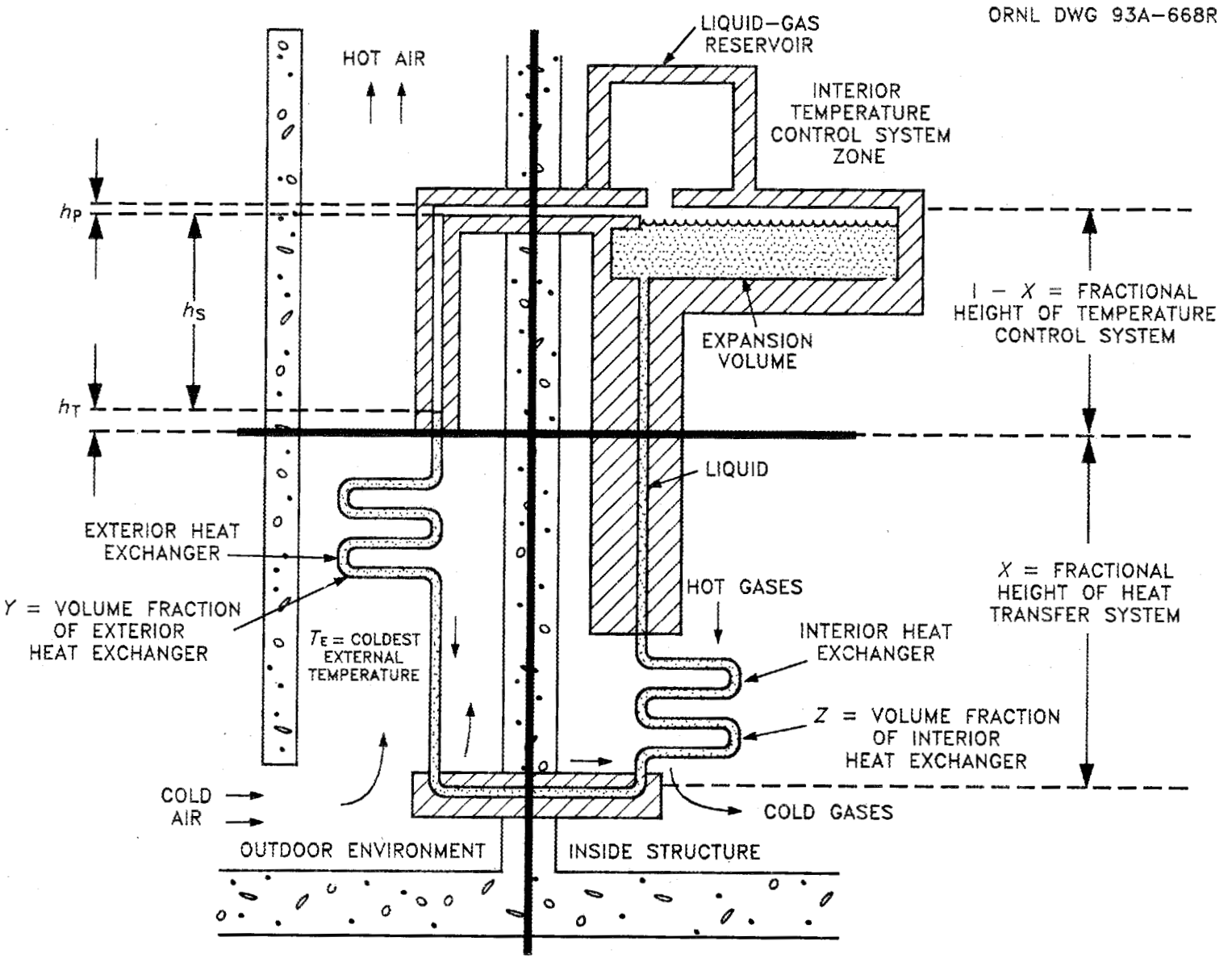

Fig. 5.2. Schematic of TIPACS model parameters.

heat exchanger. The gas bubbles are pushed upward in the fluid by buoyancy forces. This rise results in slow circulation of fluid. The liquid-gas reservoir allows an early startup and controlled heat transfer, but full performance occurs only when a single-phase fluid above the critical point is created. Startup below the critical temperature does allow the height of the TCS to be reduced.

5.3 HEAT DIODE

The TIPACS acts as a heat diode. Heat can flow from inside the reactor cavity to the exterior environment if the inside temperature exceeds both the operating temperature and the outside temperature. Heat can not flow from outside to inside if outside temperatures exceed inside temperatures.

The TIPACS is a heat diode because the outside heat exchanger is at a higher elevation than the inside heat exchanger. If outside temperatures exceed inside temperatures, hot, low-density fluid fills the TCS with colder, higher-density fluid at the bottom of the RCHTS. This is a stable configuration that can exist where there is no fluid circulation.

6. OTHER ISSUES

6.1 ALTERNATIVE DESIGN OPTIONS

A series of alternative design options can be chosen for specific applications. A brief description of each follows.

- For warm climate conditions, the RCHTS can be used without the TCS. Such a system will be a two-phase RCHTS when temperatures and pressures are below the critical conditions of CO_2 and will be a single-phase system when temperatures and pressures are above the critical temperature of CO_2. The RCHTS design and performance characteristics would be similar to those described in this report. Such a system may retain some of the characteristics of TIPACS with a TCS in that the heat-transfer capabilities become more efficient once the critical point of the fluid is exceeded. This reflects the change in physical properties that occur near the critical point.

- TIPACS can be used in conjunction with other systems. For example, a variety of systems have been proposed to absorb decay heat in an emergency for limited time periods (water in tubes, etc.). TIPACS creates the option for such systems to provide short-term cooling while TIPACS provides long-term safety.

- Other operating fluids can be used for TIPACS operation. Most of these have lower operating pressures than does CO_2, but they have other limitations, such as flammability.

- Alternative ultimate heat sinks can be coupled to the TIPACS. Specifically, the silo-reactor-cavity elevation allows the use of the small pond as a heat sink to provide long-term evaporative water cooling. Because water is a very good heat-transfer agent, a pond reduces the size of the external heat exchanger significantly. It also tends to reduce the size of the internal heat exchanger because of the lower heat-rejection temperature to the atmosphere. Earlier studies have examined pond cooling for ultimate heat sinks.

6.2 MONITORING OF PERFORMANCE

A requirement for practical systems in nuclear applications is to monitor the performance of the system so that one has confidence that the system is operational. For TIPACS, this monitoring is relatively simple.

TIPACS can be continuously monitored for leakage of CO_2 by using the same acoustic techniques previously used to monitor for leaks in pressure vessels (Hutton 1993; Kupperman 1993). Alternatively, the inventory of CO_2 can be continuously determined during TIPACS operation. The required instrumentation includes a pressure sensor and several temperature sensors in different parts of the system. TIPACS is a single-phase system during operation and has a sealed inventory of fluid. Given the known internal volume of the system and CO_2 properties, system inventory can be calculated from a pressure measurement and several temperature measurements.

System performance can be monitored with the previous instrumentation and four other temperature measurements: (a) inlet-air temperatures, (b) outlet-air temperatures, (c) reactor-cavity-wall temperatures, and (d) reactor-vessel temperature. With any three of these four measurements, the forth temperature can be calculated. Comparisons among calculations and measurements provide real-time measurements that performance is as predicted and can assess many forms of degraded performance. Causes of degraded performance could included partial blockage of air coolers, changes in thermal radiation-adsorption properties of the pressure vessel, and other long-term degradation mechanisms. The same measurements would also monitor conditions during reactor transient or accident conditions with real-time monitoring of reactor-cavity temperatures and rates of heat removal from the reactor. Such sophisticated levels of system monitoring may not be required. Pressure and temperature measurements for inventory determinations would identify if TIPACS performance were degrading, but they would not necessarily provide the cause of such problems.

6.3 EQUIPMENT AVAILABILITY

The components and instrumentation necessary to build TIPACS are commercially available. The soft drink industry currently handles large quantities of CO_2 for carbonated beverages (Coke®, Pepsi®, etc.). The CO_2 is usually supplied as a liquid CO_2. Public health standards require high-purity CO_2. The vaporization of liquid CO_2 is often achieved with natural-draft air coolers to minimize energy costs. Because CO_2 forms solid dry ice at lower pressures, these air-cooled heat exchangers are high-pressure heat

exchangers. There is a 60+ year experience-base with such technology. CO_2 has also been used in certain industrial air conditioning systems for over 60 years. There is also a CO_2 dry ice industry. These large industries have resulted in a large supply industry for heat exchangers, pumps, storage vessels, and instrumentation.

There is large-scale nuclear experience with CO_2. The British Magnox power reactors are cooled with CO_2. This provides more than 30 years of nuclear power experience in the use of CO_2 in nuclear applications. The radiation levels and temperatures of CO_2 in Magnox reactors are much higher than corresponding radiation levels and temperatures in an MHTGR reactor cavity; thus, there is high confidence that TIPACS can withstand these temperature and radiation levels.

7. UNCERTAINTIES AND UNKNOWNS

The initial evaluation of TIPACS indicates the feasibility and limiting design conditions for TIPACS. However, significant uncertainties remain that require additional work.

7.1 MHTGR DESIGN TRADE-OFFS

The general design requirements for the MHTGR are known, but there are engineering trade-offs among various systems to meet the general requirements. TIPACS has a different set of characteristics than does the existing RCCS. The optimum design of TIPACS will involve different trade-offs than the currently proposed system. This analysis is a first iteration to understand the TIPACS. The MHTGR program has recently committed to an advanced gas-turbine-power cycle to replace the steam-power cycle. This changes the reactor-cavity cooling requirements. The new power cycle will result in reactor vessel temperatures of ~450 vs the 220°C assumed herein. This necessitates alternative heat exchanger designs such as internal heat exchanger—Option B.

7.2 MODEL OF THE TIPACS UNDER ALL EXPECTED CONDITIONS

The behavior of the TIPACS under the full range of design conditions must be evaluated. This will require a detailed numerical model of the TIPACS to evaluate design options and operation under all expected conditions including transient conditions.

7.3 PROOF-OF-PRINCIPLE EXPERIMENT

The evaluation of TIPACS has been based on theoretical conditions. A proof-of-principle experiment is required to confirm that major assumptions are correct and that basic operation is as expected. A proof-of-principle experiment must show that quantitative performance of TIPACS matches calculated performance.

7.4 ENGINEERING SCALE TEST

If TIPACS is to be used, an engineering test is required to validate models of TIPACS performance, test critical components, and ensure integration of the TIPACS into containment design. An engineering test requires (1) significant scale of operation to be ensured that all phenomena in full-scale operation are represented, (2) performance measurements of key components such as heat exchangers, and (3) ability to change out critical components to test different designs.

7.5 DEVELOPMENT OF ENGINEERING METHODOLOGY

An engineering methodology must be developed so that the TIPACS systems can be reliability designed for different conditions without requiring prototype testing of equipment for a wide range of conditions. This methodology would be based on the results of earlier modeling work, proof-of-principle experiments, and engineering scale tests. A key component of development of the methodology is determining the sensitivity of various design parameters based on theory and experiment.

8. CONCLUSIONS

The initial evaluation of the TIPACS indicates the potential for a high-performance RCCS with significant advantages over the existing air duct system. These advantages include

- Less equipment volume in the reactor cavity which simplifies design and may reduce costs. This is a consequence of a high-density heat-transfer fluid in a high-performance RCHTS.

- Better reactor cavity isolation. The TIPACS is a sealed RCHTS. It provides two high-pressure (>1000 psi) barriers between the inside of the reactor cavity and the environment; these barriers must fail before possible release of radionuclides can occur. It creates the option of a sealed containment building. The presence of these barriers converts the RCCS from the weakest isolation link in the containment system to the strongest.

- Cooling cutoff under cold weather conditions. TIPACS does not cool the reactor cavity below a preset temperature.

- Optional emergency reactor cooling via conduction of heat to the ground. The TIPACS is transparent to heat transfer from the reactor vessel to the soil in the event of a total TIPACS failure. This provides an additional inherent level of safety to ensure that MHTGR fuel can never be heated sufficiently to cause sufficient release of radionuclides, even in "beyond design basis" events of extremely low probability.

There is one major disadvantage of TIPACS. It is a new technology, and it has not been tested. Because there are significant uncertainties, there is the potential for unforeseen problems that would limit performance. Consequently, additional development effort is required. There is one minor disadvantage of TIPACS. It is mechanically a simple system, but it is complex to design. This is, in part, a result of the requirement that it operate near the critical point of the heat-transfer fluid.

9. REFERENCES

Ball, S. J., *ORECA-I: A Digital Computer Code for Simulating the Dynamics of HTGR Cores for Emergency Cooling Analyses,* ORNL/TM-5159, Union Carbide Corp., Nuclear Division, Oak Ridge National Laboratory, Oak Ridge, Tennessee, 1976.

Conklin, J. C., *Modeling and Performance of the MHTGR Reactor Cavity Cooling System,* NUREG/CR-5514, ORNL/TM-1145, Martin Marietta Energy Systems, Inc., Oak Ridge National Laboratory, Oak Ridge, Tennessee, 1990.

Forsberg, C. W., "Temperature Initiated Passive Cooling System," patent application to the U.S. Commissioner of Patents and Trademarks, application No. 08/098,550, July 28, 1993.

Forsberg, C. W., et al., *Proposed and Existing Passive and Inherent Safety-Related Structures, Systems and Components (Building Blocks) for Advanced Light Water Reactors,* ORNL-6554, Martin Marietta Energy Systems, Inc., Oak Ridge National Laboratory, Oak Ridge, Tennessee, October 1989.

Friend, D. G., *NIST Thermophysical Properties of Pure Fluids,* Version 3.0, National Institute of Standards and Technology, Gaithersburg, Maryland., 1992.

Ganapathy, V., "Specify Packaged Steam Generators Properly," *Chem. Engr. Prog.* 89(9), 62 (September 1993).

Green, D. W. and Maloney, J. D., *Perry's Chemical Engineers' Handbook: Sixth Edition,* McGraw-Hill Book Company, New York, 1984.

Hahne, E. W. P., "Natural Convection in the Near Critical Region and Its Application in Heat Pipes," pp. 774–826 in *Natural Convection Fundamentals and Applications,* S. Kakaç et. al., eds., Hemisphere, New York, 1984.

Hutton, P. H., "Listening To Reactor Pressure Boundaries For The Sounds Of Cracks And Leaks," *Nuc. Eng. Int.* 38(47), 38 (December 1993).

Kays, W. M. and London, A. L., *Compact Heat Exchangers, Third Edition,* McGraw-Hill Book Company, New York, 1984.

Kupperman, D., "Considering Options For Leak Detection," *Nuc. Eng. Int.* 38(47), 41 (December 1993).

National Academy of Science, *Nuclear Power: Technical and Institutional Options for the Future,* Washington, D.C., June 17, 1993.

Oka, Y. and Koshizuka, S., "Concept and Design of a Supercritical-Pressure, Direct-Cycle Light Water Reactor," *Nuclear Technology* **103**(3), 295 (September 1993).

Polyakov, A. F. "Heat Transfer under Supercritical Pressures," pp. 1-53 in *Advances in Heat Transfer, Vol. 21,* Academic Press, New York, 1991.

Watts, M. J. and Chou, C. T., "Mixed Convection Heat Transfer to Supercritical Pressure Water," pp. 495–500 in *Proc. Seventh International Heat Transfer Conference, Vol. 3*, U. Grigull et al., eds., Hemisphere, New York, 1982.

White, F. M., *Fluid Mechanics,* McGraw-Hill Book Company, New York, 1979.

Appendix A

CRITICAL PROPERTIES OF FLUIDS

Appendix A: CRITICAL PROPERTIES OF FLUIDS

The temperatures at which the TIPACS operates depends on the critical properties of the heat transfer fluid. With appropriate selection of fluid, the TIPACS can initiate operation at any desired temperature. Table A.1 lists a representative set of fluids that are candidates for the TIPACS at different temperatures.

Table A.1. Critical properties

Substance	t_c, °C	P_c, atm	ρ_c, g/cm^3
Helium	−267.96	2.261	0.06930
Neon	−228.71	26.86	0.4835
Nitrogen-14	−146.89	33.54	0.3110
Air	−140.6	37.2	0.313
Argon	−122.44	48.00	0.5307
Oxygen	−118.38	50.14	0.419
Methane	−82.60	45.44	0.162
Krypton	−63.75	54.20	0.9085
Perfluoromethane (tetrafluoromethane)	−45.6	36.9	0.630
Silicon tetrafluoride	−14.1	36.7	
Boron trifluoride	−12.3	49.2	
Xenon	16.59	57.62	1.105
Perfluoroethane	19.7		0.617
Trifluoromethane	25.74	47.73	0.525
1,1-Difluoroethylene	30.1	43.75	0.417
CO_2	31.04	72.85	0.468
Ethane	32.28	48.16	0.203
Perfluoroethene (tetrafluoroethylene)	33.3	38.92	0.58
Fluoromethane	44.55	58.0	0.300
Sulfur hexafluoride	45.55	37.11	0.734
Perfluoro-*n*-propane	71.9	26.45	0.628
1,1,1-Trifluoroethane	73.1	37.09	0.434
Dichlorodifluoromethane (R-12)	111.80	40.71	0.558
Perfluoro-*n*-butane	113.2	22.93	0.629

Table A.1. Critical properties (continued)

Substance	t_c, °C	P_c, atm	ρ_c, g/cm^3
1,1-Difluoroethane	113.5	44.37	0.365
Ammonia	132.4	111.3	0.235
1,2-Dichloro-1,1,2, 2-tetrafluoroethane (R-114)	145.7	32.2	0.582
Perfluoro-*n*-pentane	149	20.1	
Silicon trichlorofluoride	165.3	35.3	
Dichlorofluoromethane (R-21)	178.5	51.0	0.522
Perfluorocyclohexane	184.0	24	
Fluorotrichloromethane (R-11)	198.0	43.2	0.554
Perfluoro-*n*-heptane	201.6	16.0	0.584
Uranium hexafluoride	230.2	45.5	
Ethanol (ethyl alcohol)	243.1	62.96	0.276
Perfluoro-*n*-decane	269.2	14.3	
Bromine	311	102	1.18
Dideuterium oxide (D_2O)	371.0	215.7	0.363
Water	374.2	218.3	0.325
Iodine	535		
Mercury	900	180	

Source: Dean, J. A., *Lange's Handbook of Chemistry: Eleventh Edition*, McGraw-Hill Book Company, New York.

Appendix B

CO_2 PHYSICAL PROPERTIES BELOW THE CRITICAL POINT

Appendix B: CO_2 PHYSICAL PROPERTIES BELOW THE CRITICAL POINT

The off-on characteristics of TIPACS depend primarily on the density of the heat-transfer fluid below its critical point. The CO_2 phase diagram is shown in Fig. B.1. Carbon dioxide density in tabular form (Table B.1) is shown herein between its triple point (solid, liquid, and gas in equilibrium) and its critical point (gas and liquid with identical properties). Density data allow calculation of the temperature of initial operation of the TIPACS for any given TIPACS geometry. TIPACS operates at a single pressure for a given set of temperatures; therefore, the data are in the form of density vs temperature for fixed pressures.

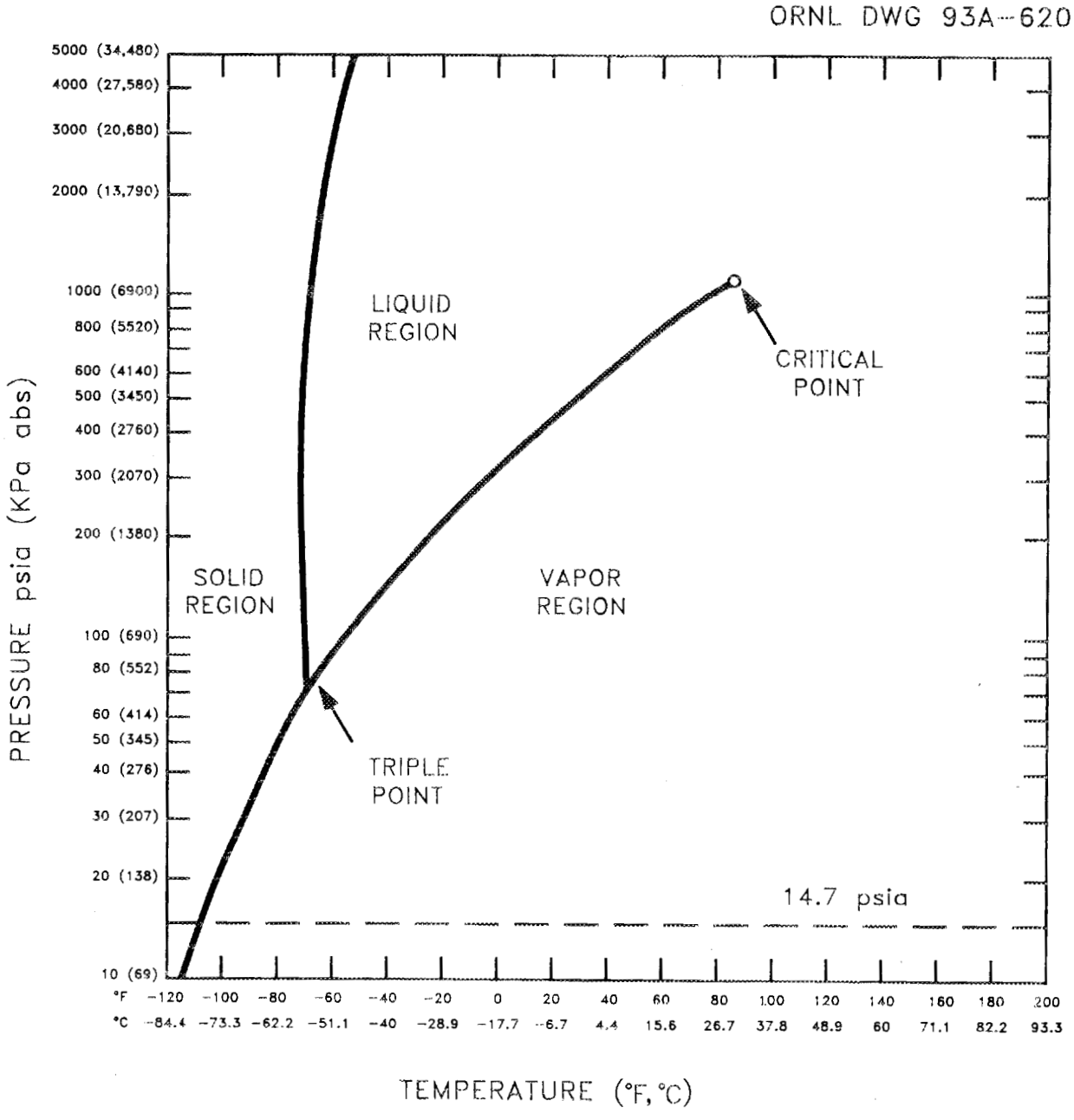

Fig. B.1. Carbon dioxide phase diagram.

Table B.1. Carbon dioxide saturation line properties and liquid properties below saturation temperature

Critical Point Data

Critical temp: 304.21 K
Critical pressure: 7384.3 kPa
Critical density: 468 kg/cu. m

Triple Point Data

Triple point temp: 216.58 K
Triple point pressure: 518.16 kPa

Saturation line data

Saturation temp (°C):	*31.2*	31	30.75	30.5	30.25	30	29	28	27	26	25	22.5	20	15	10	5	0	-10	-20	-30	-40	-50	-54
Saturation pressure (kPa):	*7384*	7347	7313	7263	7230	7180	7018	6860	6705	6553	6404	6044	5702	5062	4480	3949	3467	2634	1958	1419	999	679	575
Gas saturation density:	*468*	400	375	358	345	335	304	282	265	250	238	212	191	159	134	114	97	71	51	37	26	18	15
Liquid saturation density:	*468*	533	557	575	589	601	636	661	681	699	714	748	776	823	863	898	929	984	1032	1076	1116	1155	1170

Density of liquid carbon dioxide (kg/cu. m) at various system pressures (in kPa as column headings)

System temperature (°C)	(K)	*7384*	7347	7313	7263	7230	7180	7018	6860	6705	6553	6404	6044	5702	5062	4480	3949	3467	2634	1958	1419	999	679	575
31.2	***304.2***	*468*	x	x	x	x	x	x	x	x	x	x	x	x	x	x	x	x	x	x	x	x	x	x
31	304.0	582	533	x	x	x	x	x	x	x	x	x	x	x	x	x	x	x	x	x	x	x	x	x
30.75	303.8	610	588	557	x	x	x	x	x	x	x	x	x	x	x	x	x	x	x	x	x	x	x	x
30.5	303.5	628	618	606	575	x	x	x	x	x	x	x	x	x	x	x	x	x	x	x	x	x	x	x
30.25	303.3	641	631	623	606	589	x	x	x	x	x	x	x	x	x	x	x	x	x	x	x	x	x	x
30	303.0	653	647	641	630	621	601	x	x	x	x	x	x	x	x	x	x	x	x	x	x	x	x	x
29	302.0	686	683	680	675	671	665	636	x	x	x	x	x	x	x	x	x	x	x	x	x	x	x	x
28	301.0	710	708	706	702	700	696	681	661	x	x	x	x	x	x	x	x	x	x	x	x	x	x	x
27	300.0	730	728	726	723	722	719	709	697	681	x	x	x	x	x	x	x	x	x	x	x	x	x	x
26	299.0	746	745	743	741	740	738	730	721	711	699	x	x	x	x	x	x	x	x	x	x	x	x	x
25	298.0	761	760	759	757	756	754	747	740	733	724	714	x	x	x	x	x	x	x	x	x	x	x	x
22.5	295.5	792	791	791	789	788	787	783	778	773	768	763	748	x	x	x	x	x	x	x	x	x	x	x
20	293.0	819	818	817	816	816	815	811	808	804	801	797	787	776	x	x	x	x	x	x	x	x	x	x
15	288.0	862	862	861	861	860	860	857	855	853	850	848	842	836	823	x	x	x	x	x	x	x	x	x
10	283.0	899	898	898	898	897	897	895	893	892	890	888	884	880	871	863	x	x	x	x	x	x	x	x
5	278.0	931	930	930	930	929	929	928	926	925	924	922	919	916	910	904	898	x	x	x	x	x	x	x
0	273.0	959	959	959	959	958	958	957	956	955	954	953	950	948	943	938	933	929	x	x	x	x	x	x
-10	263.0	1010	1010	1010	1009	1009	1009	1008	1007	1007	1006	1005	1003	1001	998	995	992	989	984	x	x	x	x	x
-20	253.0	1055	1054	1054	1054	1054	1054	1053	1053	1052	1051	1051	1049	1048	1045	1043	1041	1039	1035	1032	x	x	x	x
-30	243.0	1095	1095	1095	1095	1095	1095	1094	1094	1093	1093	1092	1091	1090	1088	1086	1084	1083	1080	1078	1076	x	x	x
-40	233.0	1134	1134	1134	1134	1133	1133	1133	1133	1132	1132	1131	1130	1129	1128	1126	1125	1123	1121	1119	1118	1116	x	x
-50	223.0	1170	1170	1170	1170	1170	1170	1170	1169	1169	1169	1168	1167	1167	1165	1164	1163	1162	1160	1158	1157	1156	1155	x
-54	219.0	1184	1184	1184	1184	1184	1184	1184	1183	1183	1183	1182	1182	1181	1180	1178	1177	1176	1174	1173	1172	1171	1170	1170

Appendix C

ANALYTICAL MODELS OF TEMPERATURE CONTROL SYSTEM PERFORMANCE

Appendix C: ANALYTICAL MODELS OF TEMPERATURE CONTROL SYSTEM PERFORMANCE

Four analytical models of TCS performance have been developed to understand design trade-offs and allow for scoping calculations of equipment size. Key parameters of the model are shown in Fig. C.1.

C.1 HEIGHT OF A TCS

The height of the TIPACS is determined by two parameters: the heights of the RCHTS and TCS, respectively. The RCHTS height is dependent on the application and the necessary elevation for efficient natural circulation. The TCS height is a function of the RCHTS height, the coldest expected external temperature (T_E) and the temperature of initial RCHTS operation (T_o).

The relative heights of the RCHTS and the TCS can be parametrically determined. Consider TIPACS of unit height, the RCHTS with fractional height (X), and the TCS with fractional height ($1 - X$). The TCS height is the transition interface zone between hot and cold fluid in the exterior TCS zone (h_T), the static hydraulic head between hot fluid and cold fluid (h_s), and some additional volume for piping (h_p). For simplified analysis, the transition zone (h_T) and the piping zone (h_p) can be assumed to have zero height. This assumption is a reasonable approximation for large systems where h_T and h_p tend to have fixed heights independent of system size. Figure C.1 is a schematic of a TIPACS with critical dimensions.

The static head is at its maximum when the difference in densities of the fluid in the interior and external zones are greatest. Maximum external fluid density occurs under the coldest external design temperature (T_E). For a cold climate, this might be -40°C. The internal fluid has the lowest density when it is at the highest temperature (T_o), just before the TIPACS begins operation. T_o is at the critical temperature or below.

For any given coldest design point, external temperature T_E and interior startup temperature T_o, X can be calculated by a force balance of fluids on the exterior side of the TIPACS and the interior side of the TIPACS at the bottom of the TIPACS.

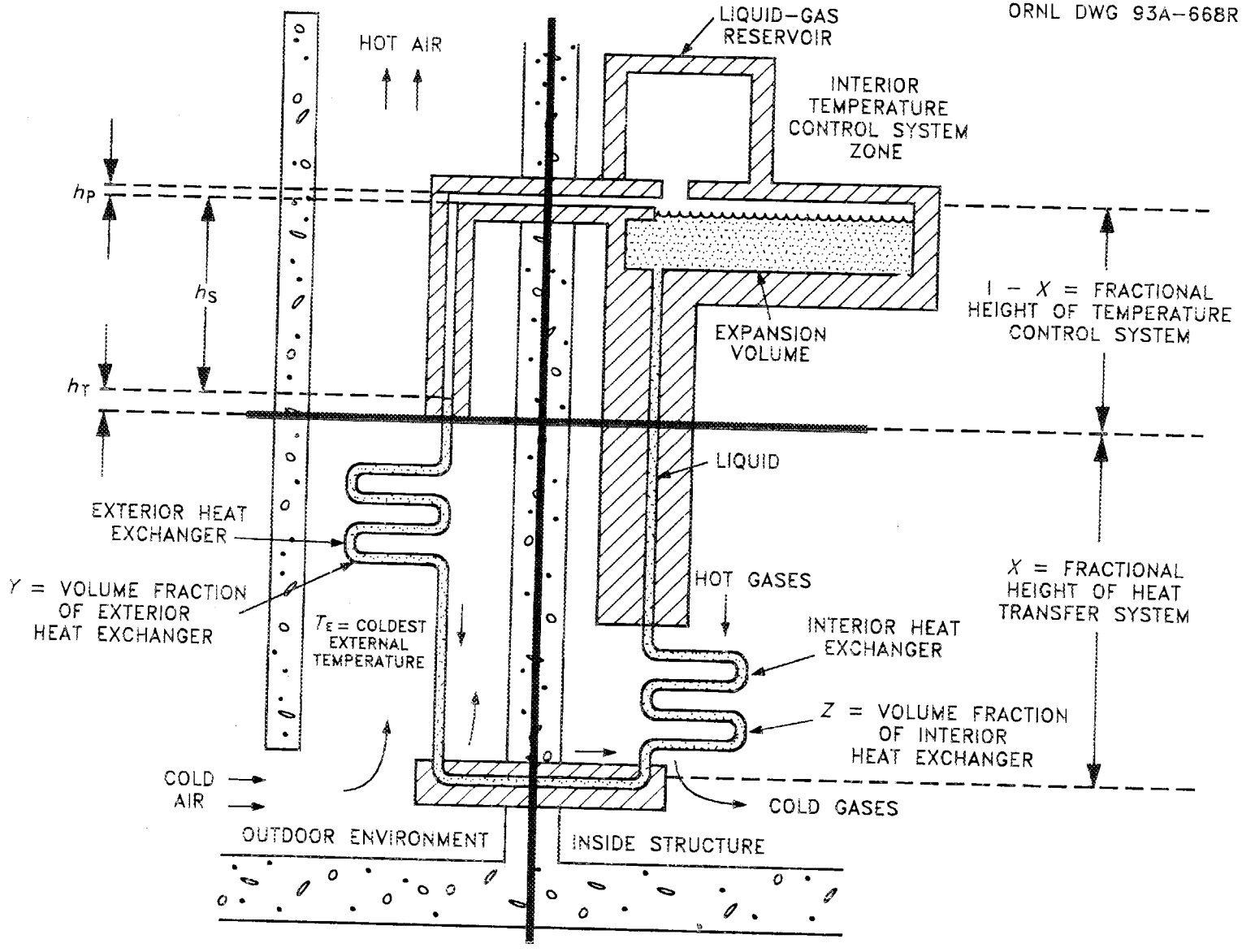

Fig. C.1. Schematic of TIPACS model parameters.

$$X\rho_{L,T_E,P_o} + (1 - X)\ \rho_{G,T_o,P_o} = [1]\ \rho_{L,T_o,P_o} \quad , \qquad \text{Eq. (C.1)}$$

where

X	=	the relative height of cold liquid = relative height of RCHTS,
$1 - X$	=	the relative height of hot gas above cold liquid =the height of TCS,
$\rho_{L,T_E P_o}$	=	the density of liquid at temperatures T_E and pressure P_o,
$\rho_{G,T_o P_o}$	=	the density of gas at temperature T_o and pressure P_o,
$\rho_{L,T_o P_o}$	=	the density of liquid at temperature T_o and pressure P_o.

This equation includes several assumptions. The liquid and gas densities do not change significantly over the height of the TIPACS because of the weight of the fluid. This is valid—except when very close to the critical point. For TIPACS heights in meters, the pressure from the fluid weight is <1% of the system pressure. It also assumes that hot-cold transition zones are flat surfaces rather than temperature transition zones over some distances.

Figure C.2 shows the relative height (X) of the RCHTS for different designs of TIPACS when using CO_2 as the fluid. The horizontal axis shows different minimum external design temperatures between -40°C and T_c. Practical designs have T_E between 0 and -40°C, depending on the climate. The full range of temperatures is shown because it shows how h_s changes with temperature.

The design lines for different initial operating temperatures (T_o) are shown. For example, if the exterior minimum design temperature is -40°C and the design operating temperature (T_o) is 25°C, the RCHTS height is 53% of the total TIPACS height, with the TCS being 47% of the total TIPACS height.

Two separate effects occur as T_o varies. First, the density of the hot, liquid CO_2 decreases rapidly as the critical temperature (T_c) is approached. This tends to increase the height of the TCS zone with the relative height of the RCHTS decreasing as T_o is changed from 15 to 25 to 30°C. Second, for any given T_o (15, 25, or 30°C), the relative height of the RCHTS does not significantly change over minimum exterior temperatures

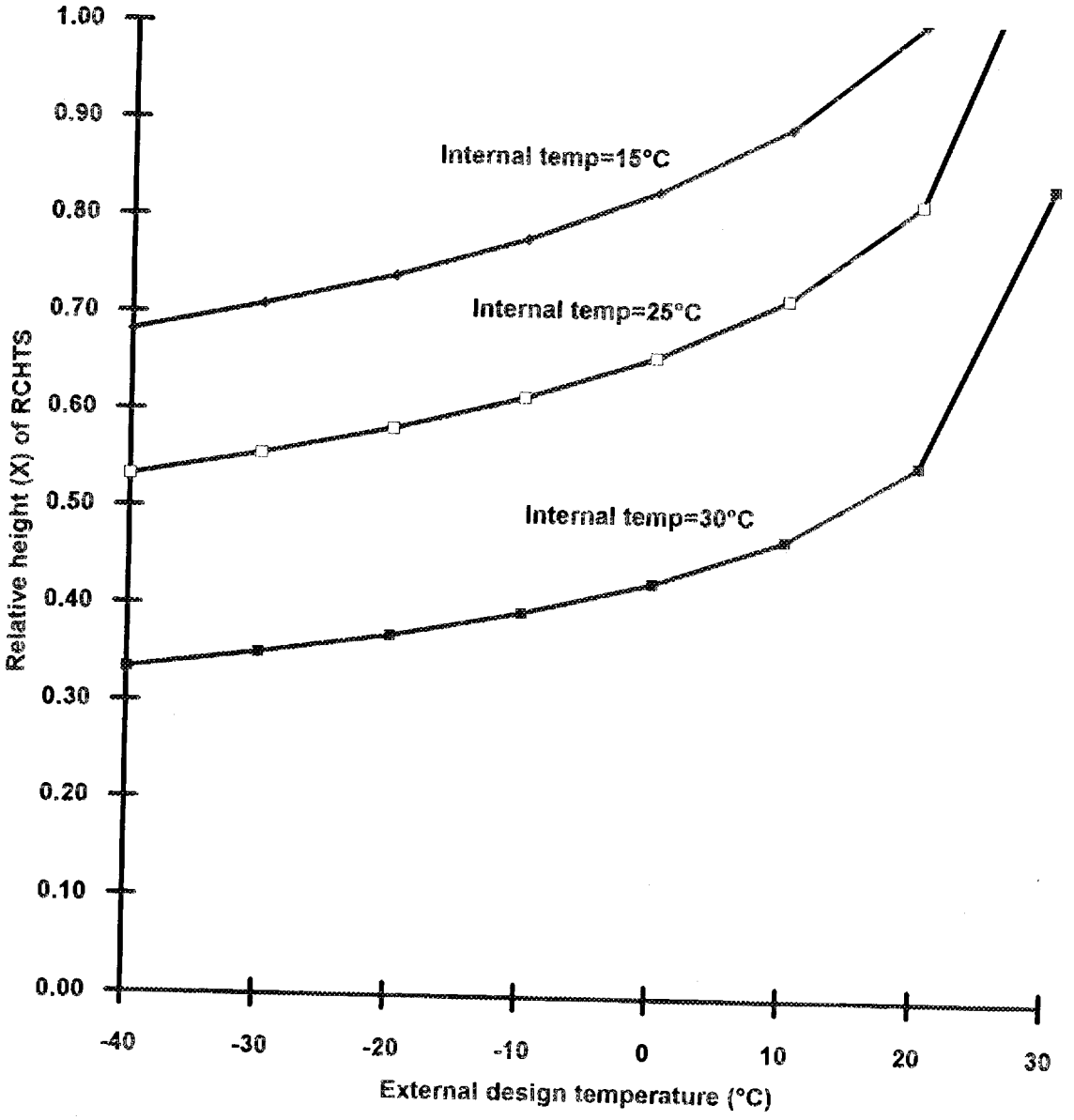

Fig. C.2. Relative height of RCHTS vs external design temperatures.

from −40 to 0°C. Note: To obtain T_o less than the critical temperature, the expansion reservoir must be reduced in size while the liquid-gas reservoir (Fig. C.1) is expanded in size. The combined volume of these two reservoirs is a constant. The reservoirs can be combined into a single reservoir where the exit to the reservoir is at a particular elevation on the side.

The design of TIPACS can be modified to minimize its height by reducing the hydraulic-pressure height of the RCHTS and, hence, the TCS (Fig. C.3). This is not required for current MHTGR designs but is an option if these were major reconfigurations of plant design. The RCHTS is divided into an upper and a lower section at the bypass flow connector. The bypass connector is a connection between the interior and external RCHTS zone. In this configuration, the lower RCHTS does not influence the sizing of the height of the TCS. The lower RCHTS looks like a dead-end, constant temperature, leg. The bypass connector flow creates isothermal conditions in the lower RCHTS leg with a static pressure balance between the interior and exterior RCHTS at the level of the connector. Calculations based on the previous equation start at this level.

If the bypass connector flow is small and the bypass connector contains a fluidic diode, it can reduce the height of the TCS without significantly altering the behavior of the RCHTS when the system is operating. In a standby mode, very low flows are necessary to ensure zero hydraulic gradient across the bypass connector. The system has static conditions. With zero hydraulic gradient at this point, the height of the TCS is determined by the height of the upper RCHTS zone. When the RCHTS is operating, there are large flows around the system and large hydraulic gradients. The bypass connector is essentially like a small leak between two zones in a natural-circulation loop. The leak effect can be further reduced by the addition of a fluidic diode. Fluidic diodes are no-moving-parts components with the characteristic that flow allowed in one direction is 10 to 100 times as much as that allowed in the other direction given a constant pressure drop (Forsberg 1989). Such devices have been developed for special nuclear and chemical applications.

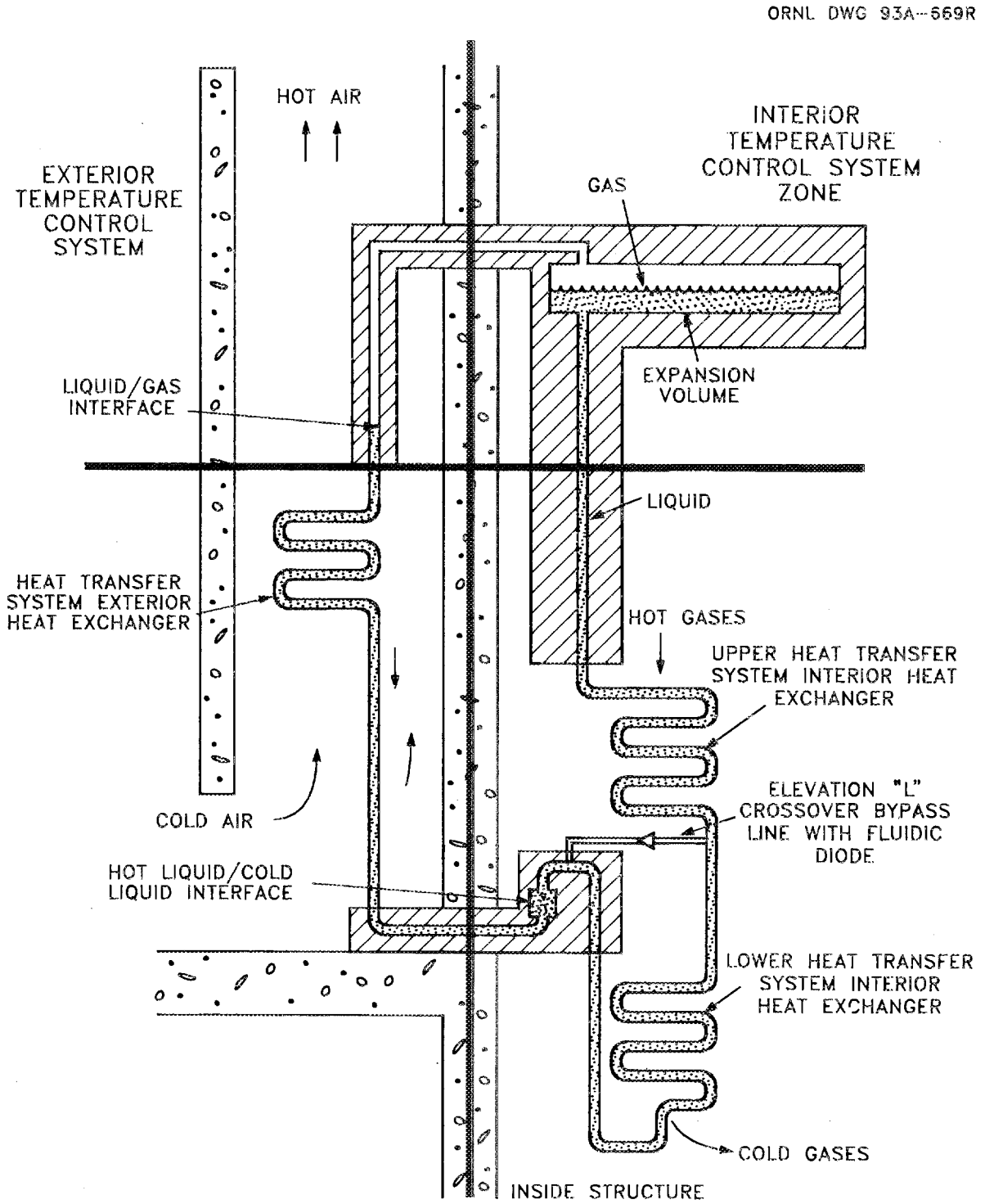

Fig. C.3. TIPACS with bypass line to minimize TCS height.

C.2 RELATIVE VOLUMES OF TCS COMPONENTS

The temperature T_o, at which TIPACS initiates operation, is primarily determined by the relative internal volumes of different components and the lowest expected external design temperature T_E. The key component to be sized is the expansion reservoir. For a parametric analysis of preferred relative volumes of different components, a system of unit internal volume is chosen where Y equals the fractional volume of the external heat exchanger, Z equals the fractional volume of the interior heat exchanger, and $(1 - Y - Z)$ is the fractional volume of the TCS zone. For purposes of understanding, consider a system where the only volume in the TCS zone is the expansion reservoir; i.e., piping volumes and gas-liquid reservoir volumes are small.

The expansion reservoir (TCS zone) is designed so that at the coldest external temperatures (T_E), it is filled with gas, while there is cold liquid to just fill the RCHTS zone (volume fractions $Y + Z$). This assumes cold conditions in both the interior and exterior zones. When TIPACS is just about to start operating, the inventory needed to fill the system is also determined by the coldest external temperature. The external heat exchanger with volume fraction Y must be filled with cold liquid. The remainder of the system with volume fraction $(1 - Y)$ must have fluid at the critical temperature, pressure, and density to provide the single-phase RCHTS. The mass of fluid under both conditions in the system must be equal; hence, a mass balance can be made. The mass of liquids and gases under coldest standby conditions equals the mass of fluids at point of operation on the coldest day:

$$(Y + Z)\ \rho_{L,T_E,P_E} + (1 - Y - Z)\ \rho_{G,T_E,P_E} = Y\ \rho_{L,T_E,P_c} + (1 - Y)\ \rho_c \quad , \quad \text{Eq. (C.2)}$$

where

ρ_{L,T_E,P_E} = the density of liquid at coldest temperature (T_E) and corresponding pressure for saturated system at P_E,

ρ_{G,T_E,P_E} = the density of gas at coldest temperature (T_E) and corresponding pressure for saturated system at P_E,

ρ_{L,T_E,P_c} = the density of liquid at coldest temperature (T_E) and pressure of fluid at the critical point, and

ρ_c = the density of fluid at the critical point.

Figure C.4 shows the external heat exchanger volume fraction Y vs minimum external temperature T_E for different internal heat exchanger volume fractions Z. (Note: The equations were derived assuming the minimum fluid in the system.) The TIPACS can operate with higher fluid inventories that imply lower temperatures for TIPACS's initial operation. Different inventories of fluid will modify this figure, as will the existence of temperature transition zones (h_T) and piping zones (h_P).

Several observations are noteworthy:

- The TIPACS designs are insensitive to the choice of coldest exterior design temperature T_o. The volume fraction of the exterior heat exchanger is insensitive to the exterior temperatures from -40 to 0°C. This is seen by the almost horizontal lines and reflects the fact that the density of liquid CO_2 does not significantly change over this range.

- The volume of the TCS ($1 - Y - Z$) is basically a function of the internal RCHTS volume fraction. Liquid CO_2 below 0°C expands ~150% when heated to the critical temperature. For example, at -40°C with an exterior heat-exchanger volume fraction of ~0.25 and an interior heat-exchanger volume fraction of 0.3, the TCS volume fraction is ~0.45. This is ~150% of 0.3.

C.3 RELATIVE VOLUMES OF INTERNAL AND EXTERNAL HEAT EXCHANGERS

The initial operating temperature T_o of the TIPACS depends upon the fluid volume fraction Y of the external heat exchangers, the fluid volume fraction Z of the interior heat exchangers, and the exterior ambient temperature T_A. The external heat exchanger has a fixed volume. At T_E, the lowest design temperature conditions, a defined mass of fluid in the internal heat exchanger = $Y\rho_{T_E}$. If the outside temperature T_A increases, the fluid in the external heat exchanger will expand, its density will decrease, and the fluid will be expelled to the rest of the TIPACS. The added liquid will cause the TIPACS to initiate

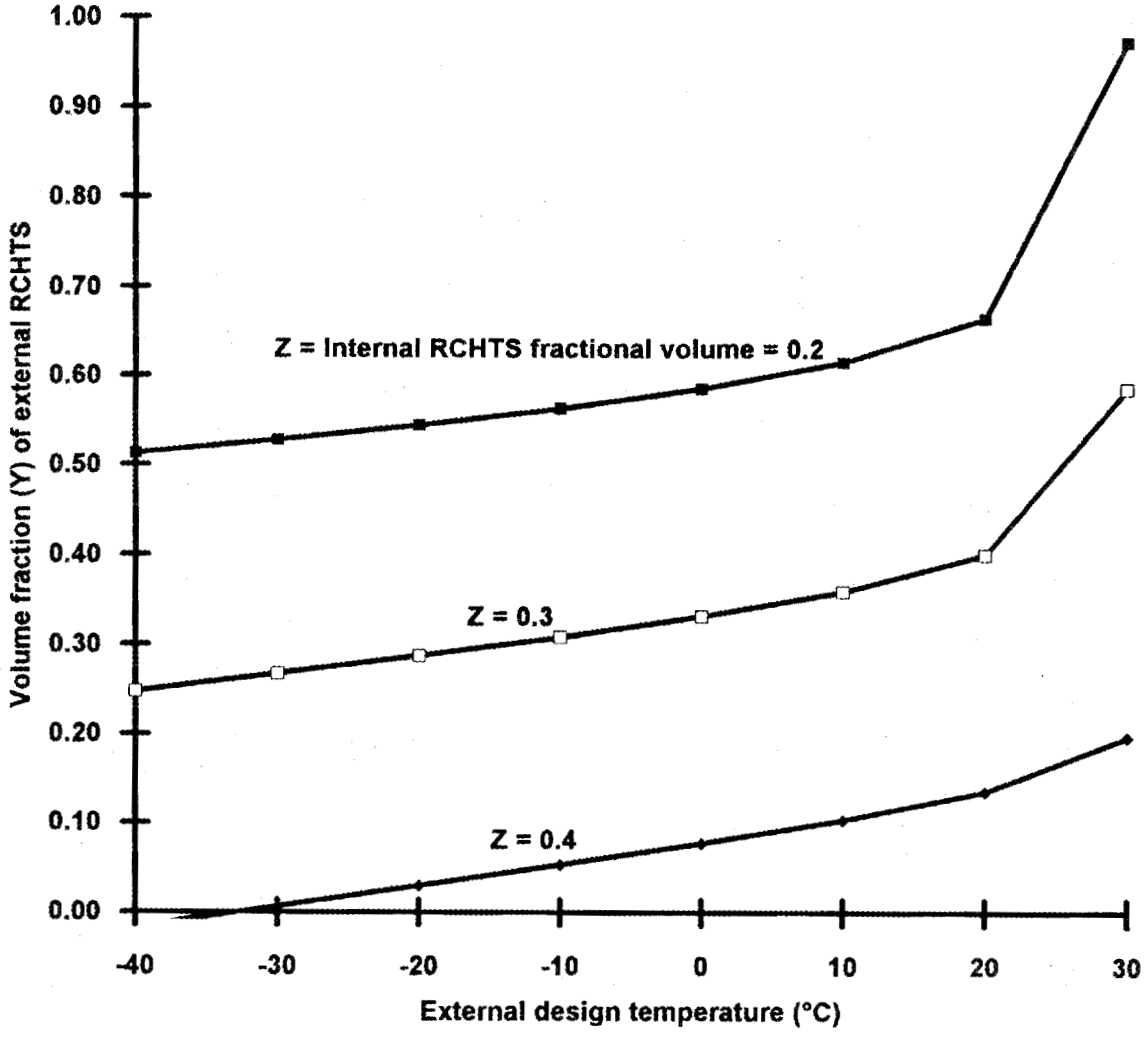

Fig. C.4. Volume fraction (Y) of external RCHTS vs external design temperature for different internal RCHTS volume fractions.

operation at a lower interior temperature. The impact of variable external ambient temperatures and design parameters on TIPACS startup temperature T_s can be parametrically studied.

The quantity of fluid expelled from the exterior heat exchanger as the ambient temperature increases above the lowest design point temperature is $Y\,[\rho_{T_E} - \rho_{T_A}]$. If this fluid is uniformly spread over the rest of the TIPACS internal volume $(1 - Y)$, it increase the average density by $Y\,(\rho_{T_E} - \rho_{T_A}) / (1 - Y)$. The interior fluid density of the TIPACS at startup is ρ_{To}. If there were no external variation in temperature, T_o would equal T_c, and the interior fluid density would be the density at the critical point $\sim\rho_c$. The actual density of the interior fluid of the TIPACS at startup (ρ_s) is the idealized startup fluid density plus what is expelled from the exterior heat exchanger when its temperature is above T_E:

$$\rho_s = \rho_c + \frac{Y(\rho_{T_E} - \rho_{T_A})}{1 - Y} \quad . \qquad \text{Eq. (C.3)}$$

The liquid density at startup can be calculated for any given exterior heat-exchanger volume fraction Y and any exterior heat exchanger temperature T_A. Given the density, the corresponding startup temperature T_s is determined given the restrictive assumptions previously discussed.

An evaluation of Eq. (C.3) shows two phenomena.

- The choice of the coldest design temperature has little impact on this feature of the design because ρ_{T_E} does not vary significantly from ~40 to 0°C.

- For small-volume-fraction external heat exchangers ($Y < 0.3$), this phenomenon alters startup temperatures by at most a few degrees. The reason for the small effect is that most of the expansion of CO_2 before the critical point occurs within a few degrees celsius of the critical point. Fluid that is expelled from the external heat exchanger is expelled to the expansion reservoir and equilibrate at expansion reservoir temperature. A small addition of fluid has little impact because most of the expansion in the expansion reservoir occurs just below the critical point.

C.4 SYSTEM PRESSURE

The system pressure is determined by (1) the design of TIPACS, (2) the external and exterior temperatures, and (3) the fluid inventory. Exact system pressure is difficult to calculate during TIPACS's operations because it depends on the temperatures of each volume of fluid in the system where temperatures vary with location. Representative average pressures can be calculated for different temperatures, assuming the same average temperature represents the system as a whole.

Equation (C.2) shows the mass of fluid for the TIPACS of a unit volume; hence, each side of the equation calculates the average density (ρ_A) of the fluid in the system. This implies that

$$\rho_A = Y \rho_{L,T_E,P_c} + (1 - Y)\, \rho_c \quad . \qquad \text{Eq. (C.4)}$$

Given the average fluid density, the operating pressure is directly determined from the equation of state for any assumed temperature. Figure C.5 shows the CO_2 density vs temperature for various pressures. For any given TIPACS system with a fixed average density, the pressure for the corresponding temperatures is on a horizonal line, as shown in Fig. C.5. Figure C.6 shows the TIPACS's pressures when CO_2 is the working fluid for different exterior heat exchanger volume fractions (Y) and different average temperatures. [Note: The results shown in Fig. C.6 depend on the assumptions used to derive Eq. (C.2) and Eq. (C.4)]. From Eq. (C.4) and Fig. C.6, several conclusions can be drawn.

- There is a strong incentive to minimize the exterior heat-exchanger volume to minimize maximum system pressure. Under the most severe conditions for initiation of TIPACS operation, the external heat exchanger is filled with cold, liquid CO_2. This liquid CO_2 increases system pressure as it warms up. The external heat exchanger volume fraction should be kept below $Y = 0.25$.

- With a fixed-volume system, pressure can increase significantly with average operating temperature.

- For the expected range of operating conditions, the pressures are below those of steam in typical coal power plants with temperatures far below power-plant-boiler temperatures. No unusual difficulties of design would be expected with such operating conditions.

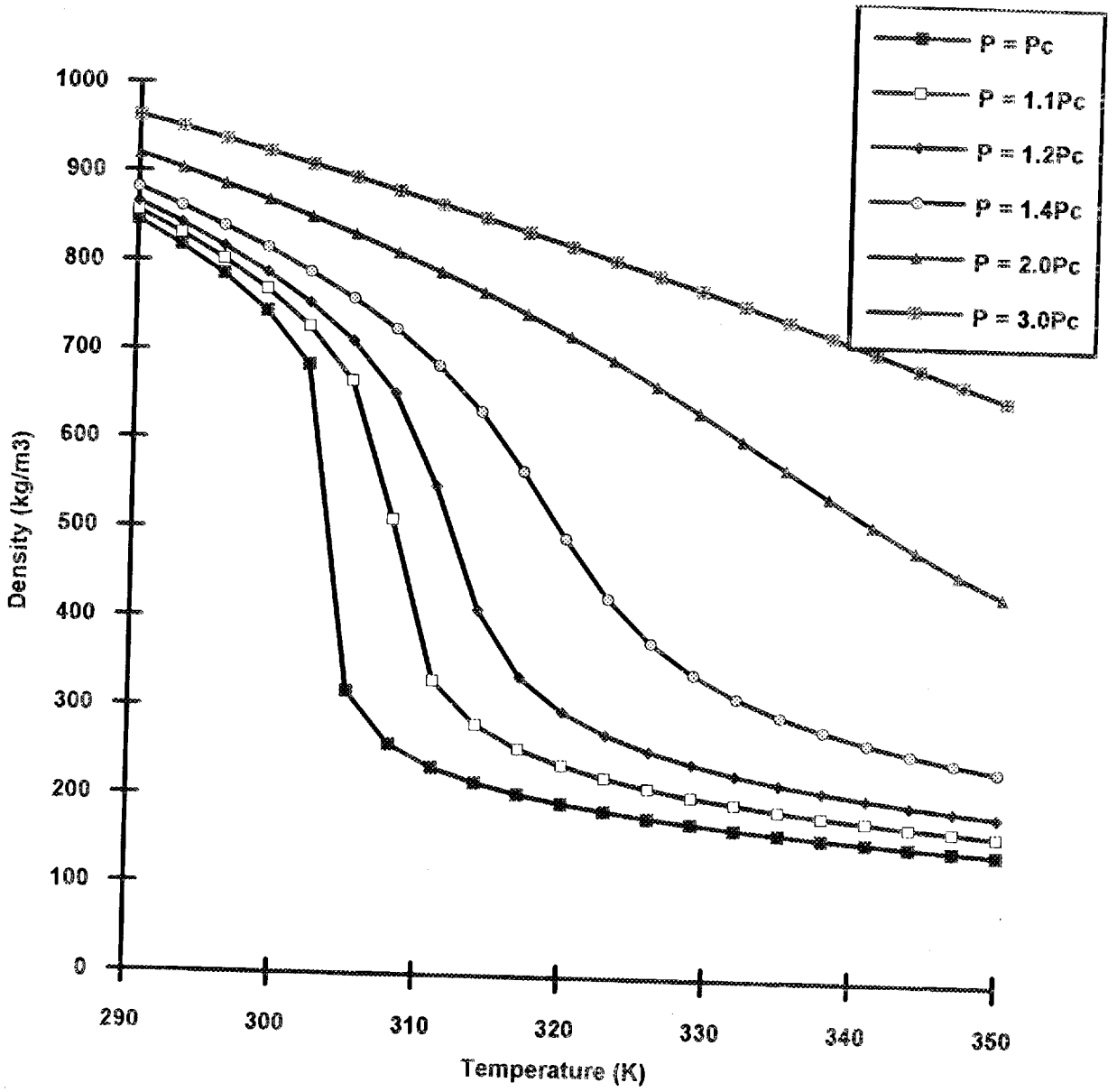

Fig. C.5. Density for CO_2 at various pressures near the critical temperature (304 K).

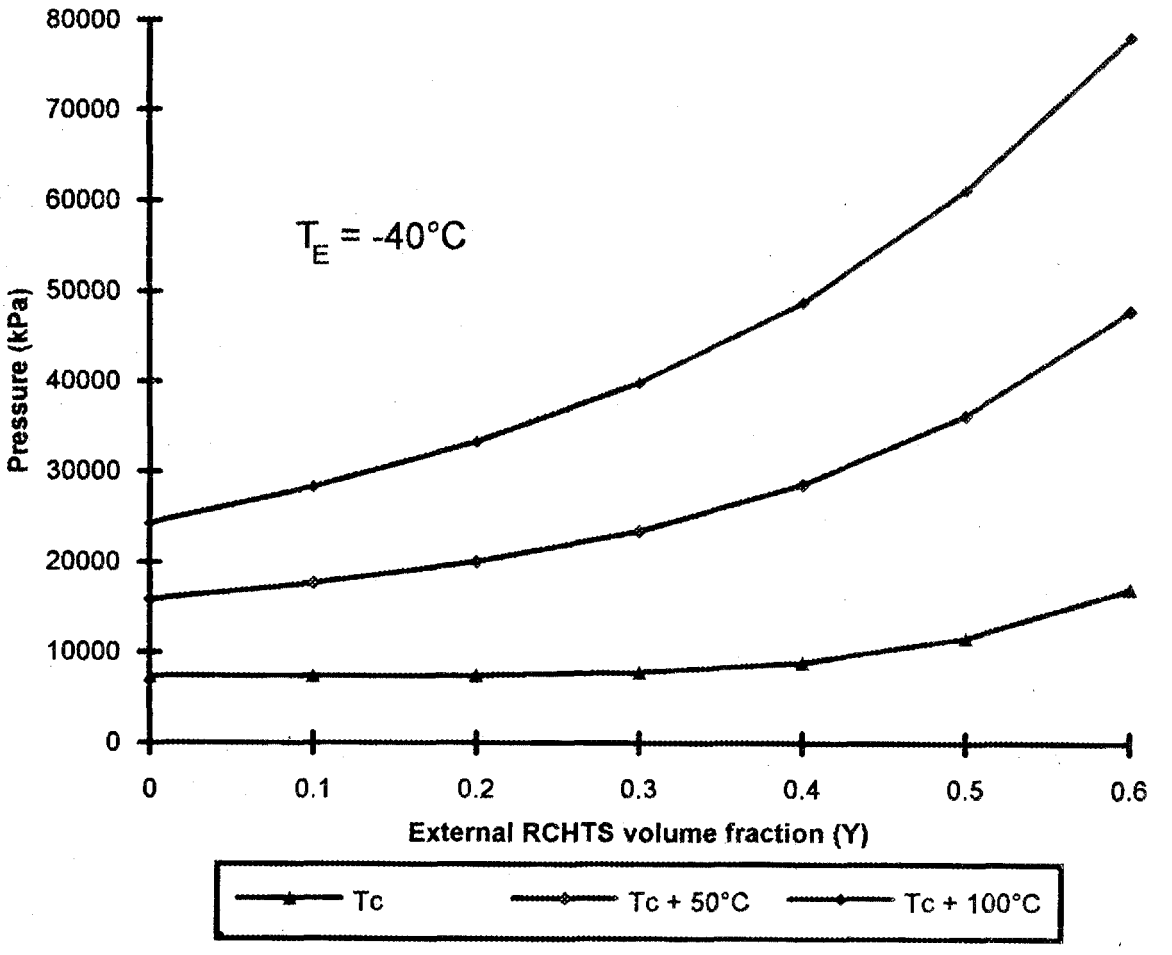

Fig. C.6. Pressure vs external RCHTS volume fraction (*Y*) at various operating temperatures.

Appendix D

ANALYSIS OF RCHTS

Appendix D: ANALYSIS OF RCHTS

D.1 INTRODUCTION

For natural convection flow, a fluid is induced to move by a buoyancy force caused by different densities which themselves are caused by different temperatures. The temperature levels throughout the system that result in density differences that induce buoyancy forces must balance with the disipative forces for fluid circulation. For TIPACS, there are two natural convection loops—the CO_2 closed loop—(removing heat from the reactor vessel cavity) and the air open loop—(rejecting heat to ambient). These two loops are coupled by the external heat exchanger. Thus, the flows of heat and fluid in one loop will affect the other. Also, the conservation of momentum and conservation of energy equations are coupled in natural convection flow. An iterative technique is used here to achieve this coupling. The following analysis and results from a simplified computational model will demonstrate this coupled effect, particularly on the supercritical CO_2 in the high-pressure, internal loop.

As in an earlier version of the RCCS, only a quadrant, or one-fourth, of the periphery of the reactor cavity will be modeled (Conklin 1990). The internal heat exchanger (riser) is modeled with an arbitrary number of computational nodes representing the riser length. Eight axial nodes gave a good representation of the temperature profile during the calculations.

D.2 GOVERNING EQUATIONS

Two simplifications are made to model the heat transfer and fluid flow in the TIPACS. The first is the assumption of steady-state conditions—this assumes that the overall heat transfer process from the reactor vessel and ultimately to the ambient air is controlled by the reactor-vessel temperature. Thus, the dynamics, or time-dependent behavior, of the TIPACS are not considered for this preliminary model. The second assumption is that the heat transfer and fluid flow can adequately be described as a one-dimensional process; that is, only spatial variations in the flow direction are considered.

Because the flow in the internal heat exchanger is driven by the radiant heat from the reactor vessel, the velocity and temperature profile normal to the flow direction may be skewed toward the hotter, or reactor-vessel, side of the tubes. However, the spatial variations of temperature and flow, entry length, or other two-dimensional transverse flow effects are neglected for this simple model. The flows in the TIPACS are modeled as a one-dimensional, turbulent convection process driven by body forces caused by density differences between the vertical portions. This assumption should be justified by an appropriate experiment using a fluid at or slightly above the critical point.

The flow of air through the external heat exchanger and out the air chimney is modeled with the algebraic, spatially integrated, one-dimensional momentum conservation equation originally developed by Ball (1976) for modeling the helium coolant flow in the MHTGR cooling channels. This equation, as modified for the air flow in the stack of the external heat exchanger, is given by the following:

$$\dot{m}_{air}^2\left(\frac{\Re}{P}\right)\left(\frac{T_{hx,out}-T_{hx,in}}{A_{hx,fr}^2}+\frac{\overline{T}_{hx}}{A_{hx,ff}^2}\frac{1}{2}f\frac{L_{hx}}{D_{hx,hyd}}\right)-g\left(\frac{P}{\Re}\right)\frac{L_{stack}}{T_{stack}}=0 \quad . \qquad \text{Eq. (D.1)}$$

For the external heat exchanger, $A_{hx,fr}$ represents the frontal area, $A_{hx,ff}$ represents the free-flow area, f represents the Moody friction factor, L_{hx} represents the flow length, and $D_{hx,hyd}$ represents the hydraulic diameter. For the air stack above the external heat exchanger, L and T have analogous representations. For simplicity in the air stack, no friction losses and no heat losses are modeled. Thus, the air flow through the external heat exchanger is a balance of the buoyant force generated by the relatively warmer air in the stack and the acceleration and friction forces opposing motion in the heat exchanger.

The heat transferred to the air is calculated by the methods presented by Kays and London (1984). The effectiveness-number-of-transfer-units (ε-NTU) method was used to calculate the heat duty given an arbitrary height, width, and length of the external heat exchanger. For simplicity, the CO_2 flow resistances and heat-transfer coefficient in the

external heat exchanger are modeled at the mean temperature, and variable thermophysical effects are considered. This simplistic assumption should be improved for a more detailed TIPACS model.

The CO_2 flow in TIPACS is modeled with a similar, algebraic, spatially integrated, one dimensional momentum conservation equation. Equation (D.1) was derived for a perfect gas, which is a good assumption for atmospheric air but not for CO_2 near the critical point. Hence, the governing equation for the CO_2 mass flow is:

$$\dot{m}^2_{co_2} \sum_i \frac{1}{2A_i^2} f_i \frac{L_i}{D_i} - g \sum_j \rho_j^2 L_j sign(\dot{m}_j) = 0 \quad , \qquad \text{Eq. D.2}$$

where the subject j represents only the vertical portions of TIPACS. The sign of the flow in the vertical components is present to account for the direction of the buoyancy force caused by the density differences, where downward flow is positive. As for the air flow, this equation represents a balance between the friction and buoyancy forces in TIPACS. Note that for the closed CO_2 loop, the acceleration momentum forces are balanced and do not appear in Eq. (D.2). Also, no minor losses resulting from pipe bends, expansions, or contractions are modeled for simplicity.

The Moody friction factor in Eq. (D.2) is computed with the Blasius approximation (White 1979) as modified for variable properties (Polyakov 1991).

$$f = 0.316 \left(\frac{\dot{m}_{co_2} D_{hyd}}{A \mu} \right)^{-1/4} \left(\frac{\rho_{wall}}{\rho} \right)^{1/3} \left(\frac{\mu_{wall}}{\mu} \right)^{1/5} . \qquad \text{Eq. (D.3)}$$

The heat transferred to the CO_2 in each modeled node of the internal heat exchanger is computed with a conservation of energy equation spatially integrated in the flow direction to give the following:

$$Q_i = \dot{m} \bar{C}_i \left(T_{i,out} - T_{i,in} \right) \quad , \qquad \text{Eq. (D.4)}$$

where the mean specific heat is used for each segment.

Because of convective heat transfer, the CO_2 temperature at the outlet of each node is computed with the exponential approach method developed by Ball (1976), where

$$T_{i,out} = T_{i,in} + \left(T_{wall,i} - T_{i,in}\right)\left[1 - \exp\left(-\frac{hA_i}{\dot{m}\bar{C}}\right)\right] \quad . \qquad \text{Eq. (D.5)}$$

Equation (D.5) is an exact solution of the differential equation for conservation of energy of the CO_2 in the riser, where the metal node temperature is uniform over the node length, the transit time is negligible, and the specific heat can be represented as a bulk mean value.

The heat-transfer coefficient h in Eq. (D.5) for the riser nodes is determined with the relationships presented by Watts and Chou (1982). They introduce a "buoyancy parameter" which has the form

$$\frac{\bar{Gr}_b}{\bar{Re}_b^{2.7}\,\bar{Pr}_b^{1/2}} \quad . \qquad \text{Eq. (D.6)}$$

Watts and Chou (1982) also claim that under variable property conditions in CO_2, the Nusselt number was correlated by

$$Nu_{varp} = 0.0183\,\bar{Re}_b^{0.82}\,\bar{Pr}_b^{1/2}\left(\frac{\rho_{wall}}{\rho_b}\right)^{0.3} \quad . \qquad \text{Eq. (D.7)}$$

This equation must be modified for heated upflow to account for two effects observed in near-critical flows of water and CO_2. If the buoyancy parameter is $>10^{-5}$ and $<\sim 10^{-4}$, there is a degradation in heat transfer because of buoyant effects suppressing near-wall turbulence. In this range, the heat transfer is given by

$$Nu = Nu_{varp}\left(1 - 3000\frac{\bar{Gr}_b}{Re_b^{2.7}\,\bar{Pr}_b^{1/2}}\right)^{0.295} \quad . \qquad \text{Eq. (D.8)}$$

If the buoyancy parameter is $>10^{-4}$, there is an augmentation in heat transfer because the buoyant effects apparently increase near-wall turbulence. In this range, the heat transfer is given by

$$Nu = Nu_{varp}\left(7000\frac{\bar{Gr}_b}{Re_b^{2.7}\,\bar{Pr}_b^{1/2}}\right)^{0.295} \quad . \qquad \text{Eq. (D.9)}$$

These "near-wall" effects that modify the Nusselt number correlation with variable properties exist only in heated upflow (or cooled downflow) for fluids with positive thermal expansion coefficients, and are not present in horizontal flow. Thus, no buoyancy effects are modeled for the horizontal CO_2 flow in the external heat exchanger.

The heat transferred to the riser-tube wall is modeled as purely one-dimensional radiation heat transfer in an annulus. Heat transferred by other mechanisms is typically $<10\%$ of the total heat load. The cross-section of the reactor cavity is modeled as two long, concentric cylinders. The heat flux from the reactor to each of the riser tube nodes, as developed by Conklin (1990), is given by

$$q_i = \frac{\varepsilon_r \varepsilon_i}{\frac{R_i}{R_r}\varepsilon_i + \varepsilon_r - \varepsilon_r \varepsilon_i}\,\sigma\left(T_r^4 - T_i^4\right) \quad . \qquad \text{Eq. (D.10)}$$

This equation represents the radiant heat transferred to each riser node from the reactor vessel. Participating media thermal radiation effects are not considered. If there is a substance in the annulus between the reactor and the risers that can absorb and emit thermal radiation, this equation must be modified to account for the resultant degraded heat transfer. CO_2 is such a radiation participating gas, as is steam.

D.3 SOLUTION METHODOLOGY

The equations representing the air and CO_2 mass flows in a TIPACS, as given by Eqs. (D.1) and (D.2), must balance according to the heat transferred and considering the varying thermophysical properties. To begin, initial riser temperatures and CO_2 and air-mass flows are assigned. First, the heat flux from the reactor is transferred to the riser, with the resulting temperatures of the metal and the flowing CO_2. Then the mass-flow equation is solved for the CO_2 closed loop with the calculated temperatures. Then the external heat-exchanger thermal performance is calculated, yielding outlet temperatures of air and CO_2 given the calculated CO_2 mass flow and specified air-inlet temperature to the heat exchanger. After convergence of the external heat-exchanger air mass flow, the calculated external heat-exchanger CO_2 outlet temperature is then the riser inlet temperature. The iterations are repeated with the new CO_2 temperature, and a new riser temperature distribution and reactor heat load are calculated. The iterations are complete when the CO_2 mass flow computed in one complete internal loop iteration agrees within a specified tolerance of the previous iteration (arbitrarily set to 0.1% for this simple model).

Calculating the heat duty of the external heat exchanger is also an iterative process because (a) the heat duty of the heat exchanger is dependent on the air flow rate through it and (b) the air flow is dependent on the heat duty, as given in Eq. (D.4). Thus, an initial air flow is guessed, and iterations are done with Eq. (D.1) and the ε-NTU relationships until convergence.

All during these flow and heat balance iterations, the algorithms computing the thermophysical properties of CO_2 and air must be invoked. The algorithms presented by Friend (1992) are used for the thermodynamic properties. The algorithms of Hahne (1982) are used for the transport properties. Simpson's rule is used if integration over an appropriate temperature interval is necessary.

Thus, a computational-intensive process results, even for the simple, one-dimensional model as described. If additional modeling detail is needed—which would be the case for an actual design—commensurate computational efforts and facilities are needed.

INTERNAL DISTRIBUTION

1. T. D. Anderson
2. S. J. Ball
3. W. P. Barthold
4. J. M. Begovich
5. C. R. Brittain
6. T. D. Burchell
7. N. E. Clapp
8-12. J. C. Conklin
13. A. G. Croff
14. J. G. Delene
15-19. C. W. Forsberg
20. E. C. Fox
21. D. H. Fry
22. W. Fulkerson
23. W. A. Gabbard
24. U. Gat
25. R. K. Genung
26. F. J. Homan
27. C. R. Hudson
28. H. Jones
29. J. E. Jones, Jr.
30. M. J. Kania
31. H. T. Kerr
32. O. F. Kimball
33. T. S. Kress
34. S. B. Ludwig
35. D. W. McDonald
36. L. E. McNeese
37. G. E. Michaels
38. D. L. Moses
39. B. F. Myers
40. E. Newman
41. J. P. Nichols
42. J. Z. Palmer
43. J. T. Parks
44. C. E. Pugh
45-49. W. J. Reich
50. P. L. Rittenhouse
51. O. M. Stansfield
52. D. B. Trauger
53. R. E. Uhrig
54. J. D. White
55. R. P. Wichner
56. B. A. Worley
57. R. G. Wymer
58. A. Zucker
59-60. Central Research Library
61-62. Laboratory Records
63. Laboratory Records-RC
64. ORNL Y-12 Technical Library
65. Document Reference Section
66. ORNL Patent Section

EXTERNAL DISTRIBUTION

67. Paul E. Allaire, Department of Mechanical, Aerospace, and Nuclear Engineering, University of Virginia, Charlottesville, VA 22903.

68. L. F. Blankner, U.S. Department of Energy, Oak Ridge Operations Office, Oak Ridge, TN 37831.

69. Linden Blue, General Atomics, P.O. Box 85608, San Diego, CA 92186-9784.

70. Albert E. Bolon, Department of Nuclear Engineering, University of Missouri-Rolla, 102 Fulton Hall, Rolla, MO 65401-0249.

71. Evelyn Bolton, Document Control Section, U.S. Department of Energy, Office of Scientific and Technical Information, P.O. Box 62, Oak Ridge, TN 37831.

72. George C. Bramblett, MHTGR Project Division, General Atomics, 3550 General Atomics Court, P.O. Box 85608, San Diego, CA 92186-9784

73. Larry Brey, PDCO-W, P.O. Box 85608, San Diego, CA 92186-9784.

74. E. C. Brolin, U.S. Department of Energy, NE-1, 1000 Independence Avenue, Washington, DC 20585.

75. Gilbert J. Brown, Program in Nuclear Engineering, Department of Chemical and Nuclear Engineering, University of Massachusetts-Lowell, One University Avenue, Lowell, MA 01854.

76. D. B. Bullen, Nuclear Engineering Program, Department of Mechanical Engineering, Iowa State University, 107 Nuclear Engineering Laboratory, Ames, IA 50011-2241.

77. H. J. Bruschi, General Manager, Advanced Technology Westinghouse Electric Corporation, Westinghouse Energy Center, P.O. Box 355, Pittsburgh, PA 15230-0355.

78. S. A. Caspersson, ABB Combustion Engineering Nuclear Power, 1000 Prospect Hill Road, M/S 9354-0422, Windsor, CT 06095-0500.

79. Ivan Catton, Building 46-147N Eng IV, Mechanical, Aerospace, and Nuclear Engineering Department, School of Engineering and Applied Science, University of California-Los Angeles, 405 Hilgard Avenue, Los Angeles, CA 90024-1597.

80. V. Charyulu, College of Engineering, Lillibridge Engineering Laboratory, Idaho State University, P.O. Box 8060, Pocatello, ID 832909.

81. Frank Y. Chen, Office of Nuclear Performance Assessment, MS EH-11, United States Department of Energy, Germantown, MD 20874.

82. Richard N. Christensen, Nuclear Engineering Program, Ohio State University, 206 West 18th Avenue, Columbia, OH 43210.

83. David D. Clark, Cornell University, Ward Laboratory of Nuclear Engineering, Ithaca, NY 14853-7701.

84. John C. Cleveland, Division of Nuclear Power, International Atomic Energy Agency, A2572, Wagramerstrasse 5, P.O. Box 100, A1400, Vienna, Austria.

85. J. P. Cook, ABB Combustion Engineering Nuclear Power, 1201 Riverfront Parkway, Room 1023A, Building #3, M/S 970-3, Chattanooga, TN 37402.

86. Michael L. Corradini, Department of Nuclear Engineering and Engineering Physics, 151 Engineering Research Boulevard, University of Wisconsin-Madison, Madison, WI 53706.

87. B. Demars, U.S. Department of Energy, Naval Reactors Office (NE-60), 3N06/NR Crystal City, Arlington, VA 22202.

88. Dave A. Dilling, Bechtel National, Inc., 50 Beale St., P.O. Box 193965, San Francisco, CA 94119-3965.

89. H. Lee Dodds, Nuclear Engineering Department, University of Tennessee-Knoxville, 315 Pasqua Engineering Building, Knoxville, TN 37996-2300.

90. J. H. Donohew, U.S. Nuclear Regulatory Commission, MS-11D23, 1 White Flint North, 11555 Rockville Pike, Rockville, MD 20551.

91. Donald J. Dudzaik, North Carolina State University, Department of Nuclear Engineering, 1110 Burlington Laboratories, Raleigh, NC 27695-7909.

92. N. Dean Eckhoff, Kansas State University, Department of Nuclear Engineering, Ward Hall, Manhattan, KS 66506-2503.

93. Donald F. Elger, Nuclear Engineering Program, Department of Mechanical Engineering, University of Idaho, Moscow, ID 83843.

94. S. El-Safwany, U.S. Department of Energy, San Francisco Operations Office, 1301 Clay Street, Oakland, CA 94612-5208.

95. M. M. El-Zeftawy, U.S. Nuclear Regulatory Commission, MS-P315, 1717 H. Street, NW, Washington, DC 20555.

96. Gilbert A. Emmert, Department of Nuclear Engineering and Engineering Physics, 151 Engineering Research Boulevard, Madison, WI 53706.

97. M. Farr, Department of Nuclear and Energy Engineering, University of Arizona, Tucson, AZ 85721.

98. Mark Forsell, General Atomics, P.O. Box 85608, San Diego, CA 92186-9784.

99. T. Kenneth Fowler, University of California, Department of Nuclear Engineering, Berkeley, CA 94720.

100. Kermit L. Garlid, University of Washington, 303 Benson Hall, BF-20, Department of Nuclear Engineering, Seattle, WA 98195.

101. Zuying Gao, Institute of Nuclear Energy Technology, Tsinghua University, P.O. Box 1021, Beijing 102201, China.

102. S. Ghose, Bechtel Group Inc., 50 Beale Street, P.O. Box 193965, San Francisco, CA 94119-3965.

103. Dan Giessing, U.S. Department of Energy, NE-42, 1000 Independence Avenue, Washington, DC 20585.

104. Pierre J. Godbout, Energy Engineering Institute, Campus de L'Université de Montreal, Ecole Polytechnique de Montreal, Montreal, Quebec, Canada H3C 3A7.

105. Michael W. Golay, Department of Nuclear Engineering, Building 24-102, Massachusetts Institute of Technology, 77 Massachusetts Avenue, Cambridge, MA 02139-4307.

106. Sim Golen, Nuclear Programs, Bechtel National, Inc., 50 Beale St., P.O. Box 193965, San Francisco, CA 94119.

107. A. A. Harms, Department of Engineering Physics, McMaster University, 1280 Main Street, West, Hamilton, Ontario, Canada L8S 4L7.

108. Makato Hishida, Japan Atomic Energy Research Institute, 319-11 Ibaraki-ken, Naka-gun, Tokai-mura, Japan.

109. M. H. Holmes, Public Service Company of Colorado, Fort St. Vrain Nuclear Generating Station, 16805 Weld County Road 19 ½, Platteville, CO 80651.

110. Richard Ireland, NUS Corporation, 910 Clopper Road, Gaithersburg, MD 20878-0962.

111. Barclay G. Jones, University of Illinois, 103 S. Goodwin Avenue, Department of Nuclear Engineering, Urbana, IL 61801.

112. H. Jones, U.S. Department of Energy, Contracts Management Office, San Francisco Operations Office, 1301 Clay Street, Oakland, CA 94612-5208.

113. Pete Karcz, HTGR Program, U.S. Department of Energy, NE-451, 19901 Germantown Road, Germantown, MD 20874.

114. Martha Kass, Nuclear and Fusion Programs, U.S. Department of Energy, P.O. Box 2008, Oak Ridge, TN 37831.

115. Paul Kasten, 341 Louisiana Avenue, Oak Ridge, TN 37830.

116. Mujid S. Kazimi, Massachusetts Institute of Technology, Department of Nuclear Engineering, 77 Massachusetts Avenue, Bldg. 24-102, Cambridge, MA 02139.

117. J. M. Kendall, PDCO, P.O. Box 85608, San Diego, CA 92186-9784.

118. Thomas W. Kerlin, University of Tennessee-Knoxville, Nuclear Engineering Department, 315 Pasqua Building, Knoxville, TN 37996-2300.

119. Edward H. Klevans, The Pennsylvania State University, Nuclear Engineering Department, 231 Sackett Building, University Park, PA 16802.

120. L. Kovach, NUCON, P.O. Box 29151, Columbus, OH 43229.

121. P. G. Kroeger, Reactor Analysis Division, Brookhaven National Laboratory, Building 475-B, Upton, NY 11973.

122. D. J. Krommenhoek, Knolls Atomic Power Laboratory, Building D-2, Room 121, P.O. Box 1072, Schenectady, NY 12301.

123. Jay F. Kunze, University of Missouri-Columbia, Nuclear Engineering Program, E2433 Engineering Building, East, Columbia, MO 65211.

124. Jurgen Kupitz, Division of Nuclear Power, A 2572, International Atomic Energy Agency HQ, Wagramerstrasse 5, A-1400, Vienna, Austria.

125. N. Kuzavkov, OKB Mechanical Engineering, Burnakovsky Proezd 15, 603 603 Nizhny Novgorod 74, Russian Federation.

126. Richard T. Lahey, Jr., Department of Nuclear Engineering and Engineering Physics, Rensselaer Polytechnic Institute, Troy, NY 12180-3590.

127. Edward N. Lambremont, Nuclear Science Center, Louisiana State University, Baton Rouge, LA 70803-5820.

128. L. Gary Leal, University of California, Department of Chemical and Nuclear Engineering, Santa Barbara, CA 93106.

129. Richard Lester, Department of Nuclear Engineering, Massachusetts Institute of Technology, Building 24-102, Cambridge, MA 02139.

130. Lawrence Lidsky, Department of Nuclear Engineering, Massachusetts Institute of Technology, Building 38-174, 77 Massachusetts Avenue, Cambridge, MA 02139.

131. Jose G. Martin, Program in Nuclear Engineering, Department of Chemical and Nuclear Engineering, University of Massachusetts-Lowell, One University Avenue, Lowell, MA 01854.

132. William R. Martin, University of Michigan, 108 Cooley Lab, North Campus, Department of Nuclear Engineering, Ann Arbor, MI 48109-2104.

133. S. Martin, Department of Energy, Oak Ridge Operations Office, Oak Ridge, Tn 37831.

134. D. Martinez, Contract Management Division, U.S. Department of Energy, 1301 Clay Street, Oakland, CA 94612-5208.

135. D. J. McGoff, NE-40, U.S. Department of Energy, Washington, DC 20036.

136. L. D. Mears, Gas Cooled Reactor Association, Suite 300, 10240 Sorrento Valley Road, San Diego, CA 92121-1605.

137. Albert Mejane, CEA-DRN, CEN Saclay, 91191 Gif sur Yvette-Cedex, France.

138. Don W. Miller, The Ohio State University, Nuclear Engineering Program, 206 West 18th Avenue, Columbus, OH 43210.

139. Ray R. Mills, MHTGR, PDCO-E, c/o Merex, Inc., Suite 300, 3206 Tower Oaks Blvd., Rockville, MD 20852.

140. I. S. Mosevitskii, Russian Research Center Kurchatov Institute, 123162 Moscow, Russian Federation.

141. Frank J. Munno, University of Maryland, Department of Materials and Nuclear Engineering, Nuclear Engineering Program, College Park, MD 20742-2115.

142. H. F. Niessen, Forschungszentrum Jülich, Postfach 1913, 52405 Jülich 1, Germany.

143. Anthony J. Neylan, General Atomics, P.O. Box 85608, San Diego, CA 92186-9784.

144. J. D. Nulton, Office of Deputy Assistant Secretary for Reactor Systems, Development and Technology, NE-40, Department of Energy, Washington, DC 20545.

145. Walter J. Parker, Stone and Webster Eng. Corp., 245 Summer St., P.O. Box 2325, Boston, MA 02107.

146. Gary A. Pertmer, Nuclear Engineering Program, Department of Materials and Nuclear Engineering, University of Maryland, College Park, MD 20742-2115.

147. Per F. Peterson, Department of Nuclear Engineering, University of California-Berkley, Berkley, CA 94720.

148. Michael Z. Podowski, Department of Nuclear Engineering and Engineering Physics, Rensselaer Polytechnic Institute, Troy, NY 12180-3590.

149. John W. Poston, Texas A&M University, Department of Nuclear Engineering, 129 Zachry Engineering Center, College Station, TX 77843.

150. Victor H. Ransom, School of Nuclear Engineering, Purdue University, West Lafayette, IN 47907-1290.

151. C. L. Reid, Modular HTGR, PDCO-East, 3206 Tower Oaks Boulevard, Suite 300, Rockville, MD 20852.

152. Alan H. Robinson, Oregon State University, Department of Nuclear Engineering, Radiation Center C116, Corvallis, OR 97331-5902.

153. Norman F. Roderick, Department of Chemical and Nuclear Engineering, Farris Engineering Center, Room 209, University of New Mexico, Albuquerque, NM 87131-1341.

154. W. J. Rowan, 504 Mountain Breeze, Knoxville, TN 37922-1516.

155. Gary M. Sandquist, University of Utah, Nuclear Engineering Program, Salt Lake City, UT 84112.

156. J. Scarborough, MS-1643, U.S. Nuclear Regulatory Commission, Washington, DC 20555.

157. R. W. Schleicher, General Atomics, P.O. Box 85608, San Diego, CA 92138.

158. George E. Schmauch, Air Products and Chemicals, Inc., 7201 Hamilton Boulevard, Allentown, PA 18195-1501.

159. Fred Silady, Systems Engineering, General Atomics, P.O. Box 85608, San Diego, CA 92186-9784.

160. Walter Simon, General Atomics, P.O. Box 85608, San Diego, CA 92186-9784.

161. S. E. Slezak, Sandia National Laboratories, P.O. Box 5800, Albuquerque, NM 87185.

162. Kim Smart, Public Service Company of Colorado, Fort St. Vrain Nuclear Generating Station, 16805 Weld County Road 19 ½, Platteville, CO 80651.

163. Jason Speyer, Mechanical, Aerospace, and Nuclear Engineering Department, School of Engineering and Applied Science, 46-147N Eng IV, University of California-Los Angeles, 405 Hilgard Avenue, Los Angeles, CA 90024-1597.

164. T. G. Theofanous, Department of Chemical and Nuclear Engineering, University of California-Santa Barbara, Santa Barbara, CA 93106.

165. N. E. Todreas, Massachusetts Institute of Technology, Department of Nuclear Engineering, 77 Massachusetts Avenue, Bldg. 24-219, Cambridge, MA 02139.

166. James S. Tulenko, University of Florida, Department of Nuclear Engineering Sciences, Room 202, Nuclear Science Center, Gainesville, FL 32611.

167. A. Van Heek, Netherlands Energy Research Foundation ECN, Postbus 1, Petten, The Netherlands.

168. L. P. Walker, MHTGR PDCO-W, c/o General Atomics, P.O. Box 85608, San Diego, CA 92186-9784.

169. Bernard W. Wehring, The University of Texas At Austin, Nuclear Engineering Program, Department of Mechanical Engineering, Austin, TX 78712.

170. A. Weinberg, Oak Ridge Associated Universities, Room E17, Vance Road, Oak Ridge, TN 37830.

171. J. Williams, U.S. Department of Energy, Financial Management Division, 1301 Clay Street, Oakland, CA 94612-5208.

172. Pete M. Williams, HTGR Division, U.S. Department of Energy, NE-451, 19901 Germantown Road, Germantown, MD 20874.

173. Jim Windmiller, NP-MHTGR Central Records Facility, EG&G Idaho, P.O. Box 1625, Idaho Falls, ID 83415-2520.

174. W. O. Winer, Nuclear Engineering and Health Physics Program, School of Mechanical Engineering, Georgia Institute of Technology, Atlanta, GA 30332-0405.

175. David Woodall, Nuclear Engineering Program, Department of Mechanical Engineering, University of Idaho, Moscow, ID 83843.

176. Hank Zeile, NPR Department, EG&G Idaho, P.O. Box 1625, Idaho Falls, ID 83415-2511.

177. Office of Assistant Manager of Energy Research and Development, P.O. Box 2008, DOE-ORO, Oak Ridge, TN 37831-6269.